AL-FARABI KAZAKH NATIONAL UNIVERSITY

UDC: 620.3 On manuscript rights

KUANYSHBEKOV TILEK KUANYSHBEKULY

Researching the properties of functionalized few-layer graphene nanostructures

6D071000 – Materials science and technology of new materials

Dissertation for the degree of Doctor of Philosophy (PhD)

Scientific consultants:
Doctor of physical-mathematical sciences
Professor A.M. Ilyin

Doctor of physical-chemistry
Professor G.W. Beall
Texas State University (San Marcos, USA)

The Republic of Kazakhstan
Almaty, 2019

CONTENTS

SYMBOLS AND ABBREVIATIONS

NFG – natural graphite powder
GO – graphene oxide
RGO – reduced graphene oxide
FFLGN – functionalized few-layer graphene nanostructures
FSLGN – functionalized single-layer graphene nanostructures
HOPG – highly oriented pyrolytic graphite
H_2SO_4 – sulfuric acid
HNO_3 – nitric acid
$KMnO_4$– potassium permanganate
$KClO_3$ – potassium chlorate
$NaClO_2$– sodium chlorite
H_3PO_4 – phosphoric acid
Ga – gallium
AFM – atomic force microscopy
XRD –X-ray diffraction
TGA – thermogravimetric analysis
SEM – scanning electron microscope
EDS – energy dispersive X-ray spectroscopy
AB – absolute humidity (g/m^3 or $grain/ft^3$)
m_w – a mass of water vapor (grams or grain)
v – the volume of air (m^3 or ft^3)
RH – relative humidity
P_V – actual partial pressure of moisture contained in the air (bars or KPa)_
P_S – saturated pressure of humid air at the same given temperature (bars or KPa)
SH – saturation of humidity (g/m^3)
m_{ws} – the mass of water vapor at saturation (g) and v is the air volume (m^3).
CO_2 – carbon dioxide
NO_2 – nitrogen dioxide
NH_3 –hydrogen nitride (ammonia)
CVD – chemical vapor deposition

INTRODUCTION

The relevance of the study

As is known, graphene is a two-dimensional hexagonal structure of carbon atoms, connected by the sp^2 electron configuration. Graphene, functionalized graphene, and its related structures remain to this day an object of increased interest in various fields of science and technology due to its unique mechanical, electrical and optical characteristics. In addition, graphene and its related structures are considered as promising materials in the production of various gas sensors, humidity sensors, electronic devices, electrical sources, in particular, lithium-ion batteries, which can be used in various fields of production, such as nanoelectronics, aviation, military technology, and medicine.

One of the main directions of graphene related research is the study of its modifications, for example, GO, which may be referred to functionalized few-layer graphene (FFLGN). Graphene oxide (FFLGN) is an oxide form of graphene, which is an atomic-thin sheet-like material dispersed in water, which has numerous oxygen-containing groups, where oxygen is introduced into graphene by chemical oxidation.

Functionalization of graphene can be carried out by various methods, in particular, the creation of radiation defects, hydrogenation, oxidation, etc. During the functionalization with strong acids such as H_2SO_4, HNO_3, $KMnO_4$, bulk graphite will have hydroxyl and epoxy groups on their plane, as well as carbonyl and carboxyl groups at the edges. As a result, the functionalized graphene becomes a semiconductor, unlike graphene, therefore its field of practical application will expand significantly.

In this regard, functionalized graphene is a relevant material and has a wide range of applications in semiconductor electronics for creating biosensors, supercapacitors, various gas sensors, humidity sensors, organic electrodes, LEDs, etc.

On the other hand, the most urgent task is to reduce such sheets of functionalized graphene by removing oxygen-containing groups. Reduced sheets of functionalized graphene are usually considered as one of the types of chemically produced graphene and have a number of other names such as functionalized few-layer graphene (FFLGN), chemically modified graphene, transformed graphene, or reduced GO.

The most attractive property of FFLGN is the change in its electrical and optical characteristics, which is realized by removing functional oxygen-containing groups using thermal reduction of FFLGN films and membranes in air and hydrogen atmosphere at optimum temperature conditions. Also, thermal reduction contributes to the production of graphene and graphene-like materials in a large-scale quantity, which is still an actual problem and to this day researchers are trying to achieve a large-scale and more affordable production technology.

The past few years demonstrate an increase in attention to the functionalization of graphene using radiation methods, for example, the formation of radiation defects and doping them with atoms of various elements such as Ga, As, N, B, S.

The resulting functionalized graphene nanostructures are promising for use in nanoelectronics, supersensitive sensors, electrical power sources, flexible electronic and power devices. However, by the moment the stable atomic configurations of graphene, functionalized with individual atoms of different elements not well understood and not clear determined the way of their production in graphene nanostructures and of obtaining the required characteristics. In some cases, solving these issues is a difficult task for experimental research and correct interpretation of data; therefore, computer modeling becomes a very effective research tool for better understanding the physical and chemical properties of functionalized graphene nanostructures and predicting their characteristics. In this regard, the presentation of the results of computer simulation of some possible stable structures of Ga-doped graphene, and few-layer graphene, as well as the study of the basic principles of their energy and structural characteristics are one of the issues of this dissertation work.

One of the important tasks of this work is the creation of a sensitive humidity sensor based on the FFLGN membrane due to its absorption properties and the study of its electrophysical characteristics, which are the great importance in measuring and controlling the humidity of the environment for industrial, agricultural and human activities. Compared to existing present-day sensors, our humidity sensor has a wide operating range of humidity measurements, the equal response and recovery times, as well as stability at various levels of surrounding humidity, and it also has the most important properties, such as low cost, not requiring high technology and stability of works in an aggressive environment.

Thus, the development of technology for producing FFLGN, films and membranes based on them, the study of the optical, electrical properties of FFLGN films with optimal thermal annealing, the study of the influence of temperature on the structure and composition of the FFLGN membrane after thermal reduction, and the use of the FFLGN membrane as a humidity sensor are an actual task in the field of materials science.

The purposes of the thesis are synthesis and computer simulation of FFLGN, obtaining of FFLGN films and membranes and investigation of their physicochemical properties after thermal reduction at various temperatures.

The tasks of the thesis:

1. Creation of computer models of FFLGN, some possible stable structures of graphene and few-layer graphene, functionalized by Ga atoms, various bonding types between graphene and oxygen and calculation of their binding energy and structural characteristics;
2. Synthesis of the FFLGN and obtaining FFLGN films and thermal reduction of these films in the air at temperatures: 80 °C, 120 °C, 160 °C, 200 °C, 240 °C, 280 °C and investigation of the optical and electrical properties of FFLGN films after thermal reduction;
3. Preparation of the FFLGN membrane and thermal reduction in a hydrogen atmosphere at temperatures: 150 °C, 300 °C, 500 °C, 900 °C and investigation of temperature influence on the structure and composition of these samples;

4. Creation of a humidity sensor based on the FFLGN membrane and the study of its electrophysical characteristics.

Objective of the thesis is the functionalized few-layer graphene nanostructures obtained by a modified Hammers method.

Subject of the research is the structure and properties of functionalized few-layer graphene nanostructures.

Methodological framework of the research

Quantum-mechanical methods; technology of obtaining FFLGN; separation of solids from liquid in a centrifuge; obtaining separate layers of material using exposure to ultrasound; obtaining free-standing films using vacuum-assisted filtration; analytical methods: SEM and EDS, Raman spectroscopy, TGA, XRD, optical microscopy, ultraviolet and visible spectroscopy.

The scientific novelty of the thesis

1. For the first time, typical configurations of graphene doped by Ga and various arrangements of their atoms, types of oxygen bonds with graphene and the binding energies of the functionalizing graphene -O and graphene -O-H groups, the model of the possible reduction process of FFLGN were calculated.

2. The simultaneous analysis of elemental composition and electrophysical characteristics of the synthesized samples demonstrates that residual impurities in the solution of FFLGN, obtained by acid exfoliation, have a critical negative effect on the properties and reduction process of FFLGN.

3. The features of the relationship between the interplanar distances in FFLGN and their dynamics during thermal reduction, with the thickness of the films, with the thermograviometric parameters of the films and their electrical and optical properties are investigated.

4. A simple and low-cost method was developed for creating of humidity sensor based on FFLGN membrane, operating in a wide range of relative humidity (5-100%), with a symmetric signal response and recovery time, with high stability (+/-2%).

The scientific and practical significance of the study

1. Computer simulation of possible stable structures of FFLGN has been created, which can be used to better understanding the unforeseen physical and chemical properties of FFLGN. A technology has been optimtized for the production of films and membranes of FFLGN;

2. The possibility of changing the electrical and optical properties of FFLGN films by removal functional oxygen-containing groups at various temperatures of thermal reduction in air and hydrogen is shown. Thermally reduced thin films FFLGN can potentially be used in optoelectronics and as a conductive coating for a wide range of uses;

3. Thermally reduced FFLGN membranes have a developed surface, which allows them to be considered as promising materials in the manufacture of electronic devices, electrical sources, and also in gas sensors;

4. Thermally reduced FFLGN membranes have a developed surface, which allows them to be considered as promising materials in the manufacture of electronic devices, electrical sources, and also in gas sensors;

The main provisions for the defense of the thesis

1. On the basis of computer simulation of the configuration of graphene nanostructures with functional groups -O and -OH, the length and energies of chemical bonds are calculated using the density functional theory (DFT) taking into account the surface (C – O = 1.45 Å) and edge (C – O = 1.2 Å) carbon atoms, and also to establish the energetically favorable position of the Ga atom between the graphene layers.

2. The interplanar distance of functionalized graphene nanostructures can be efficiently controlled from 1.07 to 0.37 nm while preserving the highly oriented structure by thermal reduction in a hydrogen atmosphere in the temperature range from 150 to 900 ^{O}C.

3. A low sheet resistivity value of thermally reduced graphene from few-layered functionalized graphene is achieved by purifying the residual impurity chlorine atoms (Cl) and sulfur (S) with a concentration not exceeding 0.5 at.%.

4. Functionalized graphene nanostructures with a low concentration of residual chlorine (Cl) and sulfur (S) impurities are a sensitive material for absorption of water molecules and allow recording relative humidity with a symmetric time response in a wide range (from 5-100%).

Experimental and theoretical methods

The composition and structure of FFLGN were studied by SEM and EDS, Raman spectroscopy, TGA, X-ray diffraction (XRD), ultraviolet and visible (UV-Vis) spectroscopy.

The personal contribution of the author

The author participated in the process of density functional theory (DFT) calculations within Dmol3 software-package using the software tools of Chem Office Materials Studio for creating computer models of FFLGN. He has worked out technology for producing FFLGN using the modified Hammers method and FFLGN films, and membranes using the vacuum filtration method. FFLGN films were thermally reduced in air and their optical and electrical properties were investigated, and the effects of temperature on the structure and composition of the FFLGN membrane after thermal reduction in a hydrogen atmosphere at different temperatures were studied. The TGA of FFLGN was performed and the optimal modes of heat treatment of films and membranes of FFLGN were determined at which the functional oxygen-containing groups were removed, as a result of which the optical and electrical characteristics changed. A humidity sensor based on an FFLGN membrane was created, and its electrophysical characteristics were studied.

Publications

Based on the materials of the thesis 9 articles were published, including 4 articles published in journals recommended by the Committee for Control in the fileld of Education and Science of the Ministry of Education and science of the Republic of Kazakhstan. Two articles were published in journals with impact factor

Sensors & Transducers, 2019 (IF 0.3); Journal of Computational and Theoretical Nanoscience, 2019 (IF 0.45) and 3 abstracts are published in national and international conferences. All of these publications were made during the Ph.D. program.

Relation of the dissertation topic with the plans of scientific works

This dissertational work was carried out in the framework of the scientific project named “Development of technology in creation of protective coatings based on functionalized graphene nanostructures and investigation of their properties”, funded under the financing grant of project № AP05130413 of the Science Committee of the Ministry of Education and Science of the Republic of Kazakhstan.

Volume and structure of the thesis

The thesis work contains a list of symbols and abbreviations, an introduction, the main part of the 3 sections, a conclusion and a list of references. The work is presented on 100 pages, contains 52 Figures, 5 tables and 206 bibliographical references.

1 LITERATURE REVIEW

1.1 Various forms of carbon

One of the enthralling elements in material science and nanotechnology is carbon, which can introduce in the following molecular types: graphite, fullerenes, and nanotubes. Figure 1 shows the molecules of fullerene C60, carbon nanotubes and graphite, which can be considered in the form of graphene sheets arranged in a hexagonal lattice.

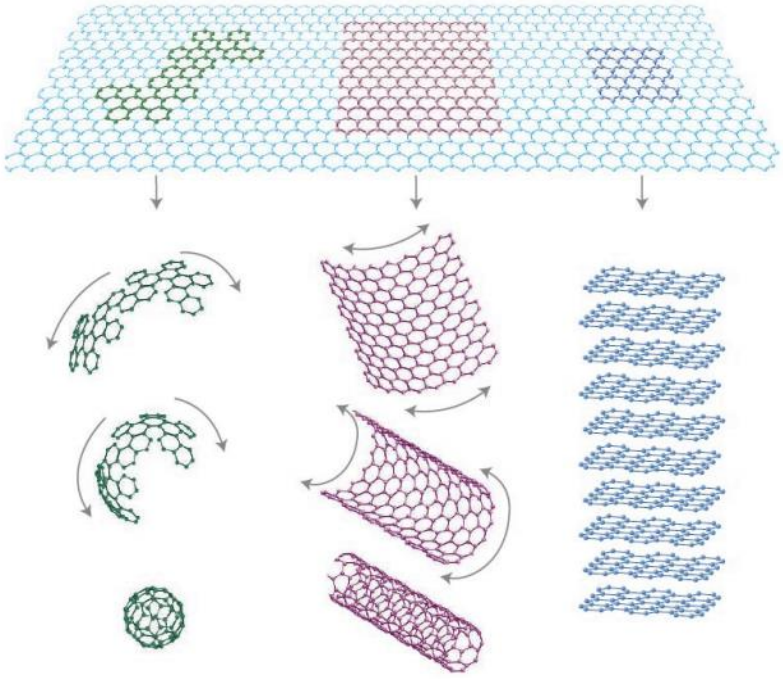

Figure 1 – C 60 fullerene molecules, carbon nanotubes and graphite [2, p. 4]

Among these carbon forms, the well-known is graphite, consisting of single layers of carbon atoms, which are stacked with hexagonal carbon sheets on above of each other. Single sheet representing the hexagonal structure was obtained in an exfoliated form in 2004 by K. Novoselov and A. Geim. Also shown that one of these single sheets, the so-called graphene, can be transferred to another substrate and the electrical characteristics can be measured [1, 2].

Graphite-like carbon nanomaterials consist of sp^2 – hybridized carbon atoms located in a hexagonal lattice, their difference in different sizes and shapes and only some common properties are similar [3].

In the history of graphene-like materials, they have been known and studied since the 1940s, but obtaining single isolated graphene and measuring its electrical characteristics was experimentally difficult and was considered almost impossible [2, 4, 5].

A detailed report was made in [6] and the history of the obtaining and characterization of graphene was shown in Table 1 [6]. From the history, we note Boehm, who invented the name of graphene in 1986 [4, 7, 8], in his work in 1962,

demonstrated the existence of single graphene. In 1962, Boehm exfoliated RGO with heteroatomic contamination, where the electrical conductivity was significantly lower compared to pure graphene, which was obtained using the “scotch tape method” [8–11]. On the basis historical time obtaining and characterization of graphene, it should be noted that all works except Boehm were observations and did not describe the distinctive properties of graphene [6, 12].

On the basis of this historical time scale for the synthesis and characterization of graphene, it should be noted that all works except Boehm were observational and did not describe the distinctive properties of graphene. Thus, according to the historical scale in 2005, Novoselov and Geim made the first report on obtaining a single layer of graphene using the “scotch tape method” without heteroatomic contamination and which describes its distinctive unique properties [6, 12].

Table 1 – The timeline of individual events in the history of graphene for its preparation, synthesis, and characterization [13, p. 3]

№	Years	Events in the history of graphene
1.	1840-1958	Graphite oxide synthesis (Schafhaeutl, Brodie, Staudenmaier, Hummers)
2.	1962	Obtain RGO, GO by chemical and thermal reduction of graphite oxide (Boehm, colleagues)
3.	1968	Obtain LEED patterns formed by absorbing a small molecule on Pt (100) (Morgan and Somorjai)
4.	1969	interpretation of Morgan and Somorjai data on the presence of a monolayer of graphite on the Pt surface
5.	1970	Obtain monolayer graphite by segregating carbon on the surface of Ni (100) (Blakely and his colleagues)
6.	1975	Prepare monolayer graphite by sublimation of silicon from silicon carbide (Van Bommel and his colleagues)
7.	1986	Using the term "graphene" to describe mono layers of graphite-like carbon recommended by Boehm and his colleagues.
8.	1997	IUPAC formalizes the definition of graphene: “The term graphene should be used only when reactions, structural relations, or other properties of multiple layers of graphene are discussed.”
9.	1999	Micromechanically exfoliate graphite into thin lamellae comprised of several layers of graphene (Ruoff, colleagues).
10.	2004	Obtain graphene by micromechanical exfoliation (Geim, colleagues).

We all know that ordinary pencil contains graphite, and when this pencil is moved on paper, the graphite is exfoliate into several thin single layers of graphite, the so-called graphene sheets. That is, fairly simple use of a pencil, which contributes to the splitting of graphite, shows that the complexity is not the manufacture of graphene structures, but simply isolation on large individual sheets in order to investigate its unique two-dimensional (2D) properties that Geim, Novoselov and their employees succeeded in.

Fullerenes were discovered by chemists in 1996 and represent a new form of molecular carbon C60, which contains 60 carbon atoms assembled in a circle shape, resembling a soccer ball, which consists of 20 hexagons and 12 pentagons that allow surfaces to form a sphere [14].

Another form of carbon structures, known since 1993, are nanotubes [15], which represent a bound quasi-one-dimensional shape and are formed from twisted graphene sheets in the form of tubes. Carbon nanotubes, like fullerenes, have hemispherical ends, and the electronic and mechanical properties of single-walled nanotubes are almost similar to graphene [5, 16–18].

Carbon nanotubes depending its layers of the walls have the following sizes: the diameters of single have 0.8-2 nm, the diameters of multi have 5-20 nm and may to 100 nm. Also, a conductance or semi conductance wall of nanotube depends on lattice orientation relative to the axis, which has the name chirality [3].

1.2 Graphene

For the first time in 2004, Geim and Novoselov, using the method of mechanical exfoliation, separated one sheet of graphene from graphite. Since then, graphene has unique physic-mechanical properties (mechanical, thermal, optical and electrical), so based on the above properties it's attracted more attention in many fields of science and technology. Graphene is a flat layer of the monatomic structure of sp^2 bound carbon atoms, which is tightly packed in a hexagonal structure [19, 20].

Graphene is a one-layer sheet of carbon, which is a flat monolayer of sp^2-hybridization carbon atoms located in a honeycomb lattice and having a carbon-carbon bond distance of 0.142 nm [21], and the height of one layer is 0.33 nm (Figure 2 (a, b)).

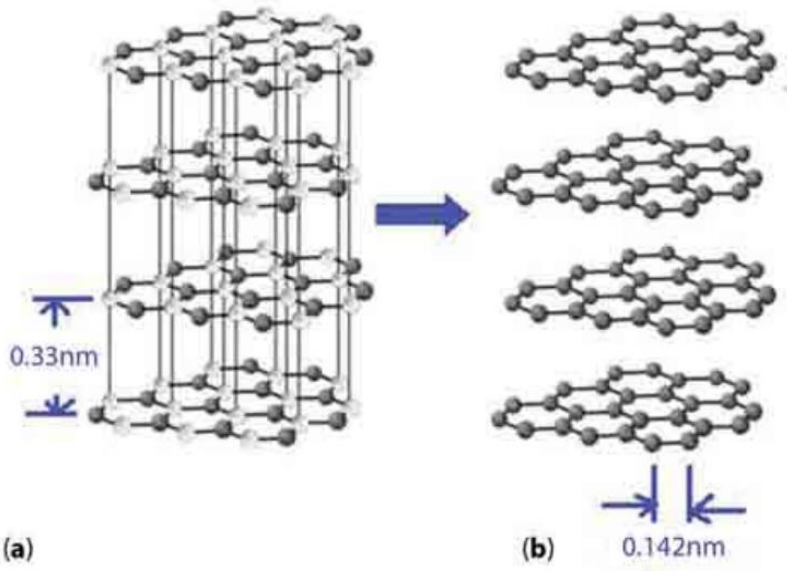

Figure 2 – Schematic diagram of (a) graphite and (b) four layers of graphene from graphite [21, p. 3].

Structure of graphene has a stable hexagonal form due to densely packed carbon atoms and sp^2 bonds in each lattice, and this -bond consists of combinations as s, p_x, and p_y orbitals [22]. The final p_z-electron is a π-bond located vertically to the plane of the lattice on which the electrical conductivity of graphene depends and the hybridization of this π -bonds contribute to the formation of the -zone and π* -zone (bands).

And also the electronic properties of graphene depend on these zones, with the help of which electrons can freely move through the half-filled bands (bands) [23]. Thus, the graphene structure consists of a densely packed one layer of carbon atoms associated with the surrounding atoms of carbon by sp^2 hybridization in the shape of a benzene ring in which each atom donates an unpaired electron for -bonds and in this case electrons can move freely with little interference at room temperature, which leads to high conductivity [24, 3].

Graphene is semimetal and lower energy of electrons can pass from the valence to the conduction bands through a small overlap, and this transition takes place without external heat exposure. Also, a certain amount of electrons can be in the conduction band and in the valence band there is a certain number of holes [25]. Figure 3 shows the conduction bands in the form of a cone-shaped structure, in which the valence band and conduction band intercept the Dirac point, also the manifestation of the anomalous quantum Hall effect and the characteristics of relativistic particles [3, 26] occur in the process of electron transfer [22, 23].

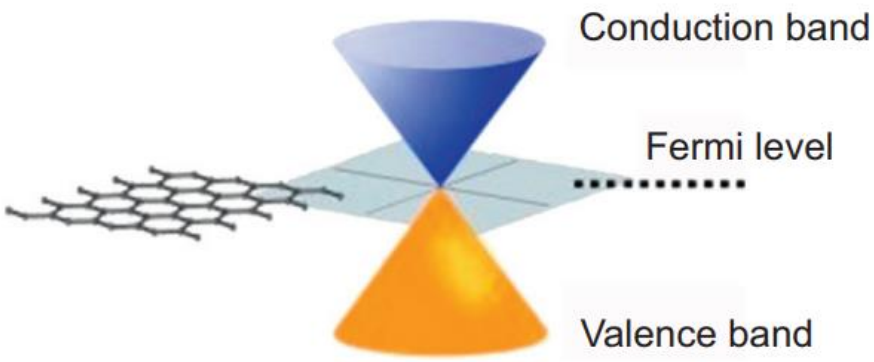

Figure 3 – Conduction zones in the form of a cone-shaped structure [3, p. 10]

Compared to other carbon materials, graphene has optical, electrical and mechanical properties. The optical property is distinguished by the fact that, regardless of the wavelength in the optical zone, graphene absorbs 2.3% of the light intensity.

Also, the transparency of graphene depends on the number of layers, that is, single-layer graphene absorbs 2.3% of visible light and has a very high transparency of 97.7%, and the transparency of two-layer graphene is less than that of single-layer and the difference between them is 2.3% [3, 27], which is shown in Figure 4 [3, p. 8]. Figure 4 shows the transparency of graphene.

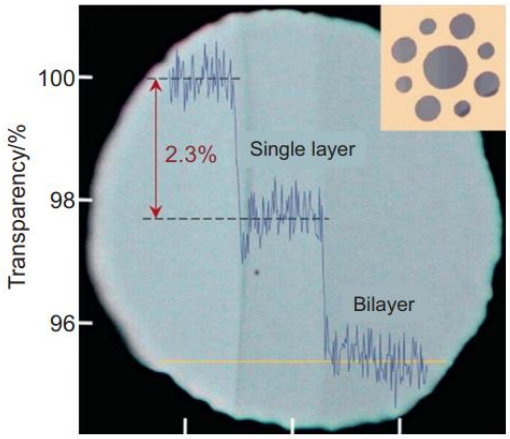

Figure 4 – Graphene Transparency [3, p. 8]

Graphene with different layers has the ability to show different colors and contrasts depending on the graphene layers according to the refraction and interference of light which this facilitates the use of graphene layers to distinguish [3, 28]. And also, depending on the different thickness of graphene, you can control the unique optical properties of this material.

Another interesting property of graphene is the mobility of electrons. In this case, the electrical conductivity of a sheet of 2D material is given by the expression and the mobility of a 2D sheet is theoretically limited to = 200,000 $cm^2V^{-1}s^{-1}$ by acoustic phonons at carrier density n = 10^{12} cm^{-2} and 140 times more mobile than silicon, and the resistivity per square is 31 Ohms. Compared with copper, the electrical conductivity of graphene with a thickness of one layer is much higher, that is, the volumetric conductivity of graphene is 0.96 × 10^6 Ohm^{-1} cm^{-1}, and copper has 0.60 × 10^6 Ohm^{-1} cm^{-1} [5].

Thus, graphene can potentially become competitive and replace indium and fluorine doped tin oxide and other traditional membranes [3] due to its optical and high conductivity properties.

The next property of graphene is the mechanical strength of graphene, which has the most rigid crystal structure among all known materials and the tensile strength and modulus of elasticity of graphene are 125 GPa and 1.1 TPa [29], respectively, its tensile strength reaches 42 N/m. If we compare the strength of steel and graphene with the same size and thickness, then graphene is approximately 100 times stronger than, for example, 1 m^2 of graphene can withstand 4 kg of weight [3, 30].

Steel has a tensile strength in the range of 250-1200 MPa = 0.25-1.2 × 109 N / m^2. For example, if it is hypothetical to take a steel film with a thickness of 3.35Å = 3.35 × 10^{-10} m as the thickness of a single graphene layer in graphite, then a two-dimensional tensile strength of steel will give 0.084-0.40 N / m, and for graphene 42 N/m, and these data show that graphene is more than 100 times stronger.

Also one of the important properties of graphene is thermal conductivity. The conductivity is10 times better than copper, which is, at room temperature, copper has 401 W $m^{-1}K^{-1}$, and graphene is approximately 5000 W $m^{-1}K^{-1}$ [5]. In addition, graphene has a high surface area of 2630 m^2/g [3, 31] and this property allows it to be

used in microsensors for gas molecules by observing a sharp change in electrical resistance in the process of adsorption and desorption of gas molecules.

1.3 Methods for the synthesis of graphene

To date graphene has attracted widespread attention, and also represents a huge potential for various scientific and practical applications, due to its physic-mechanical properties. Graphene is characterized as a 2D sheet of sp^2-hybridized carbon atoms located in a hexagonal lattice [32].

One of the important processes is the synthesis of graphene. By graphene, synthesis is meant to obtain graphene of the desired size, purity, crystallinity using various methods [32]. In this case, The most commonly used methods for the synthesis of graphene are mechanical splitting [32]; epitaxial growth; chemical vapor deposition (CVD); electrochemical peeling [24, 32, 33, 34]. Figure 5 shows the different methods for the synthesis of graphene.

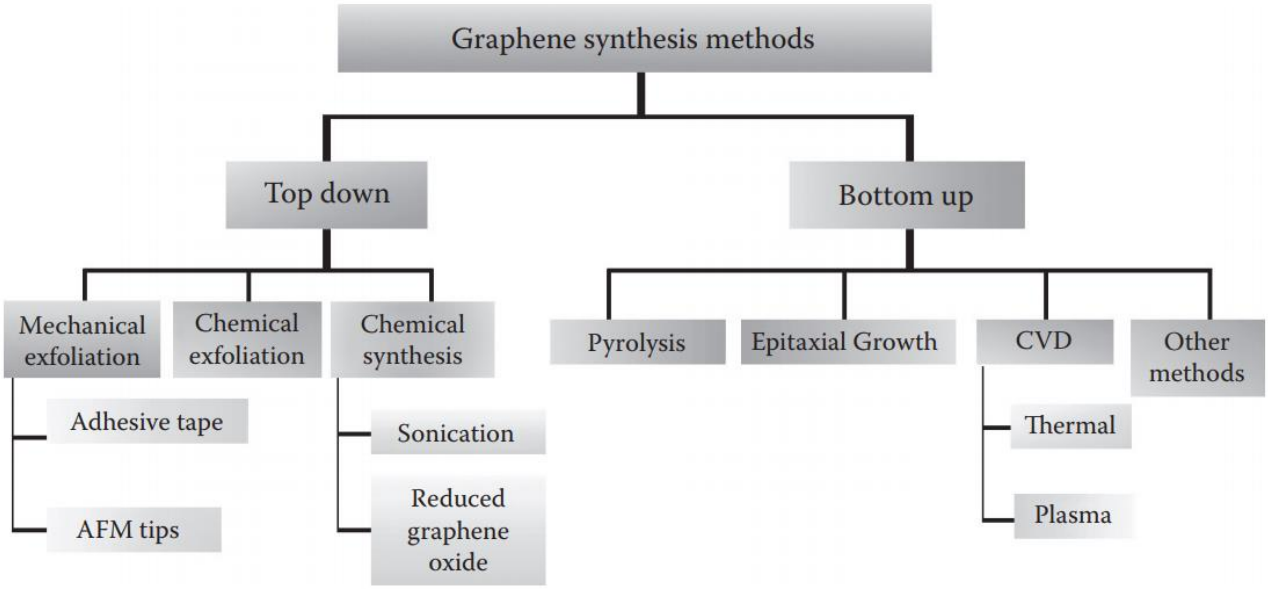

Figure 5 – Various methods for the synthesis of graphene [35, p. 29]

To obtain graphene by the method of mechanical splitting, thin layers of HOPG are placed between adhesive tapes and the graphite film is cleaved off time after time until a thin layer is obtained [32].

The next important method is epitaxial growth of graphene, where graphene is grown on monocrystalline silicon carbide (SiC) [33]. In this method, silicon carbide (SiC) is heated under a temperature of about 1200C under vacuum, resulting in the sublimation of Si atoms, forming carbon layers on SiC, which can be double-layered, multi-layered, or monolayer [24].

Synthesis of graphene in the CVD method carried out directly on next transition metal substrates, such as Ni, Cu, Co, Au, and Ru. Also, the process of saturating carbon carried out under the influence of the next various gaseous hydrocarbons: methane, ethylene, acetylene, and benzene at high temperature [34].

There are differences between hot and cold wall CVD processes, that in the hot wall substrate is heated by radiation from the heated chamber walls and temperature is relatively constant everywhere because the chamber is heated by an external source of energy. In the cold wall reactor, the sample is heated using the following ways: current pass through the sample, using a heater of the substrate, using induction, and the chamber walls have room temperature [36].

The next method of obtaining graphene is electrochemical exfoliation of graphite. Choice the electrodes and electrolyte one of the important processes in the electrochemical exfoliation, which affects the increase in charge transfer and functionalization of obtaining graphene sheets. Many different electrodes and electrolytes are used for this method and most commonly used electrodes are: HOPG, graphite, Cu, Pt., and the next electrolytes: HBr, HCl, HNO_3, and H_2SO_4, as well as acid electrolytes and alkaline electrolyte KOH, diluted with distilled water, which is ideal for exfoliating graphite [37-39].

In this process, two graphite electrodes or other types are first inserted into the solution. Then about 10 V is applied to the electrodes and the intercalating ion of the solution penetrates between the graphite layers and exfoliates into FLG sheets. After separating graphite particles from the graphene solution is exposed to centrifugation or ultrasound to improve the exfoliations. At the finish of the process, the solution is dried [40, 41].

Thus, until today, the synthesis of graphene and graphene-like materials is relevant due to the unique physic-mechanical properties, therefore, many works are aimed at finding ways to obtain graphene under such conditions as low cost, a fairly simple synthesis method, scalability and capabilities turn it into graphene. One of the most appropriate methods for the synthesis of graphene, given the above conditions, is to obtain FFLGN, which will be discussed in subsequent sections of this work.

1.4 FFLGN and FFLGN membrane

Graphene, GO and its related structures to this day continue to show interest in various fields of science and technology due to their physicochemical properties. Today, after the appearance of graphene in 2004, monoatomic carbon layer of graphene oxide has names as FFLGN.

One of the main directions of graphene related research is the study of its modifications, for example, graphene oxide, in the process of functionalization of graphene, which is the oxidation of graphite by strong oxidizing agents such as H_2SO_4, HNO_3, $KMnO_4$ as a result of which bulk graphite becomes functionalized with hydroxyl and epoxy groups on their main plane and at the edges of the carbonyl and carboxyl groups [42-45]. Then, from this bulk functionalized graphite using the most common ultrasound, it is possible to easily obtain exfoliated GO nanosheets, which may be referred to as functionalized few-layer graphene (FFLGN). So, FFLGN – is an oxide form of graphene, which is an atomic-thin sheet-like material dispersed in water, which has numerous oxygen-containing groups, where oxygen is introduced into graphene by chemical oxidation.

Today, functionalization of graphene can be carried out by various methods, in particular, the creation of radiation defects, hydrogenation, oxidation, etc. [46, 47]. In [48] it was considered that there are two basic types of functionalization of graphene: chemical and non-chemical. The chemical functionalization method is understood as chemical modification of the surface by various groups of atoms, as a result of which new covalent bonds between atoms native to reduced FFLGN/FFLGN and the guest functional groups are formed. In the case of nonchemical functionalization, mainly physical interaction occurs and functionalization occurs on the basis of π interaction between guest molecules and reduced FFLGN/FFLGN. Both categories of functionalization contribute to changes in the properties of graphene, but the most effective is chemical modification [49, 50].

Compared with pure graphene, functionalized graphene has a wide range of applications in semiconductor electronics for creating biosensors, supercapacitors, various gas sensors, organic electrodes, LEDs, etc. [51, 52].

Thereby, one of the important moments is the large-scale production of graphene, which is necessary for applications in various fields of science and technology. In work [19] it was considered that initially one of the ways to obtain graphene in large quantities was mechanical peeling of graphite using scotch tape and epitaxial chemical vapor deposition, but these methods are ineffective for large-scale production since it is laborious, low yield and takes more time [32, 53]. Therefore, at present, large-scale production of graphene is relevant and of great interest.

In this regard, FFLGN is of great interest because of its low cost, a fairly simple synthesis method, availability, the ability to convert to graphene, also its scalability, which are an important feature [54, 55-58]. In addition, in reports [59, 60] that FFLGN attracted much attention due to its broad ability to be used in energy, electronics, water purification membranes, etc.

FFLGN is an important precursor for the synthesis of graphene, which is implemented using chemical or thermal reduction processes. FFLGN is a single sheet of the crystal lattice of graphite oxide, which is a compound of carbon, hydrogen, and oxygen in different ratios, which is formed when graphite is processed with strong oxidizing agents [61].

In [62] and [63] et al., It is stated that graphite and FFLGN have a layered structure, although, compared with graphite, FFLGN contains functional groups with high oxygen density, such as hydroxyl and epoxy groups on its basal plane and on its edge with less carboxyl, carbonyl, phenol, lactone and quinone which contribute expand of interplanar distance, and also makes it hydrophilic. [62-67].

Above, we indicated that one of the important points in the production of graphene-like materials is the process of graphene functionalization, which is the oxidation of graphite by strong oxidizing agents as a result of which bulk graphite becomes functionalized with hydroxyl and epoxy groups on their base plane and on the edges of the carbonyl and carboxyl groups [68-71].

At the first time 150 years ago graphite oxide obtained by Brodie, in the experimental processing graphite functionalized by $KClO_3$ and HNO_3 [72]. FFLGN

has been modified for 150 years with various chemicals, such as $KMnO_4$, H_2SO_4, H_3PO_4 [73, 74].

At this time, the synthesis of FFLGN is performed by oxidizing NFG by the next main approaches [75]: Staudenmaier [76], Hofmann [77], Hummers [73] and Tour [78]. The Hummers methods developed by Brodie or Staudenmaier have a number of advantages over the currently existing methods for producing GO [73, 75, 76, 79]. First, it takes a little time in the process of synthesis, which can be completed within a few hours. Secondly, $KClO_3$ was replaced with $KMnO_4$for improving the safety of the reaction to eliminate the occurrence of explosive ClO_2. $KClO_3$. Third, using the $NaNO_3$ instead of HNO_3 eliminates the formation of acid mist, smoke [75], so based above process for improving the synthesis and purity of the final product, various modifications of this method were introduced [80].

Currently, the main method of obtaining FFLGN and large-scale production of graphene is the Hammers method. Graphite is usually chosen as the initial material because of its availability and low cost. The synthesis FFLGN consists mainly of two stages: such as oxidation of graphite and exfoliation of graphite oxide, which is shown in Figure 6 [72, 73, 76–78, 81].

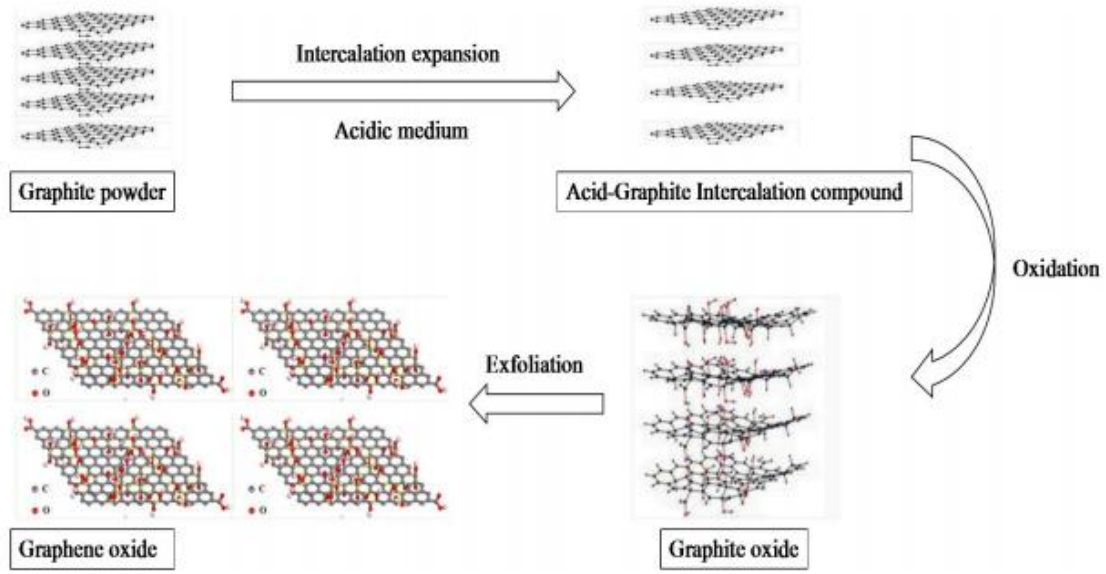

Figure 3. Schematic illustration of GO preparation process.

Figure 6 – The main stages of the synthesis FFLGN [81, p. 3]

Proportional amounts of oxidizing agents, such as $KMnO_4$, $NaNO_3$ and concentrated H_2SO_4, are mixed in order with graphite. Then a 3 phase process is carried out with low, medium and high-temperature reactions, each of which occurs separately in time. Graphite is oxidized to GO using these procedures. The implantation of oxygen-containing functional groups overcome between Van der Waals sheets and contributes to the expansion of the distance between the layers, as well as these groups are attached to both sides of the graphite sheet. Then, oxidized graphite to obtain one or few layers of graphene, these oxidized layers are exposed to

ultrasound, as a result of which it exfoliated into single-layer, few layers to formation GO, FFLGN [49], and after oxidation, graphene sheets have a large number of different defect levels, which depends on the added amount of oxidant and the time of oxidation [82, 68].

Also today, besides the obtain of large-scale amounts of FFLGN it is relevant to study of its optical, electrical, mechanical, and other properties. Due to the violation of the sp^2 bond, the properties of FFLGN as GO are often described as dielectric, but in fact, this is not true. Basically, the conductivity of FFLGN depends on the functionalization, that is, on the amount of oxidation, as well as on the method of synthesis, which can fundamentally change the electrical properties. In this case, there are various methods of functionalization, in which few-layer graphene nanostructures can be functionalized, depending on the required application.

As mentioned above, the structure and properties of FFLGN depend on the synthesis method and degree of oxidation; therefore, chemical synthesis using the Hammers method [69] has found the widest application. This synthesis method used can be changed by decreasing or increasing the levels of oxidation used to exfoliate graphite flakes, which affects the change in electrical and other properties [70].

Thus, the synthesis of FFLGN with the oxidation of bulk graphite with strong oxidizing agents, then followed by exfoliation into FLG sheets helps to obtain graphene, graphene-like materials in large quantities, with low cost, a simple method of synthesis and the ability to turn it into graphene. In addition, one of the important processes in the study of FFLGN is the reduction of FFLGN, which will be discussed in the next subsection.

Also, except obtaining FFLGN, the synthesis of the FFLGN membrane from a FFLGN solution is the most important for application in science and technology, in partically for creating humidity sensors and studying its electrophysical characteristics, which are discussed in Chapter 3.2.8 of this work.

For the manufacture of the FFLGN membrane, the following methods are used: filtration (vacuum, pressure filtration); casting-plating (spinning casting-plating, drop casting, two-piece coating); layer-by-layer assembly; evaporation; alignment method related with the shift and hybrid method [81].

From all the above methods in our experimental work, we chose vacuum filtration because its availability, low labor intensity, nano-sized control over the membrane thickness and the possibility of high-scale production of FFLGN membranes. FFLGN membranes using vacuum filtration were first obtained in work [84], in which FFLGN monolayers were connected almost in parallel, and also in this work, it is stated that during the preparation process, the physicochemical properties of FFLGN monolayers do not change [81, 84].

The synthesis of an FFLGN membrane using vacuum filtration consists of the following main processes: the selection of the appropriate concentration of FFLGN solution; FFLGN membrane is deposited by passing FFLGN solution through a porous film, then after the completion of the filtration, the resulting FFLGN membrane is dried [81, 83]. The result is a uniform dispersibility membrane with a

relatively flat surface due to the fluidity of water in the solution filtration process, and the control of the film thickness depends on the concentration chosen.

Thus, obtaining FFLGN and FFLGN membranes are important for obtaining graphene in large quantities, as well as its application in many areas of science engineering.

1.5 Reduction of FFLGN

The most attractive feature of FFLGN is the thermal reduction of graphene-like sheets, as a result of which oxygen-containing functional groups are removed, whereupon it's electrical, optical and other properties change. Also, a reduced sheet of FFLGN is usually considered as one of the types of chemically produced graphene and has a number of other names such as functionalized graphene, chemical modified graphene, chemically transformed graphene, or reduced graphene [71].

Currently, the properties of pure graphene and reduced FFLGN are close. Therefore, the reduction of FFLGN is one of the actual processes that allows obtaining graphene-like materials in large quantities and their application is important in science and technology. In this regard, to obtain graphene in a large quantities the following methods of the reducing process are used: chemical, thermal and electrochemical. As mentioned above, the use of these methods results in obtaining FFLGN whose electrical, thermal, mechanical properties are close to graphene [85].

Various chemical reagents are used in chemical reduction process, but one of the most common is hydrazine monohydrate, which is a good chemical reagent for the reduction of FFLGN [86]. The process of reducing FFLGN with hydrazine and its derivatives such as hydrazine and dimethyl hydrazine hydrate is the addition to the aqueous dispersion of FFLGN [87].

FFLGN can be reduced by heat treatment and this process is called reducing using thermal annealing [88]. Thermal annealing is usually carried out by thermal radiation. Some non-standard heating means such as microwave irradiation [89] and photo irradiation [90] for thermal reduction are used as an alternative. Also, the main advantage of microwave irradiation compared with conventional methods of heating is to heat the substance evenly and quickly [89]. In addition to the above methods, thermal reduction in a flow tube in various atmospheres (argon, vacuum, hydrogen, hydrogen/argon) is currently widely used [91]. Another method that shows promise for the reduction of FFLGN relies on the electrochemical removal of the oxygen function [85].

Electrochemical reduction of FFLGN sheets or films is performed in an electrochemical cell using an aqueous buffer solution at room temperature. Reduction, as a rule, does not require a special chemical and is mainly due to the electronic exchange between FFLGN and electrodes [92, 93].

One of the important points in the process of temperature reduction of FFLGN, which includes temperature zones at which functional oxygen-containing groups are removed in a hydrogen stream in a flow tube under the influence of various temperatures. The process of temperature reduction of FFLGN to 2000 °C has 6 important temperature zones: 140-180 °C, 180-600 °C, 600-800 °C, 800-1000 °C,

and 1000-2000 °C. At a temperature of 130 °C, due to the mild evaporation of intercalated H_2O molecules, a continuous intensive compression of GO crystals occurs. In the range of 140-180 °C, due to the rapid evaporation of intercalated H_2O molecules, GO crystals are partially exfoliated. In the range of 180-600 °C, the intermediate layers for all types of graphene and GO are contracted with the removal of the basic carboxyl groups. Within 600-800 °C, the residual carboxyl and partially hydroxyl groups are removed as gases. Within the range, of 800-1000 °C, residual hydroxyl and partially epoxy groups are removed. In the range, of 1000-2000 °C, a decrease in the number of defects is observed [94, 95].

Thus, the difference in FFLGN and reduced FFLGN is that FFLGN is highly oxygenated, with the presence of many oxygen-containing functional groups that are smaller in reduced FFLGN. These oxygen-containing functional groups, such as epoxy, hydroxyl, carbonyl and carboxyl groups on its main plane [83] can be removed in the process of chemical and thermal reduction, as a result of which the physicochemical properties of reduced FFLGN are changing, and can also find wide application in science and technology. The experimental part of the synthesis and the study of the optical and electrical properties of FFLGN films, and also changing the structure of the FFLGN membrane after thermal reduction are given in Chapter 4, and application as a humidity sensor based on the FFLGN membrane is discussed in Chapter 5 of this work.

1.6. Characterization of FFLGN by Raman spectroscopy

The Raman spectra of FFLGN, like graphene, have G and D bands, the first order of scattering of the E_{2g} phonon of sp^2 carbon atoms, G, the band is reflected around 1580 cm^{-1}, and also occurs due to stretching the C–C bond in the basal plane, which is characteristic of all sp^2 hybridized carbon materials, and the D band appears in zone of 1200–1400 cm^{-1} and indicates a certain amount of disorder, defect (disorder) or edges in the carbon structure [96, 97].

D and G bands have certain differences compared to graphite and graphene. In FFLGN, the D band is wider and more intense, while the G band is suppressed [98, 99] and significantly broadened and sometimes slightly mixed to higher frequencies [71, 100]. This shift may be due to the doping effects [101], with the result that doping will affect the mixing of the G band [102, 103].

D, G, and 2D Raman scattering bands are the basis for characterizing the reduced FFLGN and determining the density of defects. In work [98] it is given that with increasing degree of functionalization, wide D, G, and 2D bands are expected, also in this paper, it is considered that the degree of functionalization cannot be determined by Raman spectroscopy.

Another issue in the Raman spectroscopy of FFLGN and reduced FFLGN is the change in spectra after reduction. The D-band in FFLGN is mainly due to chemical functionalization and the expanded quantity of sp^3 C atoms, also structural defects inside the carbon skeleton. Functional groups are removed by reducing from π surfaces and from structural defects, such as vacancies or rebuilt carbon structures (five-membered or seven-membered rings) dominate [98].

As described above, the D band in graphene can be caused by structural defects or functional additions, as in FFLGN. Thus, by removing and adding functional groups, carbon integrity can be studied.

To determine the relative content of defects in the sp^2 carbon lattice, the most convenient measure is the ratio between the intensities I_D/I_G. The I_D/I_G ratio in FFLGN is more than graphene or graphite, where the D-band is often indistinguishable from the background and the I_D/I_G is of the order of 0.01. To use this ratio to quantify disorder, it is important to consider two defect modes [97]. Since the disorder in the graphene lattice begins to increase with a low-density defect, the I_D/I_G ratio also increases at first. With a further increase in the density of defects, ultimately lead to the loss of the carbon lattice, the I_D/I_G ratio begins to decrease due to nonlinear damping of all the peaks of Raman scattering when the material begins to turn into amorphous carbon [97].

In the low-density density mode, I_D/I_G can be approximated by an empirical formula linking the relation to the distance between two adjacent defects, L_a:

$$I_D/I_G = C(\lambda)/L_a^2 \quad (1)$$

where λ is the excitation wavelength of Raman scattering and C (λ) is an empirical parameter: C (λ) = 102 nm^2 for the excitation wavelength λ = 514 nm [97]. For FFLGN, L_a determines the size of graphite regions (domains) surrounded by oxygen-containing functional groups. For edge defects, another formula (2), the Tuinstra-Koenig ratio [104], is more appropriate:

$$I_D/I_G = C(\lambda)/L_a \quad (2)$$

Here, C (λ) = (2.4 × 10-10 nm^{-3})×λ^4 [105], and λ is the wavelength of the excitation of Raman scattering. How unlike low defect density, in the high-density-defect mode, the I_D/I_G ratio depends directly on the size of the graphite cluster [106, 107]:

$$I_D/I_G = C(\lambda)/L_a \quad (3)$$

Here C '(514 nm) = 0.55 nm^{-2} [106, 107]. As a result, the ratio between the intensities of the Raman scattering bands can serve as an estimate of the defect density in FFLGN, as well as the L_a value of graphite sp^2 hybridized carbon clusters surrounded by sp^3 hybridized functionalized sites.

In consideration of this I_D/I_G dependence on the density of oxygen-containing functional groups, we expect significant changes in the Raman spectra depending on the oxidation. This was observed in experiments on oxidative etching on single and layered graphite substrates [108]: I_D/I_G increased with oxidation, which indicates a decrease in the size of graphite carbon zones.

Due to significant oxidation, at a certain time a number of defects in the graphite structure can reach an enriched point at which, due to the degradation of six-membered rings, the intensity D of the Raman band begins to decrease. At such high

defect densities, the I_D/I_G ratio decreases with decreasing size of the graphite cluster according to (3).

The combination of I_D/I_G dependencies on the size of sp^2-hybridized zones with low and high defect density modes provides a suitable theoretical explanation for the observed behavior and allows us to estimate that the size of the graphite zones of L_a decreases to ~ 1 nm during oxidation. As well as in other works on the sizes of the sp^2 zones in FFLGN thin films and bulk FFLGN samples obtained by the Hammers method reaches up to 2.5–6 nm [109, 110].

In the reverse process, of the reduction FFLGN, the I_D/I_G ratio changes differently for different experiments with different reduction procedures. Some studies on the chemical reduction of FFLGN showed no difference in I_D/I_G [109, 110], implying that although the oxygen-containing groups were removed by reduction and the places of defects left by these groups were not cured. Other studies show a decrease in the I_D/I_G ratio, which indicates the elimination of defects through reduction [111–113], and there are works in which an increase in the I_D/I_G ratio [114–116] is considered.

This may result from an increase in the number of disorders in the system and an increase in the intensity of the D band due to the random nucleation of small sp^2 zones. A no monotonic trend in the I_D/I_G ratio was also observed for experiments with gradual chemical reduction: with the first intensity ratio, D/G was reduced and then increased [117]. This is due to the growth of the sp^2 zones during the initial reduction leading to a decrease in the I_D/I_G ratio, followed by the random formation of smaller sp^2 zones within the sp^3 clusters, which increased the lattice disorder and the I_D/I_G ratio [96, 118-122].

Thus, the characterization changes of the Raman spectra of FFLGN before and after thermal reduction plays an important role in the analysis and identifying certain structural characteristics of the samples.

1.7 Basics of computer simulation

Computational science begins to play an important role in research and development. Nowadays modern scientific research initially based on experiment and its theoretical interpretation, which is become a triad of experiment, theory and computer simulation. So this is because the analysis of modeling complex systems can be a gate for the discovery of important, but still unnoticed, simplifications and patterns. Computing tools play an important role in the development and testing of new engineering products, also the simulation results are the basis for many decision policies [123].

At this time computer modeling has such interchangeable terms as computer modeling and simulations, which are successfully used in the following areas of science and technology: design, production management, business, science, technology, architecture, entertainment, government, military and logistics/transportation.

Computer modeling is used to reduce the risk associated with creating new systems or making changes to existing ones. More than ever, modern organizations

want to be sure that investment will lead to expected results. For example, an assembly line may be required to produce a certain number of cars during an eight-hour shift. Complex, interacting factors affect the work, so powerful tools are needed to develop an accurate analysis.

Over the past few decades, computer modeling software, along with statistical analysis methods have evolved to provide developers with the tools that fit this task. Due to the development of technics and technology, each time the world becomes technical and therefore accuracy without errors is becoming increasingly important. When developing systems, business, industry, and government cannot afford to make reasonable assumptions and therefore computer modeling is more important than ever.

Compared to decision-making methods, using computer simulation for analysis has the following advantages [124]:

- allows to experiment without failures in existing systems, new ideas that are difficult, costly or impossible, as well as develop a model and compare it with the system to ensure that it accurately reflects current work. The advantages of the modeling process are that first you can make any desired modification to the model, the impact on the system under study, and then you can make a real system;

- using computer simulation it is possible to, check an advanced idea before setting, which allows identifying unexpected disadvantages in the construction and these disadvantages useful for improvement construct as instructions;

- the next advantage is the speed in the analysis in the simulation. The advantages of this process are that after developing a model, you can run a simulated system at speeds far exceeding those achievable in the real world. With many modeling languages, you can conduct and run several experiments, which saves time.

To get results, the finished model can take from a few seconds to several hours, so this process is important for factory manufacturers to control the assembly process, for example, every morning before production starts, engineers enter the expected system input data into their model and predict how long it will take daily work. All of the above mention advantages of computer modeling have a common advantage, which is to reduce the risk, and also reduce uncertainty, therefore, increases confidence regarding the expected operation of the new system or the consequences in the existent construction.

In addition to the above advantages in computer modeling, there are general limitations as follows:

- one of the flaws is an expensive analysis method for creating a computer model, but, despite this drawback, low-cost modeling packages are available, and most of the large-scale modeling work is the main enclosure in training, software, hardware, analysis.

- the next disadvantage is laboriousness (labor intensity), which does not always give a quick answer to the questions, in most cases, data collection, model development, analysis and report generation take considerable time. Using two methods in the simulation process can be accelerated: reducing the specification (detailing, scaling) and the use of universal code libraries. Sodecline the level of

detail, you can get answers to the questions of the general concept much faster, but in the process of using this approach, care should be taken when removal key details that may affect the accuracy of the model. Creating a universal simulation or code library is used during the performance of many similar simulations, this reusable resource preclude re-invention for each simulation project, which is considered the basic idea.

- gives only approximate answers when modeling discrete events, which is based on the use of random number generators and in the process of modeling, the input has a random element, some uncertainty is also associated with the output.

- it is difficult to verify one of the limitations of computer modeling. Basically, the complexity of testing is reflected when the system does not yet exist, and it is important to know that the computer model accurately represents the system being studied. In such a case, the verification most often relies on the opinions of experts and intuition as a means of ensuring that the model works in the same way as the system, but whenever judgment and opinion are used, there is a possibility of error. It is often better to stick to a conservative point of view and make sure that the predicted performance of the system is no better than the expectations of the actual work. In addition, the human factor in a computer simulation can be very accurate for accurate capture and simulation [124].

Thus, the use of computer simulation is very important in research and development and allows to explore unforeseen physical or chemical properties of atoms and molecules.

1.8 Classification of computer simulation methods

Today wide spread approaches of computer modeling are molecular dynamics (MD) and Monte Carlo (MC), and also there are hybrid techniques that combine the features of both.

MD allows to anticipate an elasticity, plasticity or destruction, without any changes in the procedure. In addition MD has another name as atomistic modeling which allows simulate materials of nanometers size, analyze and understand the motion of each atom in the material, understand how a material exposed deformation, phase changes, also extracting information from atomistic dynamics. Sometimes MD is called the “first principles approach to understanding the behavior of atoms and determining interatomic potentials (how atoms interact) all properties of materials (infinite possibilities and problems) [125, 126].

The next most important type of computer simulation is Monte Carlo, which was named after the city. Monte-Carlo, like MD, will be used to solve some problems, unforeseen risks, in science, technology, in finance, etc. In comparison with the MD method in this method the process is modeled by generating random processes, objects, quantities, which in turn is repeated several times and on the basis of the obtained random data, the probabilistic characteristics of the process being studied or the problem being solved are calculated. During the modeling, these random objects can be “natural”, which is part of the simulation of the real system or are introduced “artificially”. Often, in many cases of simulation, random objects are

introduced “artificially”. Also, the Monte Carlo method is actually used for modeling physical processes, for solving quantitative problems of science, technology, and also in materials related science, where they are used to develop and analyze new materials and structures. In addition, the Monte Carlo method is applied to the design of virtual materials, which in turn allows you to get more data than physical experiments [127, 128].

Thus, MD and Monte-Carlo are widespread approaches of computer modeling, which in turn allows to study the properties of materials, analyze and understand the motion of each atom in the material, determine the interatomic potentials (how atoms interact), and also apply when studying random structures and graphs arising in statistical physics, probability theory.

1.9 Computer simulation of FFLGN, Ga-doped graphene

It is very well known that graphene [32] and FFLGN are considered as exceptionally promising materials which are in many applications of more interest than graphene itself [32, 46, 129].

One more interesting material – FFLGN (GO) [42-45] that is graphene, functionalized with oxygen-containing chemical groups. This material is promising as an intermediate product for producing graphene in large scales. Additionally, it can be used for producing new materials for electronics, materials science. In the last few years, there has been an increase of attention to functionalization of graphene with radiation techniques, for example, forming radiation defects and doping them by atoms of different elements [46, 129-132]. This conception represents a new way of producing graphene-based 2D nanostructures functionalized with elements like Ga, As, N, B, S. Such materials are promising for prospective applications in nanoelectronics, supersensitive sensors, electrical power sources, flexible electronic and power devices. But it is not yet well understood about stable atomic configurations of graphene, functionalized with individual atoms of different elements in which way they can be produced in graphene nanostructures and how to obtain characteristics needed. It is in some cases rather difficult problem for experimental research and proper interpretation of data. In this situation, computational simulation and study of functionalized graphene-based nanostructures become a very effective research tool for better understanding the physical and chemical properties of such materials [129, 131-134] and predicting their characteristics. In this section, we demonstrate results of computer simulations of some possible stable structures of Ga-doped graphene and few-layer graphene and first-principles study of their energetic and structural characteristics [198]. It is known that Ga in its common state is a metal with a very low melting point ($\approx 30\ ^{o}C$), but when Ga atoms are arranged separately in a two-dimensional graphene’s structure, all basic properties can change very essentially.

Further, in sections 3.1.1, 3.1.2. we present results of computer simulation and density functional theory (DFT) calculations within Dmol3 software-package [132-134] of possible stable configurations of few-layer graphene, functionalized by Ga atoms. All calculations were performed using local density approximation and very

effective method of energy optimization [131, 132], with using periodic boundary conditions, with convergence tolerance on energy 0.001 eV.

1.10 Basics of humidity and types of humidity sensitive elements

At present, the creation and application of a humidity sensor plays an important role in industrial and domestic applications for human convenience, as a result of which, depending on the operating conditions, there are different types of humidity sensitive elements based on operating principles, on a unit of measurement, and also on various types of sensitive materials.

The basic units of humidity measurement are relative humidity and absolute humidity and based on these measurement parameters, the sensors are divided into the following main types: sensors of relative humidity and absolute humidity. The unit of absolute humidity has another concept as vapor density and is determined by the ratio of the mass of water vapor in the air to the volume of air and is expressed by the following formula (4) [135, 136]:

$$AB = m_w/v \quad (4)$$

(here AB – the absolute humidity (g/m^3),m_w - a mass of water (grams),v – volume of air (m^3)).

The next unit of measurement is relative humidity, which is determined by the ratio of the moisture content of air to a saturated (maximum) humidity level. In this case, the relative humidity depends on the temperature and is therefore called relative measurement and is expressed by the following formula (5):

$$RH\% = P_V/P_S*100 \quad (5)$$

(here RH – relative humidity, P_V– the actual partial pressure of moisture that is contained in the air, P_S– the saturated pressure of humid air)

Also the most important is the determination of moisture saturation, which depends on temperature and presents the ratio of the mass of water vapor at saturation to the volume of air and is expressed by the following formula (6):

$$SH = m_{ws}/v \quad (6)$$

(here SH –moisture saturation (g/m^3), m_{ws} – the mass of water vapor at saturation (g) *и* v the volume of air (m^3)) [135].

According to the unit of measurement relative compared to absolute humidity, relative humidity is most widely used because of its simplicity and low cost.

As mentioned above, the classification of humidity sensors can be subdivided on the next basis: types of sensitive materials, principles of operation, and also the type

of conductivity into resistive, capacitive, ionic, electronic (charge carriers) and the sensitivity mechanism into electronic, proton and electrolytic.

Currently, humidity sensors according to the types of sensitive materials are classified into: ceramic, organic polymers, semiconductor, organic/inorganic (polymer/ceramics) [135, 136].

Thus, to create humidity sensors and its application in industrial and domestic applications for human convenience, the most important is the choice of a suitable sensor type and the choice of material that will affect the sensitivity, stability of the device.

1.11 Application of FFLGN membrane as a humidity sensor and comparison of its performance

This section provides an overview of the application of a humidity sensor based on graphene, graphene oxide, FFLGN membrane, and other carbon materials, in turn, these materials are durable and have high thermal conductivity, as well as excellent adsorption characteristics [137], therefore they are important practical application as a humidity sensor.

The membrane based on FFLGN, GO, compared with other carbon materials, contains functional groups such as hydroxyl, carbonyl, and carboxyl on their basal plane and this makes it hydrophilic; therefore, sensors based on such materials are moisture-sensitive [137].

Therefore, according to the above-listed properties, FFLGN is currently an important material for creating humidity sensors with high sensitivity, which is necessary for such fields of engineering and science as medicine, textile industry, agriculture, biological products, scientific and technical centers, food industry and other industries [138].

To create humidity sensors, the most important electrophysical characteristics are: faster response and short recovery time; stability of work at various levels of humidity and in aggressive environments; a wide range of moisture detection, as well as the most important are the ease of manufacture technologies, low cost, which are necessary to satisfy consumers.

To achieve the above listed characteristics over the years, much attention has been paid to the creation of various types of sensors with high sensitivity based on such materials as: metal oxide nanowires; ceramic nanomaterials; silicon; semiconductor nanoparticles, etc., but despite this the creation of sensors with the above-listed characteristics remains an unsolved task to this day [139].

In this regard, as the initial material, we choose the FFLGN membrane, which is one of the potential materials to satisfy the above characteristics, and the choice of a suitable material is considered the most important factor in creating a sensitive sensor.

Due to the physicomechanical and important electronic properties of graphene and graphene-like materials, there has been more research and many studies have been done on the creation and use it as sensors for determining various gases and humidity.

The use of graphene in sensors for the determination of various gases was first demonstrated in [140], then its related structures such as FLG, GO have become more investigated and used to create nanoscale sensors [135].

Humidity sensors using graphene structures were created for the determination of NO_2, NH_3, and CO_2 gases, which were demonstrated on the basis of the following materials and principles of operation of thermally reduced graphene; epitaxial graphene; carbon nanotubes and graphene; coarse-grained GO thin film; FLG, microscale capacitive humidity sensor based on GO film; high proton conductivity GO; capacitive humidity sensor based on the Electro-spun PVDF/Graphene Membrane [139, 141-150].

We made a comparison of the performance of humidity sensors based on FFLGN with similar types of humidity sensors [146, 150-157] according to the following characteristics: dynamics of response and recovery, humidity detection range (Table 2). According to the table 2, compared to the sensors listed below, our device [206] has an advantage in response and recovery time, which has the same time of 360 s, as well as a wide range of humidity from 5-100%, and its electrophysical characteristics presented in section 3.2.8.

Of all the sensors listed, the longest response and recovery time (1200 s) in [157], besides this, the long recovery time (2300 s) is shown in [152], and in the same work the smallest response time, which is (50 s). Compared with our sensor [206], a wide range of humidity detection (0-100%) is shown in [157] and a narrow range (20-36%) in [156], the disadvantages of these devices are long response and recovery times.

Table 2 – Characteristics of humidity sensors

№	Name of works	Sensor type	Material used	Humidity Detection Range (%)	Response time (sec)	Recovery time (sec)
1	2	3	4	5	6	7
1	A Capacitive Humidity Sensor Based on an Electrospun PVDF/Graphene [150].	capacitive	Electrospun PVDF/Graphene	50-90	1000-1400	15-230
2	Gas Sensors Based on Graphene [153]	conduct metric sensor	Scotch tape graphene	5-75	1200	1000-1200
3	Polyimide-Based Capacitive Humidity Sensor [154]	capacitive	Polyimide	5-85	400-600	400

Table continuation 2

1	2	3	4	5	6	7
4	NO_2 and humidity sensing characteristics of few-layer graphene [155]	impedance	Few-layer graphene	4-84	300	Several hours
5	Resistive graphene humidity sensors with rapid and direct electrical readout [151]	resistive	Graphene	0-25	130-150	70-100
6	Graphene-Based Humidity Sensors: The Origin of Alternating Resistance Change [156]	impedance	Graphene	20-36	480	240
7	Graphene-based CO_2 sensing and it's cross sensitivity with humidity [152]	impedance	Graphene	1-67	50	2300
8	Room-Temperature Humidity Sensing Using Graphene Oxide Thin Films [146].	impedance	GO	30-60	100	2200
9	A Capacitive humidity sensor based on ordered macroporous silicon with thin film surface coating [157]	capacitive	macroporous silicon with a Ta_2O_5 thin film coating	0-100	1200	1200
10	Humidity sensor based on FFLGN membrane [206]	impedance	FFLGN membrane	5-100	360	360

Thus, graphene and its related structures, based on the above-listed works, as well as due to physicomechanical properties, have found potential practical applications as humidity sensors and today considered as promising materials in electronics and technology, in particular, for the creation of sensitive elements. In this regard, we created a humidity sensor based on the FFLGN membrane and determined its electrophysical characteristics, which are discussed in the section 3.2.8. In comparison with similar sensors, the sensor presented by us is a potential device for a commercially available product that has such advantages as a wide range of humidity, faster response, and recovery, low cost, does not require high technology and is resistant to aggressive media [204-206].

Conclusions for section 1

There are 2 types of functionalization of graphene: chemical and non-chemical. Both categories of functionalization contribute to changes in the properties of graphene, but the most effective is a chemical modification.

FFLGN is an important precursor for the large-scale production of graphene, which is implemented using chemical or thermal reduction processes. There are 4

main methods of synthesis of FFLGN: Staudenmaier, Hofmann, Hummers, and Tour, but the most effective is the Hammers method.

It is stated that graphite and FFLGN have a layered structure, although, compared with graphite, FFLGN contains functional groups with high oxygen density, such as hydroxyl and epoxy groups on its basal plane and on its edge with less carboxyl, carbonyl, phenol, lactone and quinone which contribute expand of interplanar distance, and also makes it hydrophilic.

Changes of the combination of I_D/I_G bands of Raman spectra dependencies on the size of sp^2-hybridized zones with low and high defect density modes provides a suitable theoretical explanation for the observed behavior and allows us to estimate that the size of the graphite zones of L_a decreases to ~ 1 nm during oxidation. As well as in other studies on the sizes of the sp^2 zones in FFLGN thin films and bulk FFLGN samples obtained by the Hammers method reaches up to 2.5–6 nm.

Computational simulation becomes a very effective research tool for better understanding and study of physical and chemical properties of FFLGN to solving a difficult problem for experimental research and proper interpretation of data, also understand about stable atomic configurations of graphene, functionalized with individual atoms of different elements.

Basically, the changes of optical, electrical, mechanical, and other properties of FFLGN depend on the functionalization, that is, on the amount of oxidation, as well as on the method of synthesis, which can fundamentally change the electrical properties, also depends on the reduction process of FFLGN at different temperature.

Compared to the other similar types of sensors, our device [206] has an advantage in response and recovery time, which has the same time of 360 s, as well as a wide range of measurable humidity from 5-100%, and its electrophysical characteristics presented in section 3.2.8.

2 RESEARCH METHODS

In this chapter the main research methods of FFLGN study are demonstrated. The main characteristics of the used research instruments are considered. During research the following methods were used: SEM and EDS; Raman spectroscopy; AFM; TGA; XRD; Optical microscope; Spectrophotometer Lambda 35.

2.1 SEM and EDS

To date, SEM in combination with EDS has found its wide application for analyzing and studying all types of solid samples in various fields of science and production. The main purpose of these methods is to determine the morphological features and to obtain an image of the surface of an object with a high spatial resolution of up to 0,4 nm, also to obtain an analysis of the chemical composition of the substrate. The SEM method is used in traditional studies of various types of samples such as metals, ceramics, polymers, as well as materials of the electronic and semiconductor industry, biological tissues, and chemistry. The principle of SEM is based on the interaction of the electron beam with the atoms of an object [158].

As a result of the interactions of electrons with atoms of the sample, one can obtain information on the morphology of the surface, on the composition, on the composition of the structure and other properties of the surface layers [159].

In the process of studying the sample surface, a finely focused electron beam scans the areas of analysis, and due to electron-matter interactions, signals appear on the sample surface that includes secondary and backscattered electrons to form an image and characteristic X-rays from elements present in the sample for composite studies [160].

Compared with traditional light microscopy and other analytical methods, modern SEM has the following advantages: improved resolution capabilities, high depth of focus, effect of three-dimensional perception, which contributes to a simple image interpretation, takes little time for preparation sample [161].

SEM consists of the following main components: electron source (“Pistol”); electronic lenses; sample sampling stage, detectors for all signals, data display/output devices [162].

To produce SEM images, secondary electrons from a sample that have low energy of less than 50 eV, which are produced by the primary electron beam and high energy back of the scattered electrons, contribute to the emission. The depth of penetration of the primary electron beam into the sample is several microns, and the yield of secondary electrons is tens or hundreds of angstroms [163]. The generation of secondary electrons near the surface of the primary beam and back-scattered electrons is shown in Fig. 7.

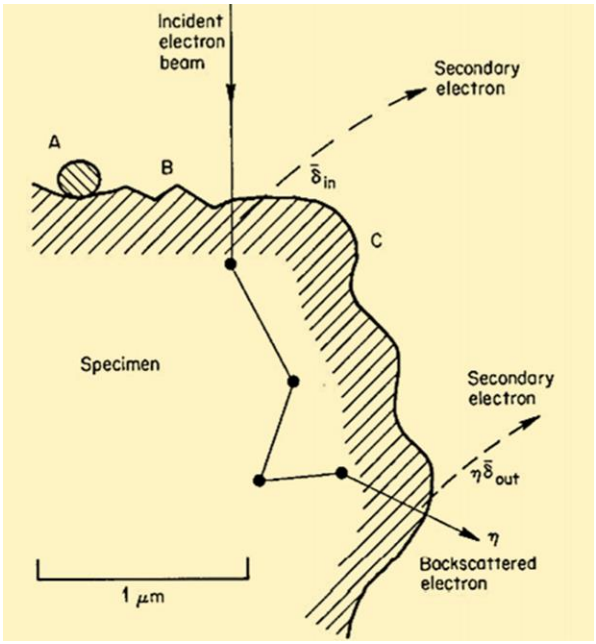

Figure 7 – Generation of secondary electrons [163, p. 43].

In the process of irradiating a sample, a beam of electrons, the so-called primary electrons, focus and transfer energy to the point volume of the sample in which the bombardment takes place, i.e., the electrons are expelled from the sample itself, which is called the secondary electrons, then these electrons are attracted and collected by the detector are then transferred to image display (Figure 8). Depending on the energy of the primary electron beam, the emission of secondary electrons from the sample increases to a certain limit, and the energy of the primary electrons is determined by the number of secondary electrons. In addition to increasing the emission of secondary electrons to a certain limit, the collected secondary electrons are reduced due to the deep penetration of the primary electrons into the sample.

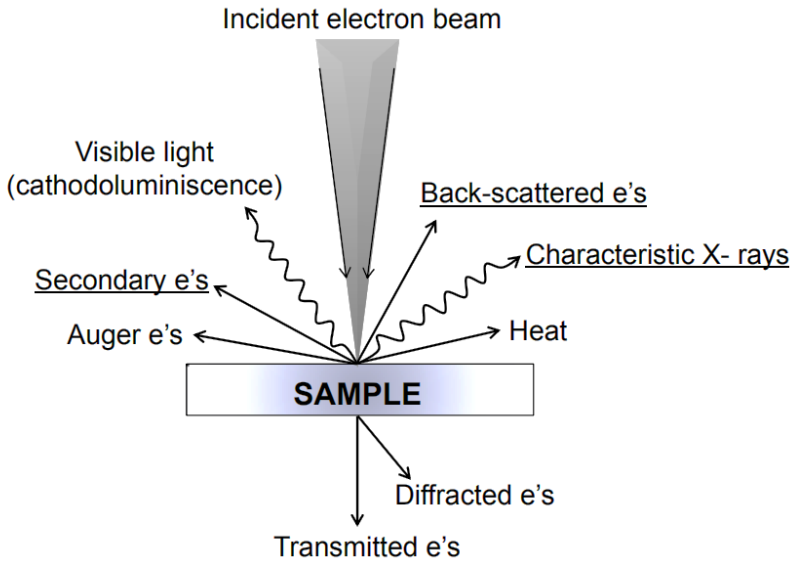

Figure 8 – Sample irradiation process [159, p. 7]

One of the main processes is obtaining an elemental analysis of a sample in which the SEM is equipped with an EDX analysis system and studies the interaction between the X-ray excitation source and a sample [159].

The main principle of operation for the spectroscopic EDS method is the determination of the presence of elements on the sample surface. During the process of affecting to sample with a focused electron beam, X-ray spectra are emitted from it, which contribute to the chemical analysis [158].

X-rays come from the atoms of the sample and are detected using EDS with atomic numbers from 4 (Be) to 92 (U), except for H, He, and Ba [172].

The interaction between the X-ray excitation source and the sample is based on the fundamental principle that each element has a unique atomic structure that allows X-rays to characterize elements of atomic structure that is uniquely identified from each other [159].

EDS consists of a qualitative analysis representing the identification of a line in the spectrum, as well as a quantitative analysis determining the concentration of elements present, which entails an intensity measurement line for each element in the sample and for the same elements in the calibration [164].

Sample preparation for the microscope and analysis include the following processes: 1. It is necessary to remove all water, solvents, or other materials that may evaporate during a vacuum; 2. Firmly install the samples; 3. The samples must be electrically conductive and non-metallic samples, such as plants, nails and ceramics must be coated so that they are electrically conductive [165]. Gold, gold/palladium, platinum, osmium, iridium, tungsten, chromium, and graphite are used to coat the samples; 4. It must be an electrical grounding to prevent the accumulation of electric charge on the surface [159].

At the electron beam source, the accelerating voltage (AV) is an important parameter for SEM and EDS, and if AV is applied, 10 kV electrons reaching the surface will have 10 keV, 20 kV will generate electrons with an energy of 20 keV, etc. In this process, the use of high electron energy contributes to the penetration deeper into the sample by several micrometers depending on the elements present, also at higher energy, the number of X-rays that are generated per electron inside the sample will be higher and this may damage the sample. In addition, depending on the application of high or low accelerating voltage will affect the resolution, that is, if high AV then the resolution is better and it is necessary to take into account the selection of the optimal AV for each sample and analysis [158].

Thus, an SEM and EDS is necessary equipment for determining morphological features and obtaining an image of the surface of an object with a high spatial resolution of up to 0,4 nanometer, also for analyzing the chemical composition of a substance.

2.2 Raman spectroscopy

By using Raman spectroscopy it is possible to study the physical state of solids, liquids, determine the chemical structures and physical forms of substances, and this

spectroscopy is based on infrared absorption and Raman scattering to detect vibrations in the molecules of a sample under study [166].

The history of the discovery of Raman spectroscopy began in 1923, by Smekal caused inelastic light scattering, and experimental work was done in 1928 by Raman and Krishnan, in which a telescope was used to focus sunlight on a sample, and another lens was placed above the sample in order to collect scattered radiation. In this process, the main characteristic of Raman spectroscopy is the change in the frequency of the scattered radiation as compared to the incident light on the sample using optical filters [166, 167].

To date, for obtaining high intensity and focusing light on a small spot in a sample in a modern Raman spectrometer, the following types of laser are used as the light source: gas lasers in particular (Ar + Ion: 488.0 and 514.5 nm; Kr + Ion: 530.9 and 647.1 nm; He, Ne: 632.8 nm); diode lasers with radiation wavelengths (785, 830, 976 nm) with a radiation power of several hundred mill watts. In addition to these types of lasers, FT-Raman spectrometers use YAG lasers with an emission wavelength of 1064 nm [167, 168].

The principle of operation of Raman spectroscopy consists of the following main components: 1) an excitation source (laser); 2) a sample lighting system and a photosensitive optical system (optical system for collecting light); 3) Wavelength selector (filter or spectrophotometer); 4) Detector (photodiode array, CCD or PMT) [169].

During spectrometer operation, a sample is illuminated with a laser beam in UV, Visor NIR range, then the sample is being excited, then the beam is scattered in all directions. Then the scattered light is collected with a lens and direct through an interference filter or spectrophotometer to obtain the Raman spectrum of the sample [169]. Figure 9 shows the illumination of the sample during the operation of the spectrometer.

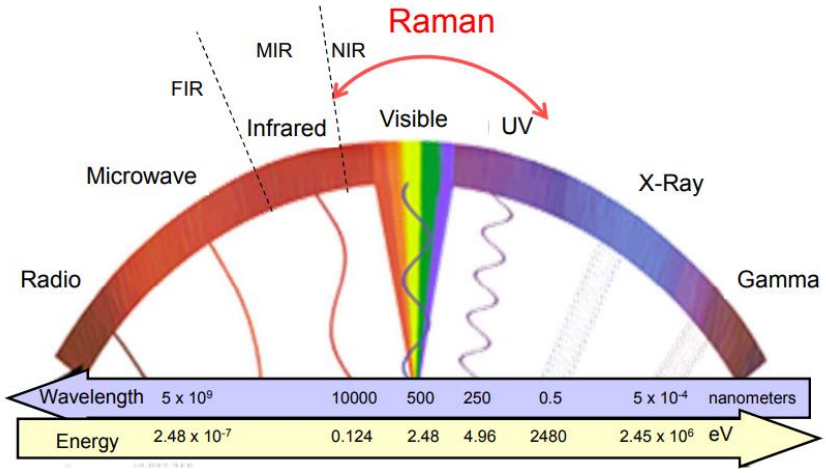

Figure 9 – Illumination of the sample with a laser beam [170, p. 3].

The operating procedure of Raman spectroscopy has the following process: 1) the laser beam excites the sample, then (2) the beam is scattered in all directions, (3)

after which the photons partially fall into the detector, which records the Raman spectrum (4) this spectrum presents Rayleigh scattering, corresponding to elastic scattering, Stokes and anti-Stokes Raman scattering, and spectral features that are characteristic of each sample [171].

When light is scattered from a molecule or a crystal, non-elastic photons appear and in this process, the scattered photons have the same energy frequencies and wavelengths, but these non-elastic photons have lower frequencies than the incident photons and this phenomenon is called the Raman effect [172].

The process of light scattering is weak, only about 106–108 photons are scattered [166]. Also in connection with the process of changing the vibrational, rotational, and electron energy of a molecule in Raman spectroscopy, there are such concepts as Rayleigh scattering, corresponding to elastic scattering and Raman scattering, which is not elastic [171, 172].

In Raman spectroscopy, shifts to lower and higher frequencies are known as Stokes and anti-Stokes Raman scattering, respectively [173]. Figure 10 shows the main processes for a single Rayleigh and Raman scattering vibration, in which there are virtual and vibrational zones, as well as Stokes and Anti-Stokes energy vibration levels. Many molecules, due to exposure to room temperature, are in a low vibrational energy level. In the process of laser interaction with electrons, polarization occurs and, as a result, a virtual zone is created, and the energy of this zone is determined by the frequency of the light source used.

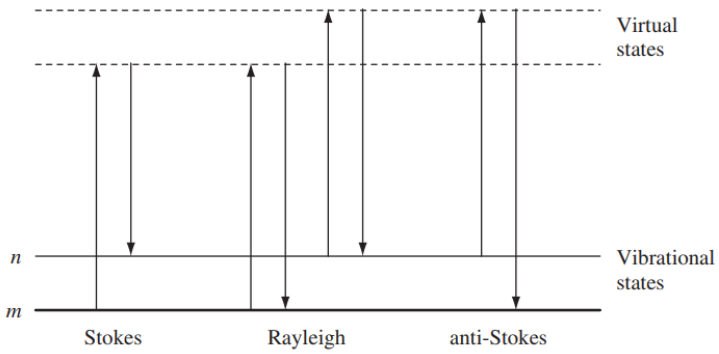

Figure 10 – Stokes Raman scattering of Raman spectroscopy [166, p. 4]

Stokes Raman scattering arises from a transition that begins with the main vibrational energy level and ends at a higher vibrational energy, as shown in Figure 10, the vibrational zone m, which contributes to the absorption of energy from a light source by the molecule, shifts to a higher vibrational energy areas (n) [166, 173]. The difference Stokes Raman scattering and from laser radiation is that it has lower energy and a higher wavelength [171].

Anti-Stokes Raman scattering compared with Stokes according to Figure 10 (a, b) due to the influence of thermal energy, some of the units of molecules are in an excited vibrational state in the vibrational zone n and such molecules are transferred from a higher vibrational level n to a lower vibrational level energy m, as a result,

appears radiation of a higher energy and a shorter wavelength than laser radiation [171, 173].

Thus, as mentioned above, Raman spectroscopy is the most important in studies of materials and new technology. Using this instrument allows to investigate the physical state of solids, liquids, determine chemical structures and physical forms of substances, also to detect vibrations in the molecules of the sample.

2.3 AFM

One of the most important tools in research in materials science is the use of integration of scanning probe microscopy and AFM, which allows simultaneously with optical observation to investigate an object using the combination of scanning probe microscopy methods such as AFM [175].

The principle of scanning probe microscopy is to scan the surface of a sample with an ultrathin probe with a tip thickness of the order of several nanometers, which is positioned above the sample and then supplied to the surface until the tip of probe interacts with the sample. The working part of the probe (tip) has dimensions of the order of ten nanometers. The characteristic distance between the probe and the surface of the samples in probe microscopes is 0.1 - 10 nm in order of magnitude [175]. The probe is placed in a certain area at the focus of the light laser beam, when the illuminated tip of the probe approaches the sample surface, the effect of a significant enhancement of Raman scattering from objects localized in the probe – the surface system appears. Then, during the scanning process, the interaction value is kept constant by changing the distance between the sample and the probe [176].

Moving the probe above the surface to the nearest thousandths of a nanometer is provided by a mechanical precision manipulator, which is made of piezo ceramic material. Figure 11 is shown the AFM.

a) AFM b) System device

Figure 11 – AFM [176]

According to Figure 12 (b), the Integration of scanning probe microscopy and AFM device consists of the following main parts:1) Confocal module including scanning mirror; 2) Direct microscope Mitutoyo; 3) 4-position lens turret; 4) AFM module with heads for various types of probes (cantilever, quartz resonator, STM needle); head for working in liquid; optical system registration of cantilever bends; 5) Measuring table, including: sample piezo scanner (100×100×10 μm); motorized sample positioner (35×35 mm); manual positioner AFM module (3×3 mm); motorized and piezo drives for focusing lens (optional); heating table (optional) [100].

Thus, when scanning by registering a Raman scattering signal from objects at each point on the surface, a map of the distribution of spectral properties in the sample is formed, this reflects the properties and topology of the surface.

2.4 TGA

The method of TGA is intended to obtain data on the heat resistance and composition of liquid, solid substances, various materials, including structural, polymers, composites, food, organic materials, biological samples, etc.

The TGA measures the mass of a sample depending on such functions as temperature, time in a certain controlled atmosphere. This method registers the mass of a substance when heating and cooling, respectively, the weight of the sample decreases or increases [177, 178].

Using thermal analysis, one can study the heat capacity, the change in mass, the coefficient of thermal expansion, the reaction in the solid state, phase transitions, also the measured mass loss curve gives data on heat resistance and changes in the composition of the substance.TGA for studying the change in the mass of a substance is divided into physical and chemical processes. Physical processes include gas adsorption and desorption; phase transitions (evaporation, sublimation), and chemical: decomposition; destruction reactions; gas reactions; chemical sorption (adsorption using chemical instead of physical forces) [179].

For the TGA process, one of the main devices is a computer that monitors and performs the following functions: provides an interface between you and the analysis tool; allows to customize experiments and enter constants; store experimental data; starts up data analysis programs [180].

TGA has following six main components (Figure 12): balance, which provides an accurate measurement of the mass of the sample and is the key to the TGA system; the sample platform, which loads and unloads the sample on the balance and back; a furnace controls atmosphere and temperature of the sample; cupboard intended for the electronics and mechanics of the system; heat exchanger designed to dissipate heat from the furnace; mass flow controllers intended for control the purge gas on the balance and in the furnace.

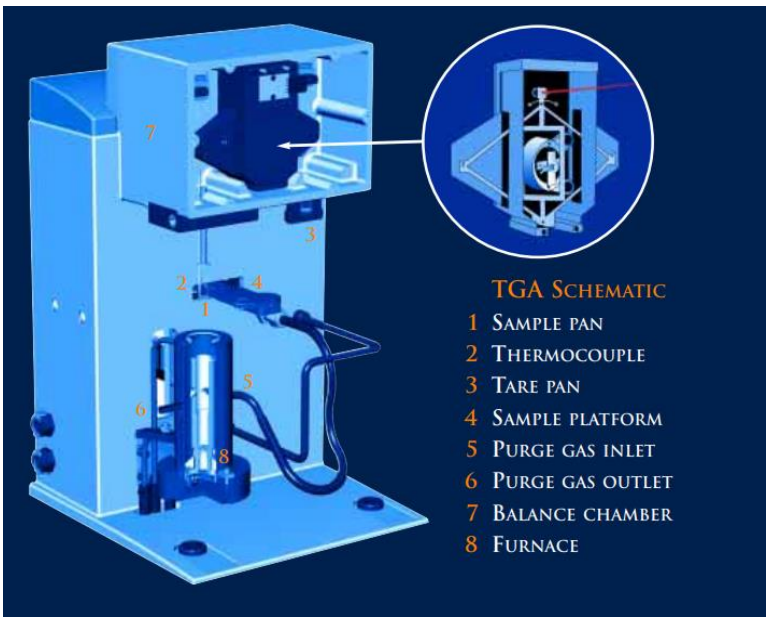

Figure 12 – The main components of TGA [181, p. 4]

In the process of TGA, depending on the capabilities of the device, the temperature can reach 1500 ° C or more, and the temperature rises at a constant rate and the change in mass are recorded depending on the temperature.

High-precision crucible scales made of platinum or ceramics are located in the electric furnace chamber, which is part of the thermal analyzer design, and the control thermocouple is under the crucible bottom [182].

The sample is inserted on the crucible hanging from a small hook, which is connected to the balance. The weight of the sample is recorded using a photodiode balance, which operates on the principle of zero balance. When the weight of the sample stays at zero position, an equal amount of light shines on 2 photodiodes, and if the balance moves from the zero position, an unequal amount of light shines on the two photodiodes and at that moment the current is applied to the counter to return the weight to the zero position. In this process, the amount of current applied is proportional to weight loss or gain. In order to apply heat to the sample, the furnace rises around the crucible and the speed and cycle of this process are controlled by the computer software.

During the furnace process, the sample is purged with nitrogen, air, or other gases, depending on the type of decomposition and the desired information. In order to protect the instrument coating from oxidative destruction or other undesirable reactions, the balance is always stored in nitrogen gas with a certain flow rate of purge gases. The recommended flow rate of purge gas for a balance of 40 ml/min, and for the sample 60 ml/min. Figure 13 shows a diagram representing the flow of purge gases [183].

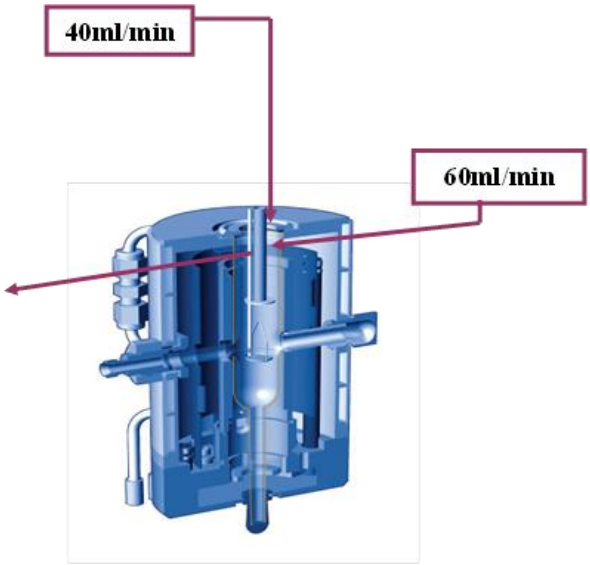

Figure 13 – TGA purge gas flow [183, p. 4]

In the purge system, gas enters the furnace through a side lever and flows directly through a sample situated in an open crucible to a vertical balance. A low volume of purge gas is directed through the balance of the chamber to prevent reverse diffusion of the primary purge of gas (if different) or decomposition products in the balance chamber.

The experimental procedure of TGA consists of the following steps:

1. Open the nitrogen gas valve and the TGA exhaust valve. It is not recommended to adjust the regulator valve;

2. Ensure that the sample crucible is clean and carefully use tweezers to place an empty crucible on the sample platform, ensuring that the crucible is correctly oriented on the platform;

3. Press the TARE button located on the console at the bottom of the tool. The tool will auto tare, which should take a couple of minutes;

4. Take a small piece of the sample and measure/record its mass using a scale.

5. After the sample has been prepared, depending on the structure and shape of the sample, the external residue (for example, oils from the fingers) is carefully removed by wiping the entire surface of the sample with Kimwipe.

6. After the instrument has completed its automatic tare sequence, place the sample in the center of the crucible. This should preferably be done without removing the sample crucible from the sample platform.

7. Enter the appropriate inputs into the Q50 TGA program:

8. Click “Apply” to save the changes.

9. Click the green button in the upper left corner of the software to start the run. TGA device will automatically perform the experiment. As the experiment ends, the instrument will automatically unload the sample onto the sample platform and begin a sequence of air cooling.

10. If there is still residue on the sample crucible, gently hold the crucible with long tweezers and clean the crucible using a propane torch flame for 2–3 seconds

(until the residue disappears). Make sure it is done in a fume hood and try to keep your hand away from the flame.

11. Raise the oven to check the internal temperature in the oven (Control - Furnace - Up). After the oven is completely sealed, check the temperature readings on the software. If the temperature returns to room temperature, proceed to the next step. If not, repeat the air cooling sequence.

12. Before leaving the lab, shut off the nitrogen gas valve and the TGA exhaust valve [99].

Thus, the method of TGA is designed to obtain data on the heat resistance and composition of liquid, solid substances, various materials, in particular, is an important method for the study of FFLGN, which is presented in section 4.7.

2.5 X-ray diffraction

XRD is one of the earliest non-destructive methods intended for research from liquids to powders and crystals, solids [184].

X-rays were discovered in 1895 by the German physicist X-rays, and the name was called because at that time their nature was not known. After that, in 1912, von Laue discovered the diffraction method, showing the structure of a crystal, where crystals diffract x-rays, also proved the wave nature of x-rays and provided a new method for studying the fine structure of substance [185].

In 1914, the first diffraction pattern of crystal was made by Knipping and von Laue, and in 1915 the theory of the crystal structure from the diffraction pattern was determined by the father and son of Bragg [186].

The interplanar spacing of FFLGN samples was calculated using the Bragg law, which is presented below:

$$n\lambda = 2d\sin\Theta \quad (7)$$

where, n– an integer, λ – x-ray wavelength (0.01-10 nm), d – interplanar grating distance generating diffraction, and θ – diffraction angle [187, 188].

Initially, XRD was used only to determine the crystal structure of substances, and today, covering a wide range of research in science and industry can provide information on crystal orientation structures, phases, deformation, crystal defects, average grain size, atomic interval [189].

Depending on the XRD object under study, there are types of diffraction experiments, such as X-ray (structural information about compounds and identification of samples; investigation of powder and monocrystal samples; obtaining X-rays using synchrotrons; using liquids and glasses for testing); The next type is electron diffraction (identification of the phase and determination of cells in small crystallites using an electron microscope, checking samples of gas phases).In addition to these types of diffraction experiments, neutrons are also used to present structural information about crystalline materials, liquids, and glasses, and is useful for spectroscopy [189]. In addition to these types of diffraction experiments, neutrons

are also used to present structural information about crystalline materials, liquids, and glasses [189].

To heat the cathode filaments, which are connected to two electrodes, they are supplied with a high voltage with several tens of kV [190].

High-speed electrons with kinetic energy elongated from the cathode filament are accelerated to the anode plate (metal target). This metal target is usually made from high-purity metals such as copper, chromium, molybdenum, or other metals (Table 3) [190]. The x-ray wavelength depends on the element from which the target is made.

Table 3 – Types of the target by the wavelength of X-rays [189].

Target	kα1	kα	kα	Filter
Cr	2.2896	2.2935	2.2909	V
Fe	1.936	1.9399	1.9373	Mn
Cu	1.5405	1.5443	1.5418	Ni
Mo	0.7093	0.7135	0.7107	Nb
Ag	0.5594	0.5638	0.5608	Pd

The electronic current between the filament and the anode is regulated by adjusting the filament current in the range of about 10 mA [191].

X-rays are produced when high-speed electrons collide with the anode plate; in this process, these electrons slow down rapidly and lose their kinetic energy, and as a result, continuous x-rays are emitted with different wavelengths [192, 190].

X-ray spectra consisting of such common components K_{α} and K_{β} are created by displacing the inner electron shells of the material of the anode plate. In turn, Kα consists, in part, of $K_{\alpha1}$ and $K_{\alpha2}$. $K_{\alpha1}$ compared to $K_{\alpha2}$ has a slightly shorter wavelength and twice the intensity [193].

Crystalline solids consist of regular arrays of atoms, ions, and molecules with an interatomic distance from 100 μm to 1 Å and therefore, in the process of XRD, the wavelength of the incident beam must be in the same order as the distance between atoms.

In diffraction, one of the important processes is the interaction of x-rays with electrons in a crystal; if the number of electrons in a crystal is larger, then the scattering of x-rays will be stronger. In addition, there is the concept of x-ray scattering efficiency, which is called the scattering coefficient denoted by the symbol f_0 and depends on the following factors: the number of electrons around an atom, the Bragg angle θ, the wavelength (λ) of x-rays [187, 194].

2.6 Optical microscope

Currently, the use of optical microscopy is relevant for micron and submicron levels of research in science and technology [195].

Optical microscopy is designed to enlarge the image of objects of small size invisible to the naked eye [196].

In our research, we used an optical microscope Leica DM 6000 M, which allows us to investigate solid and liquid; transparent, translucent and opaque objects with a resolution of up to 200 nm (x / y).

The Leica digital optical microscope has high-resolution digital cameras and software for image analysis and storage. The microscope we use has an automated incident light mode (reflection) for the light and dark field methods and an automated transmitted light mode (through the light).

In addition, the system of this microscope has automated regulators, changes in the aperture and diaphragm of the illuminator, also a motorized drive z of the focus and a motorized stagethat is responsible for x, y,and z movement.

Another important elements of this microscope is this motorized, coded turret with 6 lenses, which has the following magnifications: in 5x, 10x, 20x, 50x, 100x, 150x times. Also, the microscope has a unique memory function for simultaneous switching of the lens and contrast method, which allows detecting small or thin elements of the sample by contrast [176].

2.7 Spectrophotometer Lambda 35

We used Lambda 35 absorption spectroscopy to obtain the absorption (transmission) spectra of FFLGN films before and after thermal reduction. With this equipment it is possible to carry out various analytical work related to the study of optical spectra in the ultraviolet and visible regions, also to measure the concentration of various organic and inorganic substances in a wide variety of samples, aqueous solutions, foods, soils, etc. [197].

The basic principle of the spectrophotometer is to measure the ratio of two light fluxes that pass through the comparison channel and the sample channel in the cuvette compartment, and the optical system is based on a monochromator with a holographic concave diffraction grating. The spectral width of the slit can vary 0.5 nm, 1 nm, 2 nm, 4 nm. An optical spectrophotometer is designed for the UV-visible-near IR region of the spectrum (190-1100 nm) and allows accurate measurements of the absorption and transmission spectra [176].

The spectrophotometer device includes photodiode detectors, which serve as photodetectors and are installed in each channel, as well as this spectrophotometer has additional accessories such as cuvettes of various lengths and different sizes, thermostatically controlled multi-cuff holders, holders of solid samples, integrating sphere, optical fiber system for study samples at a distance, flow injection system. To control the measurement process, use special software that allows you to perform the following processes: configure the device, optimize their parameters, manage their work, process the output information, etc. [176, 197].

Thus, having the above characteristics, this device has found wide application in optical research, measurement of parameters of optical materials, reflective and anti-reflective coatings, band-pass filters in the UV, visible and near IR spectral regions, and in our case it is used to study FFLGN films, the results of which are presented in subsection 3.2.2.

Conclusions for section 2

SEM and EDS methods are determine the morphological features and obtain an image of the surface of an object with a high spatial resolution of up to 0,4 nm, also to obtain an analysis of the chemical composition of the substrate. The depth of penetration of the primary electron beam into the sample is several microns, and the yield of secondary electrons is 10 or 100 of angstroms. X-rays come from the atoms of the sample and are detected using EDS with atomic numbers from 4 (Be) to 92 (U), except for H, He, and Ba.

The principle of scanning probe microscopy is to scan the surface of a sample with an ultrathin probe with a tip thickness of the order of several nanometers, which is positioned above the sample and then supplied to the surface until the tip of probe interacts with the sample. The working part of the probe (tip) has dimensions of the order of ten nanometers. The characteristic distance between the probe and the surface of the samples in probe microscopes is 0.1 -10 nm in order of magnitude.

In TGA during the furnace process, the temperature can reach 1500 ° C, the sample is purged with nitrogen, air, or other gases, depending on the type of decomposition and the desired information. In order to protect the instrument coating from oxidative destruction or other undesirable reactions, the balance is always stored in nitrogen gas, which recommended a flow rate of purge gas for a balance of 40 ml/min, and for the sample 60 ml/min.

3 INVESTIGATION OF THE PROPERTIES OF FFLGN

In this chapter, we present the results of computer simulation of some possible stable structures of graphene and few-layer graphene, Ga doped graphene, FFLGN, reduced FFLGN; synthesis of FFLGN, preparation of FFLGN films and FFLGN membranes, thermal reduction of FFLGN films and membranes at various temperatures and investigation of their optical, electrical properties, creation of a humidity sensor based on FFLGN membrane. The most detailed results are presented on the influence of temperature on the composition and structure of the FFLGN membrane, as well as the changes in the thickness of the FFLGN films and membranes, also changes in the interplanar distance and intensities and the ratio of the Raman spectroscopy bands of the membrane after thermal reduction. In addition, the electro-physical characteristics of the humidity sensor based on the FFLGN membrane and performance comparison with other similar sensors are presented.

3.1 COMPUTER SIMULATION

3.1.1 Computer simulation of possible stable structures of graphene and few-layer graphene functionalized Ga

Computer modeling of molecular dynamics (MD) has become a very useful technique for studying many types of properties of layered nanomaterials, such as graphene, GO, few-layer graphene nanostructures, FFLGN, which have wide interest in various fields of science and technology, such as military technology, biotechnology, nanoscience, biomedicine, etc. In addition, research of its physical, chemical and electronic properties has paid considerable attention from researchers.

We present results of computer simulation and density functional theory (DFT) calculations of possible stable configurations of few-layer graphene, functionalized by Ga atoms [198]. As mentioned in the section 1.9 all calculations were performed by using local density approximation and very effective method of energy optimization, with periodic boundary conditions and, convergence tolerance on energy 0.001 eV.

Figure 14 presents possible adsorption sites for Ga atoms with high symmetry: namely: A, H, and B respectively. H site of adsorption (over the center of the hexagon) has the largest adsorption energy, therefore, it is the favored site for Ga atom adsorption.

Figure 15 shows a possible stable atomic complex of Ga- vacancy which was formed after using the procedure of energy optimization. In such a case, the Ga atom takes place outside the graphene sheet with forming a 3D complex defect.

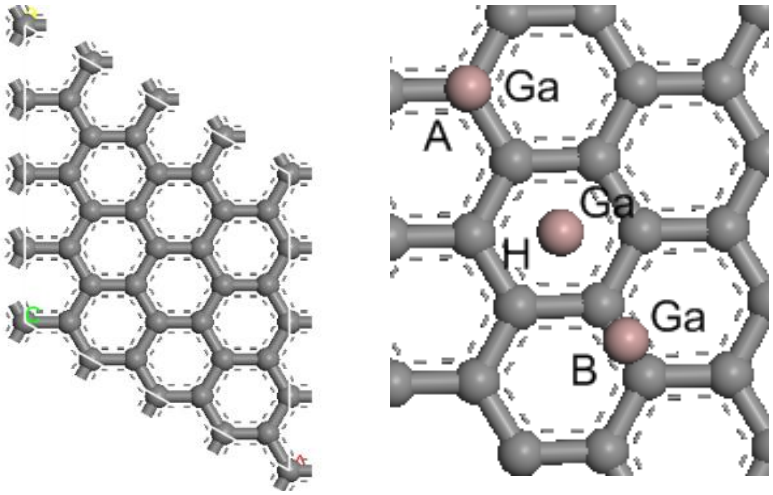

a) b)

Figure 14 – a) The unit cell for the graphene sheet within periodic boundary conditions calculations adopted a 4x4 structure; b) Some of calculated adsorption sites on graphene surface with a high symmetry: A) over the C atom; H) over the center of a hexagon; B) over the center of the C-C-bond. In all positions binding energy of Ga rather low: H – 0.73 eV, A – 0.57 eV, B – 0.40 eV. The distance between the Ga atom and graphene plane is 0.22 nm.

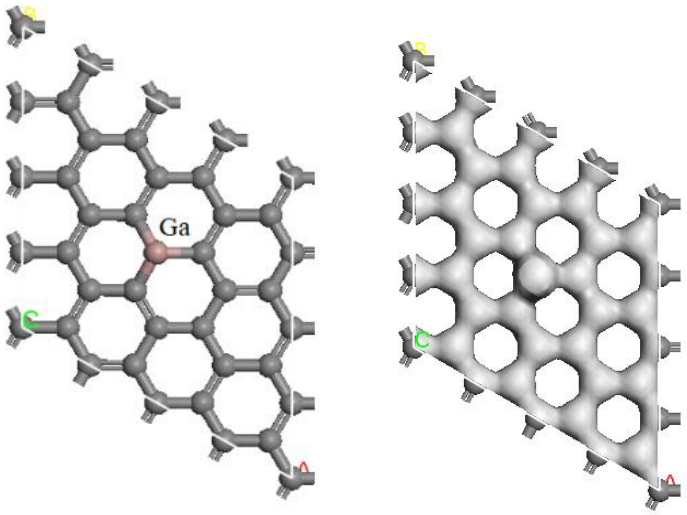

a) b)

Figure 15 – Computer models of atomic configurations Ga- graphene. a) an atomic configuration of Ga-atom bonded with a vacancy. The binding energy of Ga atom = 1.92 eV, the distance of Ga atom from graphene sheet equals 1.53 Å; b) The map of electron charge distribution for density 200 el /nm^3. In this case, gallium shows valence equal to three

Figure 16 illustrates a stable complex atomic configuration with the binding energy of Ga 1.71 eV and the distance from the graphene plane equals 0.8 Å. In this defect configuration, Ga demonstrate two-valence state.

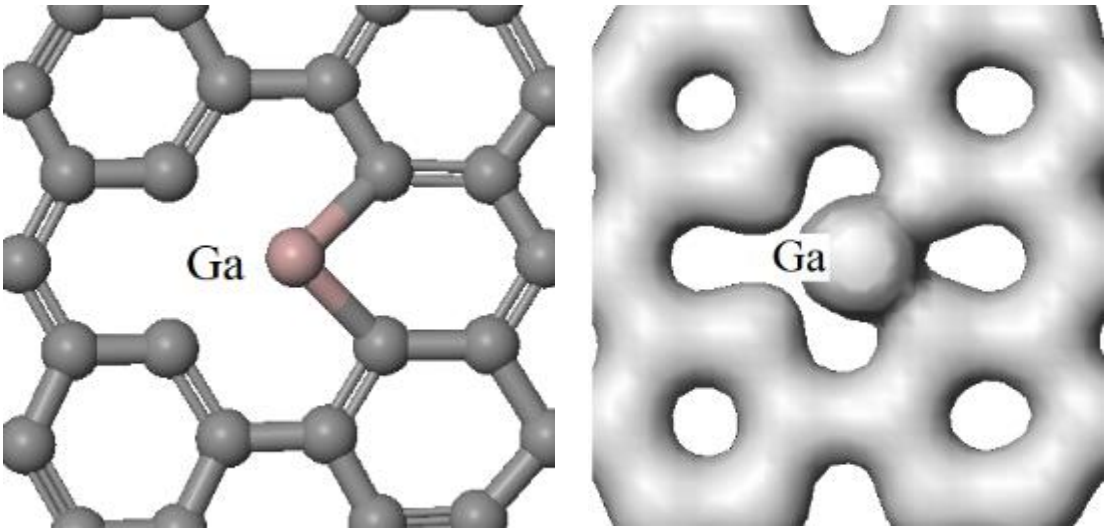

a) b)

Figure 16 – A possible structure of Ga-atom - vacancy: a) atomic configuration; b) a map of the distribution of the electron charge for density 410 el / nm^3.

Complex defect configuration – a bridge-like defect [121, 123, 124] based on a gallium atom is shown in figure 17.

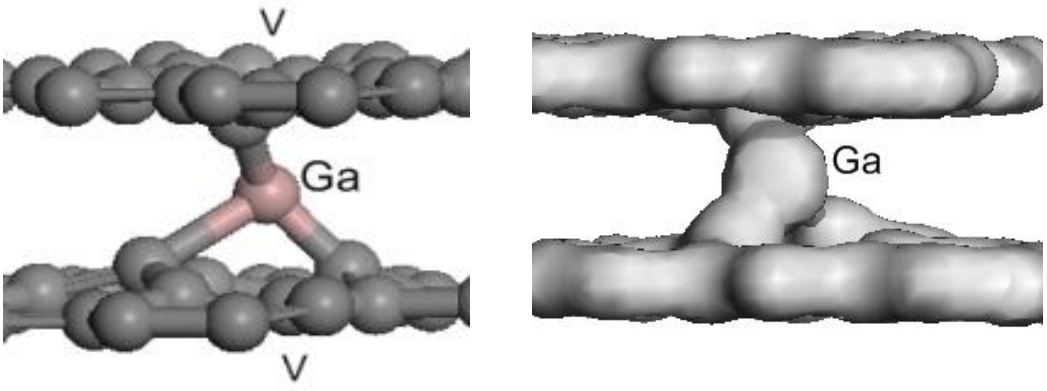

a) b)

Figure 17 – A bridge-like defect, based on Ga-atom, which connects two graphene sheets by fast covalent bond (E_{bind}= 3.28 eV): a) atomic structure of the complex defect based on a Ga- atom captured between two vacancies V in the graphene sheets; b) The map of the electron charge distribution for density 900 el/nm^3. This configuration shows three valence state of Ga.

Results of simulation and calculations have shown that the stability of Ga-graphene composition is much higher when the Ga atom is linked with a structural defect. It should be noted, that maps of the electron charge distribution (figures 15-17) show, that the electron transfer between Ga and C, in general, is in a good agreement with well-known electronegativity data for carbon and gallium (by Pauling Scale).

In this way, computer simulations and DFT calculations of structural and energetic characteristics of some possible stable configurations of Ga-graphene nanostructures were performed. Similar atomic structures in graphene and few-layer graphene can be experimentally produced by low-energy irradiation with Ga^+ ions in the SEM devices. Results of the work can be useful for production close to 2D-Ga-graphene nanostructures, for applications in nanoelectronic devices as well as for storing Ga in graphene nanostructures in atomic form.

In addition, one of the most important processes of FFLGN study is the functionalization of graphene with strong acids, as a result of which graphene becomes functionalized with hydroxyl and epoxy groups on their main plane and at the edges of the carbonyl and carboxyl groups [199-202], which was discussed in the section 1.4, and the FFLGN computer simulation and quantum-mechanical calculations will be presented in detail in the next section 3.1.2.

3.1.2 Computer Simulation of FSLGN

In this section, we have created a computer simulation of FSLGN using the molecular dynamics method by the Chem Office Materials Studio software tools. FSLGN has significant relevance in various areas because of its unique structural and dynamic properties, which can be used to investigate unforeseen physical or chemical properties of atoms and molecules (GO molecules have many crystalline properties, for example, swelling (edema) due to strong oxidation) in periodic boundary conditions. In the process of performing computer simulation of complex polyatomic systems, calculations were performed using the density functional theory and molecular dynamics methods, as well as energy optimization procedures were used to obtain the most correct complete nanostructures. Many calculations on the characteristics of nanostructures were performed using one of the reliable functionals in the DMol3 computational environment. During the calculation, the accuracy of the energy characteristics of nanostructures was up to 0.02 eV [129-134, 198].

Fragments of the computer model are shown in Fig. 18, which demonstrate FSLGN configurations with different atomic positions created by using density functional theory (DFT). According to the image, after oxidation reactions, one can see single and double configurations on the surface and edge configuration (Figure 18, a).

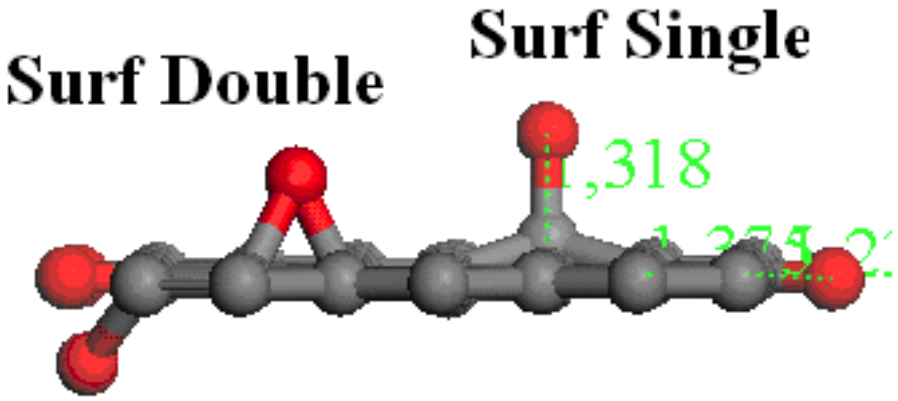

a)

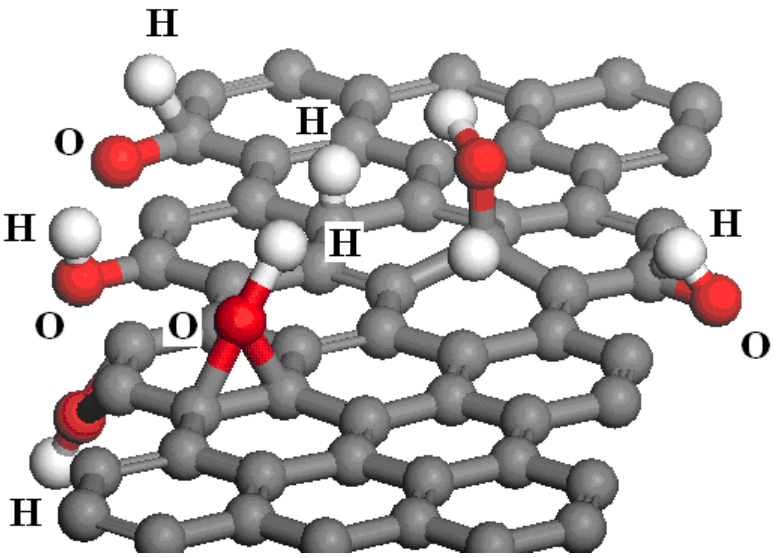

b)

a) side view after oxidation reactions; b) graphene + O-H groups after the combined action of oxidation

Figure 18– Fragments of computer models of FSLGN

Figure 18 (b) shows the behavior of the FSLGN system after additional exposure to hydrogen, which reflects possible stable configurations of graphene compositions with hydrogen and oxygen. According to the figure, it can be observed that the vacancy serves as a higher concentration of hydrogen atoms, as a result of which configurations of the O–H radical type appear, and these radicals can be desorbed from the surface of functionalized graphene.

To calculate the change in electronic properties under conditions of an increase in the level of oxidation, we created computer models of functionalized graphene, which are shown in Figure 19 (a, b, c).

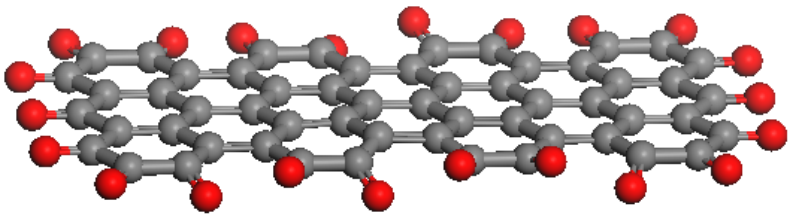

a) H-L = 0.2
graphene -O bond length = 1.2 A
Possible configurations with O

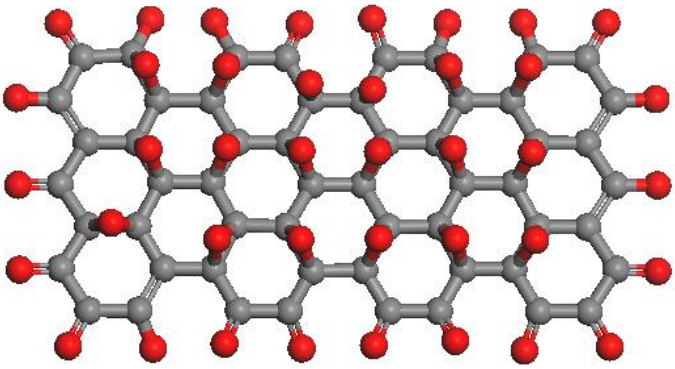

b) 0.6 eV, O/C = 40/ 56

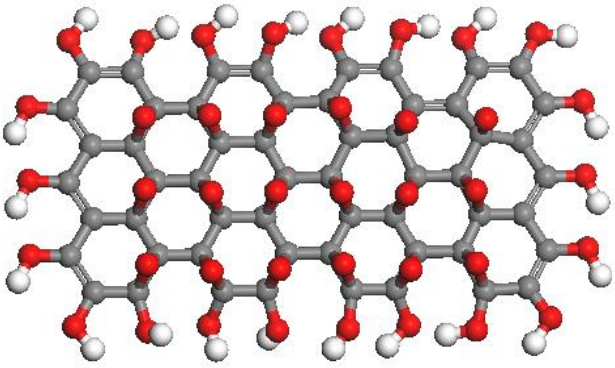

c) H-L =0.6 eV

Figure 19 – FSLGN computer model for calculating the change in electronic properties under conditions of increasing HOMO - LUMO oxidation level

Figure 20 shows possible computer models of FSLGN. According to Figure 25, one can see configurations of the OH-H radical type, which cover the ends, as well as possible configurations of 2-sided oxygen H – L = 0.8 eV

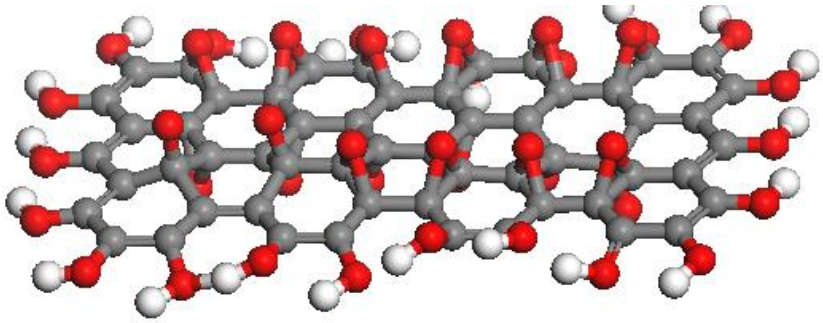

Figure 20 – 2-sided oxygen H-L = 0.8 eV, the ends are covered with O-H radicals

Figure 21 (a, b) shows computer models of possible stable configurations of the bond atom C – atom O, O-H radicals. According to Figure 21 (a), one can see the created computer models of possible stable configurations of the C atom, an O atom, which can form on the surface and on the edges, as well as configurations of the OH radical type. The length of the bonds of the configuration atom C – the atom O of the surface is 1.45 A, the edge 1.2 A, and the O–H radicals are 1.0 A.

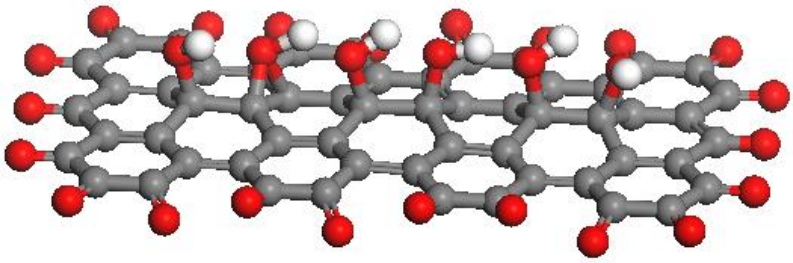

a) C – O = 1.45 A (surface), C – O = 1.2 (edges), O – H = 1.0 A

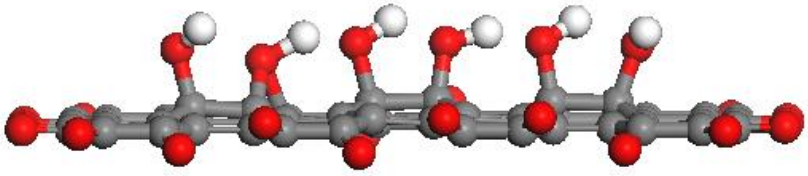

b) Binding energy of O: edges 0.5 eV, surface: 4 eV, bond surface: O – H: 2.1 eV, H - 0.9 eV (from O – H)

Figure 21 – Computer models of possible stable configurations of the bond atom C – atom O, O-H radicals

Based on calculations of DFT, the binding energy of the C atom and the O atom configurations at the edges equal to 0.5 eV, 4 eV on the surface, and the OH bond radical energy on the surface is 2.1 eV, and the H of OH radicals is 0.9 eV, which are in Figure 21 (b). The carbon atoms associated with OH radicals rise from the sheet by about 0.3 A.

Figure 22 (a, b, c) presents computer models of functionalized graphene and their typical configurations of graphene -O and O-H radicals. According to Figure 22 (a), C – O = 1.3 (surface), C–O 1.2 (edges), also the bond length of C–O of the O–H configurations radicals is 1.4 A, and the binding energy Eb (O–H)-graphene = 1.4 eV; Eb (H) = 3 eV, H-L = 0.03 (Figure 22 (b, c)), and the distance C-sheet = 0.2 A.

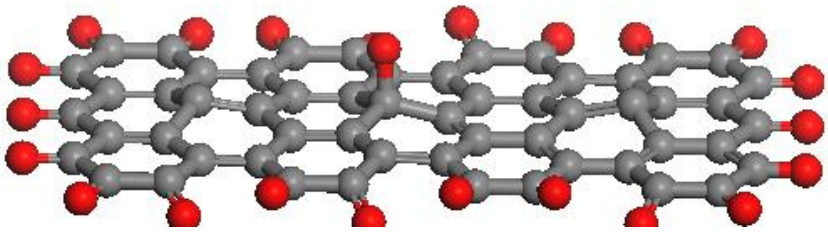

a)

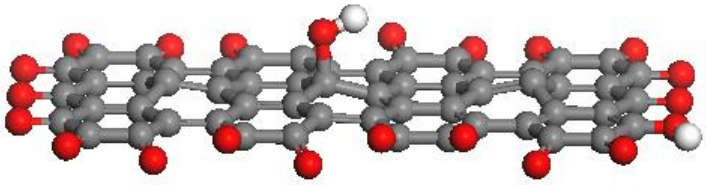

b)

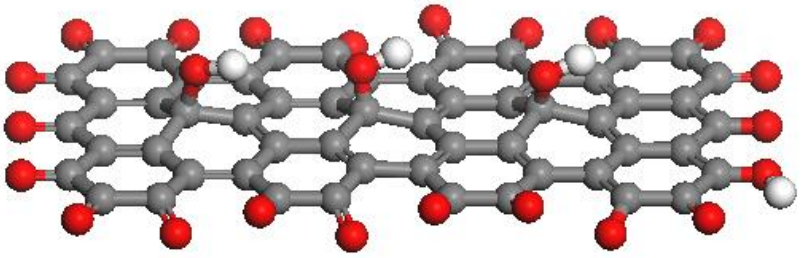

c)

Figure 22 – FSLGN computer configuration models:
a) configuration of C – O atoms;
b, c) configurations of OH radicals

The pure structure of functionalized graphene is shown in Figure 23 (a), and also in Figure 23 (b) a computer model is presented after optimization, as a result of which defects are formed in the structure of graphene. According to Figure 27 (b), the

configuration of graphene – the oxygen structure is changed, and also based on DFT calculations, the length of bond energy in the structure is C-C (O) = 1.6 A, graphene - O = 1.38 A, and near defects it is 1.7 A. In addition, binding energies were calculated, which represent the following data: a single bond in the O = 7 eV position, a double position E = 2.5 eV. C atoms bonded with O are shifted from the graphene sheet about 0.3 A.

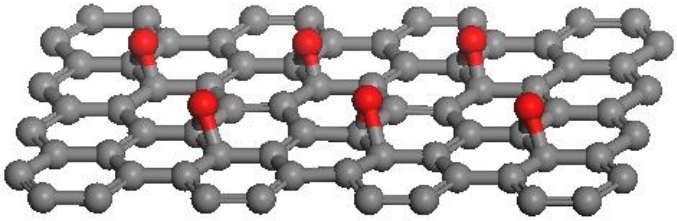

a) pristine structure

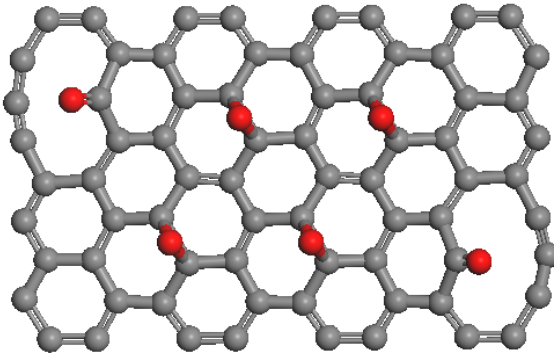

b) configuration after optimization

Figure 23 – FSLGN computer configuration models

A possible configuration of the types of bonds of oxygen with graphene was modeled, which in turn are divided into single edge E = 7 eV, single plane 2.7 eV, double plane E = 3.1 eV (Figure 24).

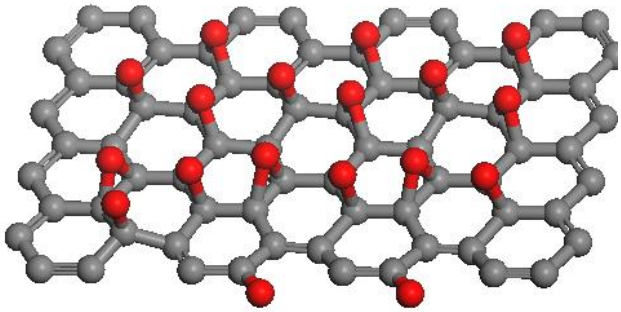

Figure 24 – Computer simulation of the types of bonds of oxygen with graphene

Figure 25 (a, b, c) shows the computer models of the FSLGN after optimization, which resulted in the formation of structural defects, hole defects are especially obvious, and the oxide is bonded on both sides according to the image.

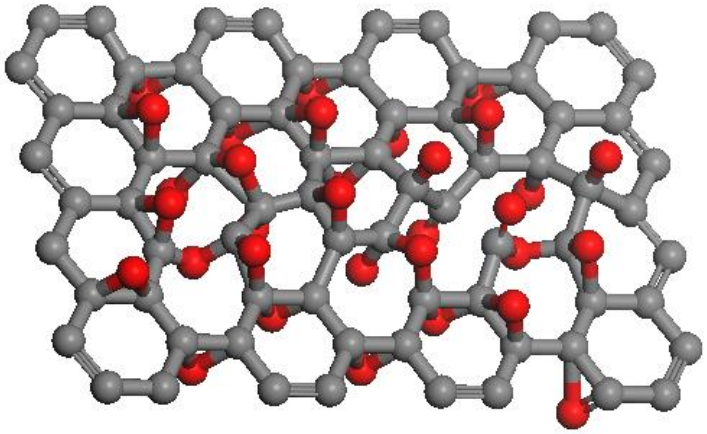

a)

.

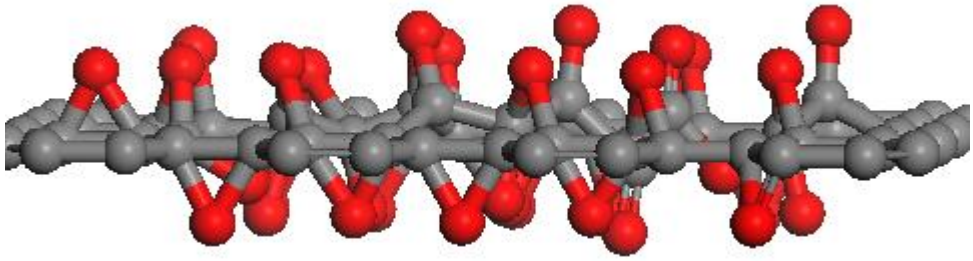

b)

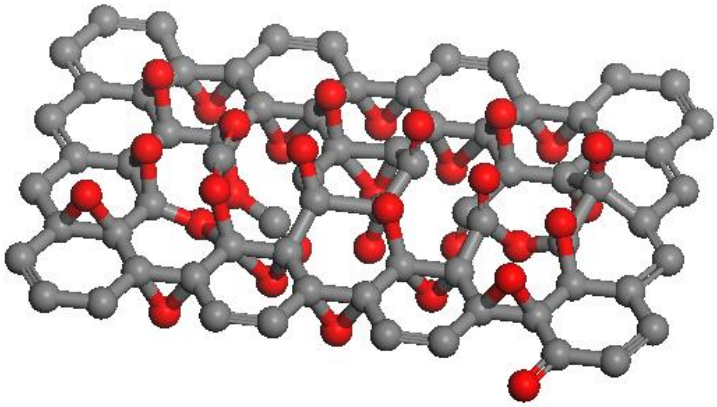

c)

Figure 25 – Computer simulation of two-sided bonds of oxide with graphene: a) view from the surface, b) from the side, c) hole defects

The charge map shows the covalent bond of oxygen with graphene, in addition, the electron charge density was calculated, which is = 0.02 e/A^3 (Figure 26).

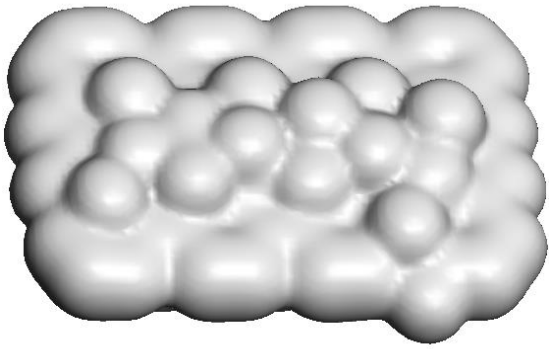

Figure 26 – Electron charge density

Figure 27 – Shows a model of a possible FSLGN reduce process with various connections: functionalizing graphene -O and graphene -O-H groups

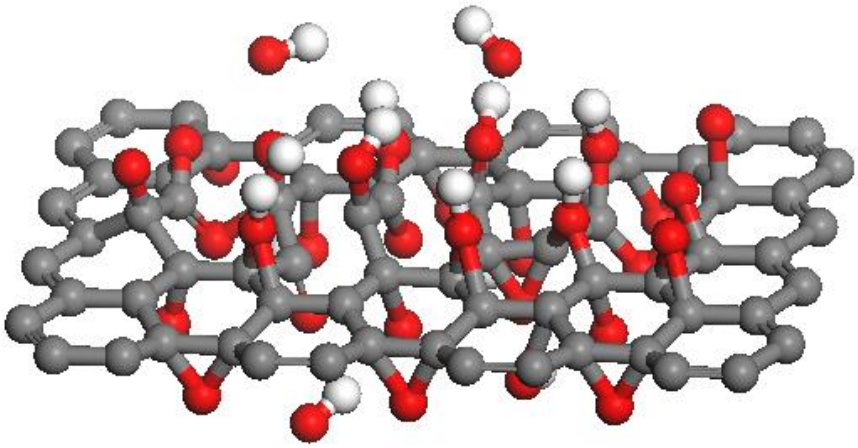

Figure 27 – Computer model of the FSLGN reducing process

Thus, the application of the density functional theory (DFT) using the molecular dynamics method with Chem Office Materials Studio software tools allows exploring unforeseen physical or chemical properties of atoms and molecules. In this section, computer models of typical configurations of FSLGN were presented, also the length and binding energies of C–O, and O–H radicals were calculated. In addition, computer models of various atomic arrangements, types of oxygen bonds with graphene, a model of the possible reduce process of FSLGN were created, and the binding energies of the graphene -O and graphene -O-H functionalizing groups were calculated.

3.2 SYNTHESIS AND RESEARCH OF FFLGN PROPERTIES

3.2.1 Synthesis of FFLGN

For several years, various methods of graphene synthesis have been performed in order to find the optimal, effective, safe method, and also ensure high performance. One of the main widespread methods of forming bulk graphene is the Hummers Method, in connection with, today this approach has attracted much interest due its high efficiency and safety during the performing reaction, also scalability. In this regard, in our work, we use the Hummers method to obtain FFLGN and investigate its properties.

FFLGN was obtained by modified Hammers method using pure natural graphite (Figure 28). The process of synthesizing FFLGN is a specific sequence, presented below. 138 ml of concentrated sulfuric acid was added to a 1500 ml flask with ice capacity at 0 °C, which was filled with graphite weighing 6 g, after which 3 g sodium nitrate was added. Then, while stirring the mixture with a magnetic stirrer, 18 g of solid potassium permanganate was gradually added, maintaining the temperature below 20 ° C for 2 hours. After raising the temperature of the mixture to 35 °C, it was maintained for 30 minutes at this temperature, then after adding deionized water, the temperature rose to 90 °C and stirred for 30 minutes. At the end, 30 % hydrogen peroxide was added until the color of the mixture changed to bright yellow and until gas emission ceased. Then the product was filtered and washed several times in 5% hydrochloric acid solution to remove metal ions, then washed with deionized water to remove acids.

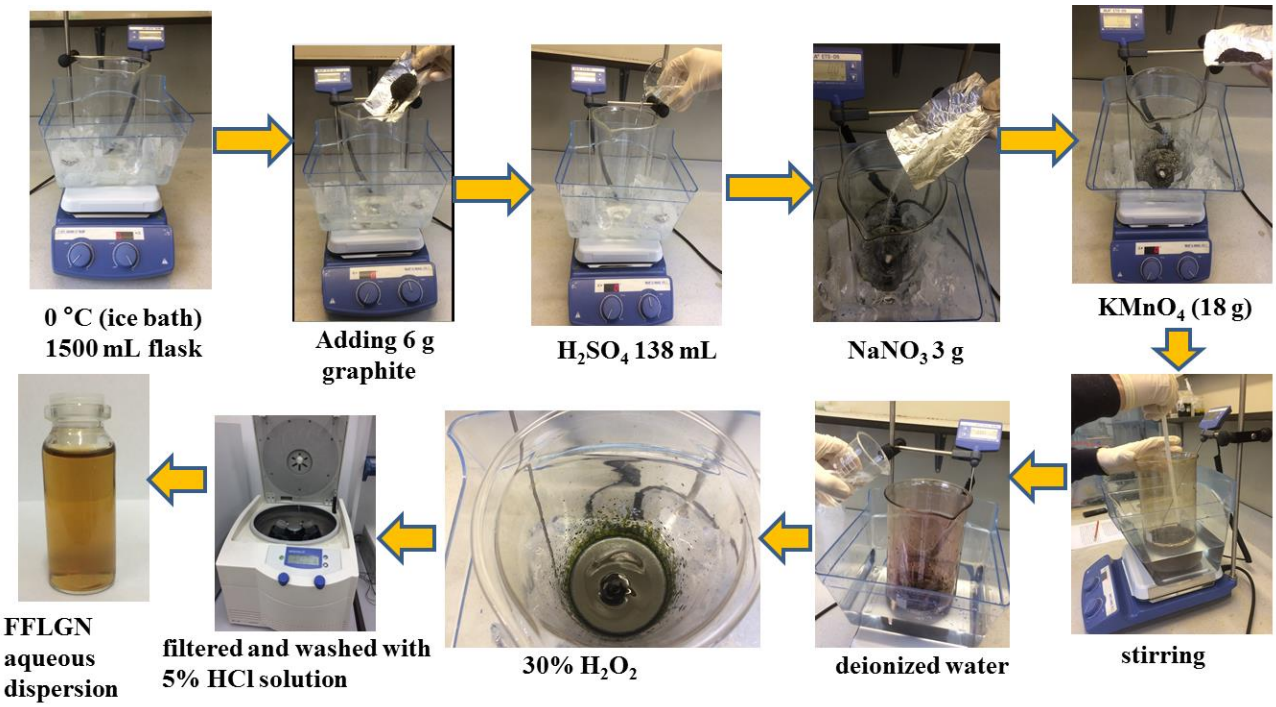

Figure 28 – Synthesis of FFLGN

It can be seen from image 29 (a, b) that the FFLGN flakes are in solution and in dry form (Figure 29 (b)), where the FFLGN sheets are placed on the surface of the substrate.

a) liquid solution FFLGN with concentration of 0.1 mg/ml

b) optical image of FFLGN on Si/SiO_2 substrate

Figure 29 – FFLGN in different forms

According to Figure 29 (a), FFLGN exfoliated into single-layer sheets of a 2D form, which is surrounded by water and alcohol molecule, also which negatively charged sheets of FFLGN promote the formation of a double layer FFLGN/water interface. In Figure 29 (b), FFLGN sheets placed on the substrate are one side in contact with the substrate, and the other side, that is, the surface with the atmosphere of air, but in any case water molecules are strongly physical sorbed on both sides of the FFLGN sheets even if they are on the surface substrates [199-202].

The EDX analysis in Figure 30 (a) shows that FFLGN contains about 67.60 at.% C, 32.40 at.% O. Figure 30 (b) shows the spectrum of FFLGN (impure), where the spectrum shows that it contains impurities such as sulfur and chlorine (69.02 at.% C, 30.04 at.% O, 0.46 at.% S, 0.49 at.% Cl)

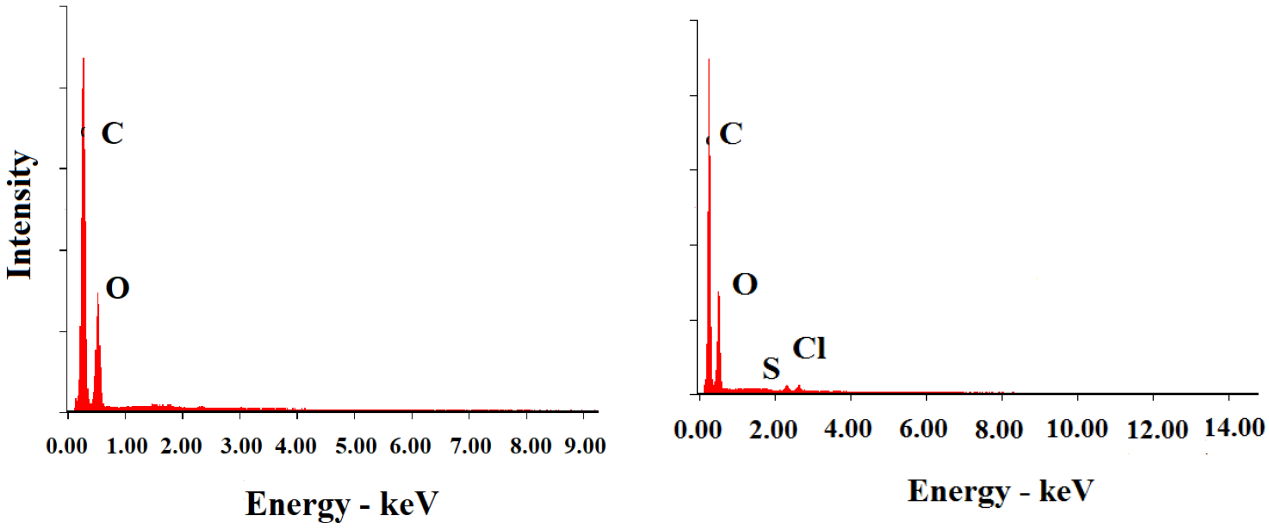

a) FFLGN b) FFLGN (impure)

Figure 30 – EDX analysis

Thus, the synthesis of FFLGN using the modified Hammers method is the most appropriate method for producing graphene, graphene-like materials in large quantities for further practical application in science and technology. Besides the synthesis of FFLGN in a large quantities, one of the most pressing problems is the study of the properties of FFLGN films after thermal annealing, the optical and electrical characteristics change, and the results of which are presented in the next subsection.

3.2.2 Optical, AFM, electrical characteristics of FFLGN films

Currently, the study of the properties of FFLGN films after thermal reduction is relevant, due to changes in their physicochemical properties. In this regard, in this work, we investigated the optical and electrical properties of FFLGN after thermal reduction in air, as a result of which reduced FFLGN thin films can potentially be used in optoelectronics, electronics, nanoelectronics, etc.

In this section, we investigated the optical, electrical properties of FFLGN after thermal reduction at temperatures of 80 °C, 120 °C, 160 °C, 200 °C, 240 °C, and 280 °C in air, where they were reduced for 20 minutes in a muffle furnace.

To obtain dry FFLGN films we used FFLGN liquid solution with a concentration of 0.1 mg/ml (Figure 29 (a)). This concentration of a solution with a mass of about 270 mg was applied to the substrate (dimensions: 15*25 mm), after application it was left overnight for drying. The mass of the applied FFLGN solution was controlled by using a Sartorius precision balance.

Figure 31 shows the initial and reduced FFLGN samples at temperatures of 80 °C, 120 °C, 160 °C, 200 °C, 240 °C, 280 °C. From the image we can see that depending on the effect of thermal reduction the color of the applied FFLGN varies from gray to dark cinnamon.

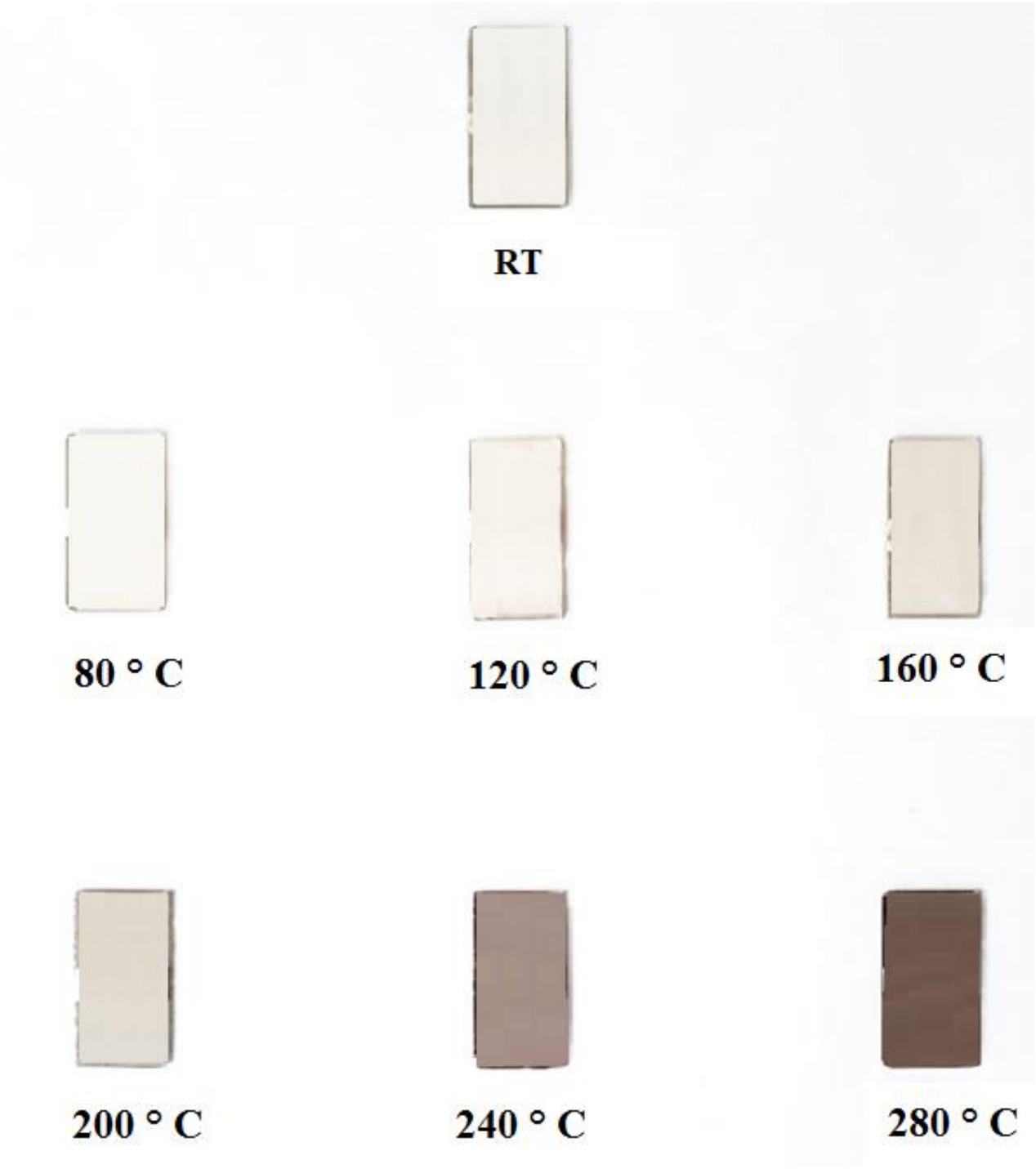

Figure 31 – Initial and reduced samples of FFLGN

After the thermal reduction of the samples, optical properties were investigated. To study the optical characteristics of FFLGN, we used ultraviolet and visible (UV-Vis) absorption spectroscopy, which measures the weakening of the light beam after it passes through the sample or after reflection from the sample surface. Using this technique, we measured the transmittance of visible light before and after the reduction of FFLGN at various temperatures in air. Optical characteristics of thermally reduced FFLGN samples investigated on UV-Vis spectroscopy are shown in Figure 32.

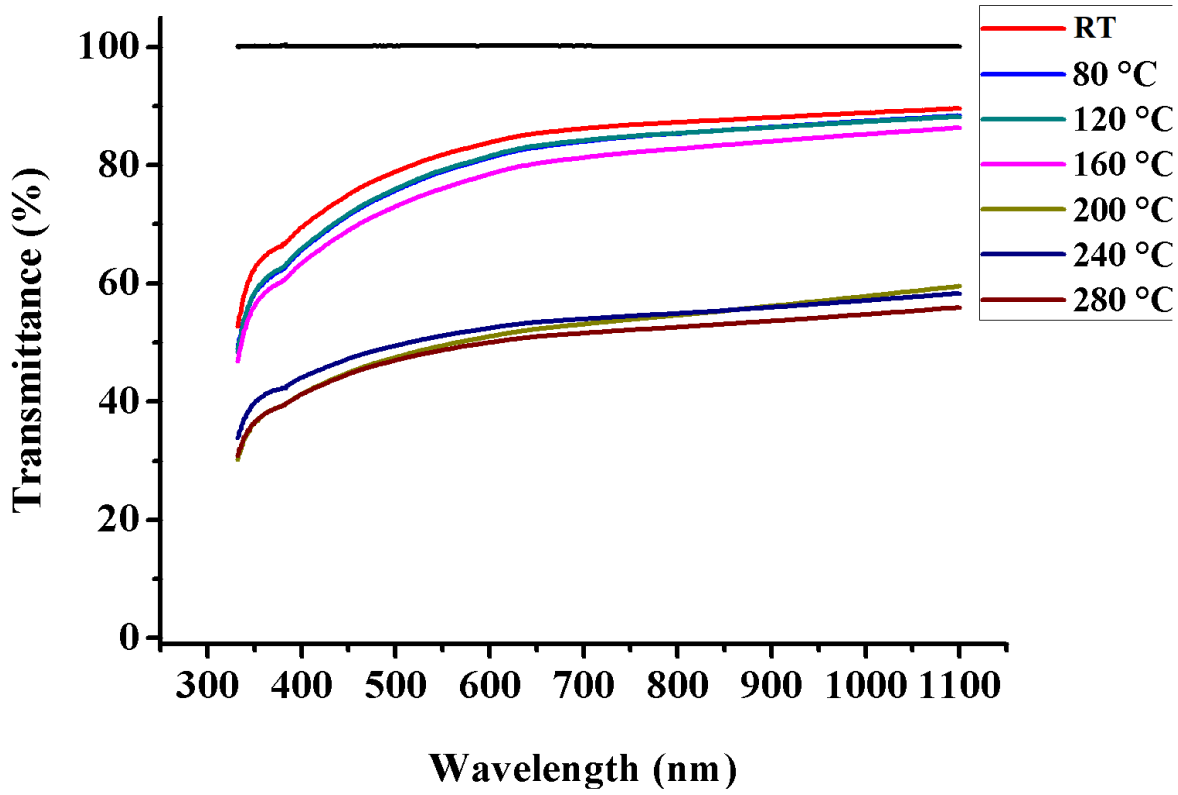

Figure 32 – Transmittance spectrum of FFLGN samples at temperatures of RT, 80 °C, 120 °C, 160 °C, 200 °C, 240 °C, 280 °C

According to figure 32, there are significant differences in spectra of FFLGN samples reduced at different temperatures. A significant change can be seen for temperatures of 160 °C and 200 °C, where the UV-Vis spectroscopy percentage decreases from 86 % to 58 % and a decrease a transmission percentage on 5 % is observed between samples corresponding to 200 °C and 280 °C, the same percentage change can be detected between the initial sample and a sample reduced at 160 °C. Thus, a significant changes in transmission of visible light through FFLGN samples before and after thermal reduction are observed between at temperatures of RT, 160 °C, 200 °C, 280 °C, which is associated with the decomposition of unstable and stable oxygen-containing groups and partial combustion of the carbon skeleton [199-202], as a result of which the percentage of visible light transmission decreases as the reduction temperature increases, therefore the samples become more absorbent.

Optical images of the initial and reduced FFLGN samples decreased in the air at temperatures of RT, 80 °C, 120 °C, 160 °C, 200 °C, 240 °C, 280 °C were investigated. At these temperatures, reduced FFLGN samples were almost identical to each other, also the initial FFLGN sample weren't observed no particular distinctive average sizes of the surface of flakes. Figure 33 shows typical images of the initial and reduced (280 °C) FFLGN samples.

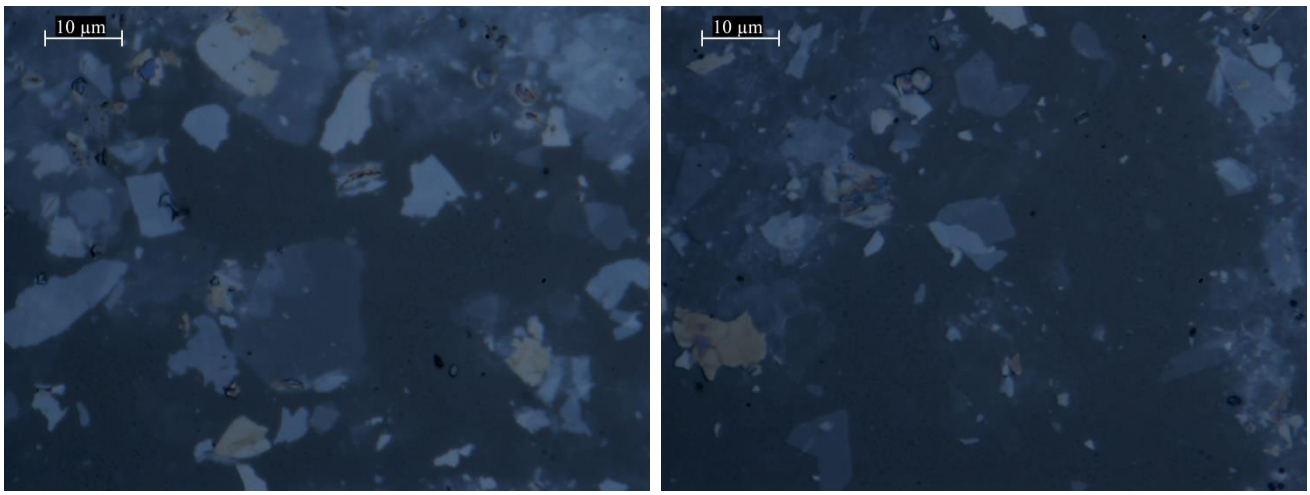

a) Profile 1 b) Profile 2

Initial FFLGN at RT

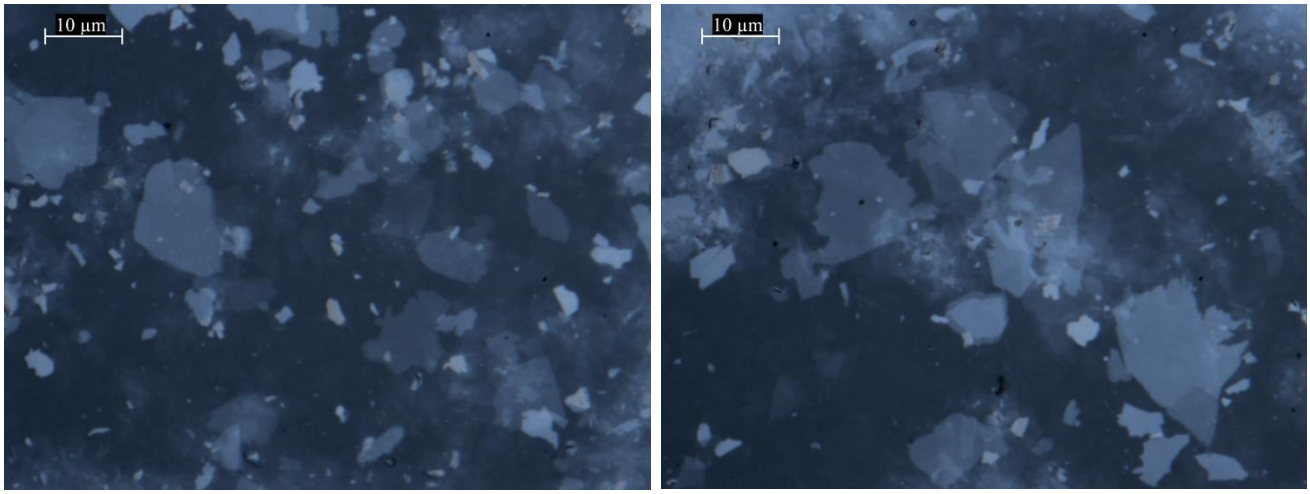

c) Profile 1 d) Profile 2

reduced FFLGN 280 °C

Figure 33 – Optical images of FFLGN films

The surface and thickness of the initial and thermally reduced FFLGN films were studied on AFM. Analyzing the AFM map, it was found that the most obvious changes in thickness from the initial sample were observed at 280 °C, where the average thickness of the reduced FFLGN decreased by 50 nm (Figure 34). According to the already known literature data, it can be assumed that the samples obtained by us with increasing reduction temperature decrease the thickness of FFLGN as a result of the removal of oxygen-containing functional groups.

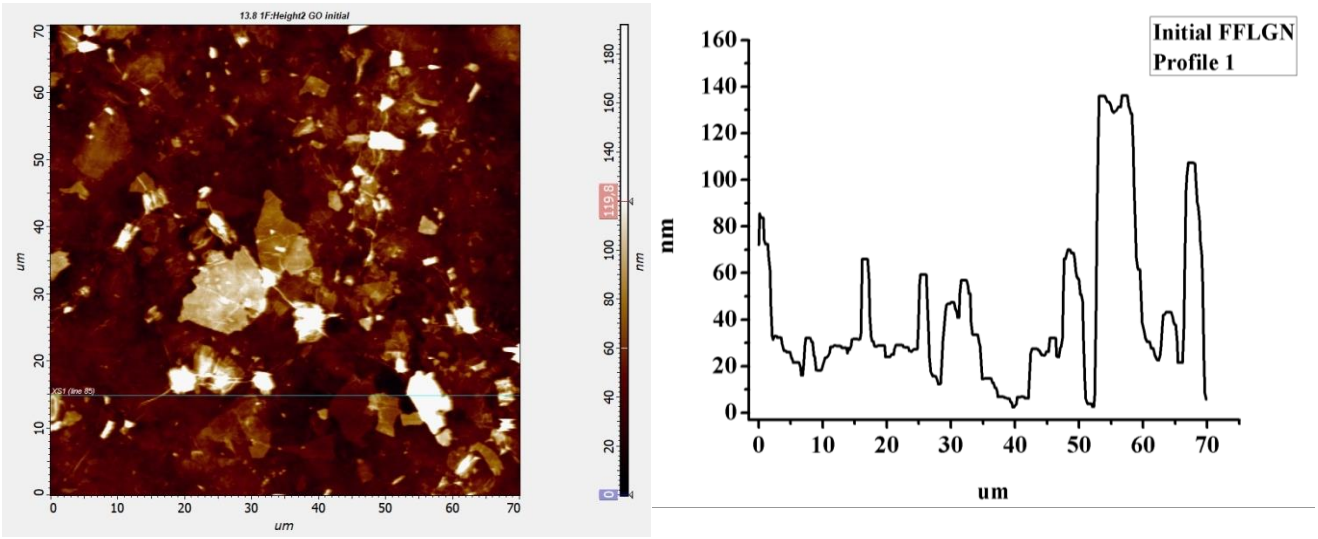

a) initial at RT (profile 1)

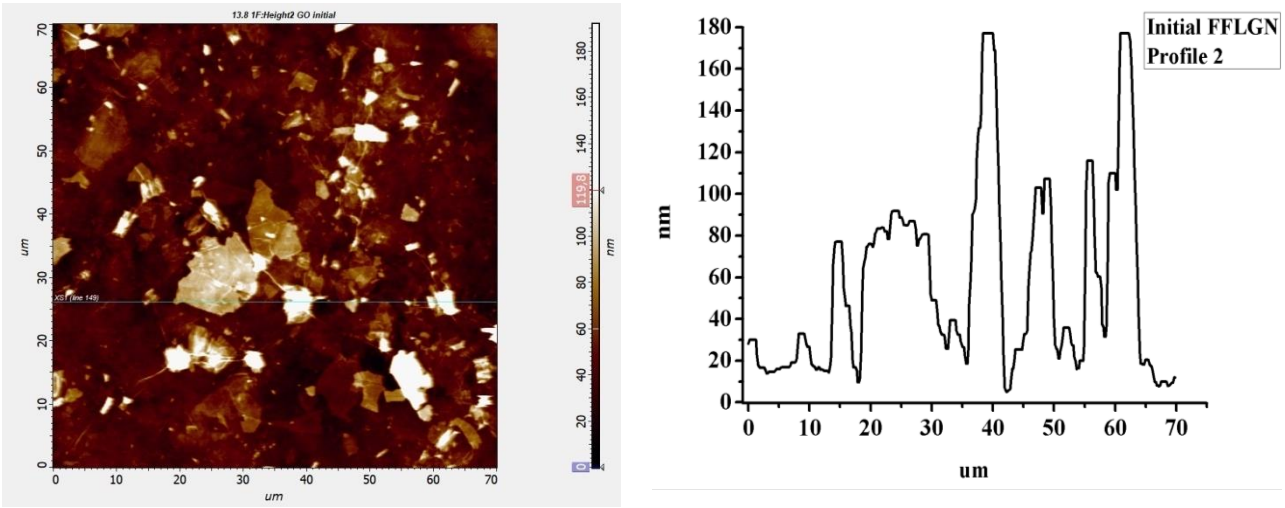

b) initial at RT (profile 2)

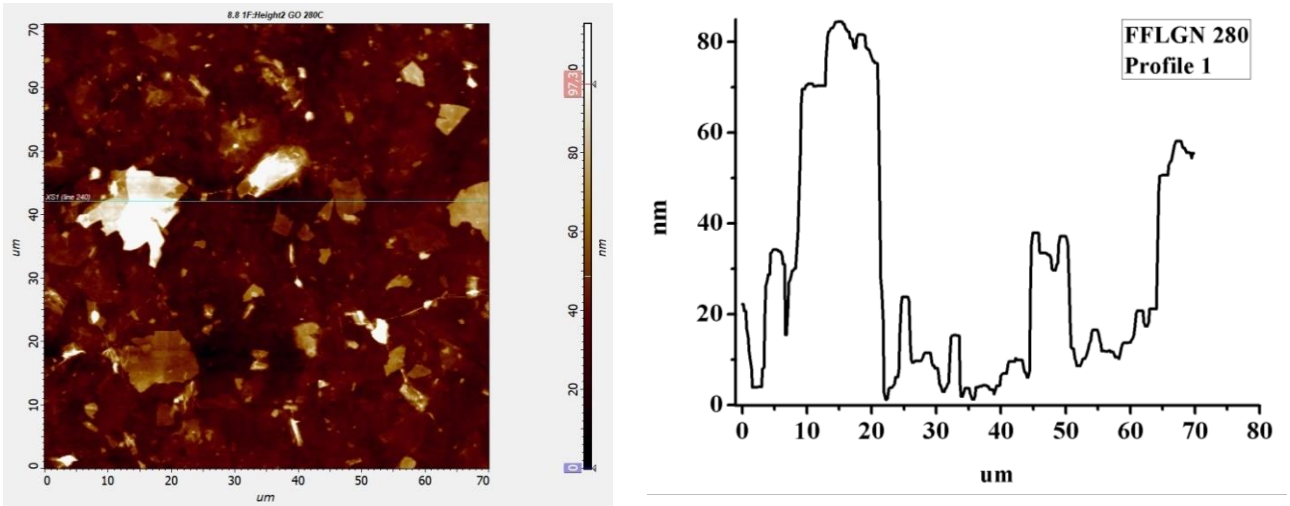

c) FFLGN 280 °C (profile 1)

Figure 34 – AFM of FFLGN, page 1

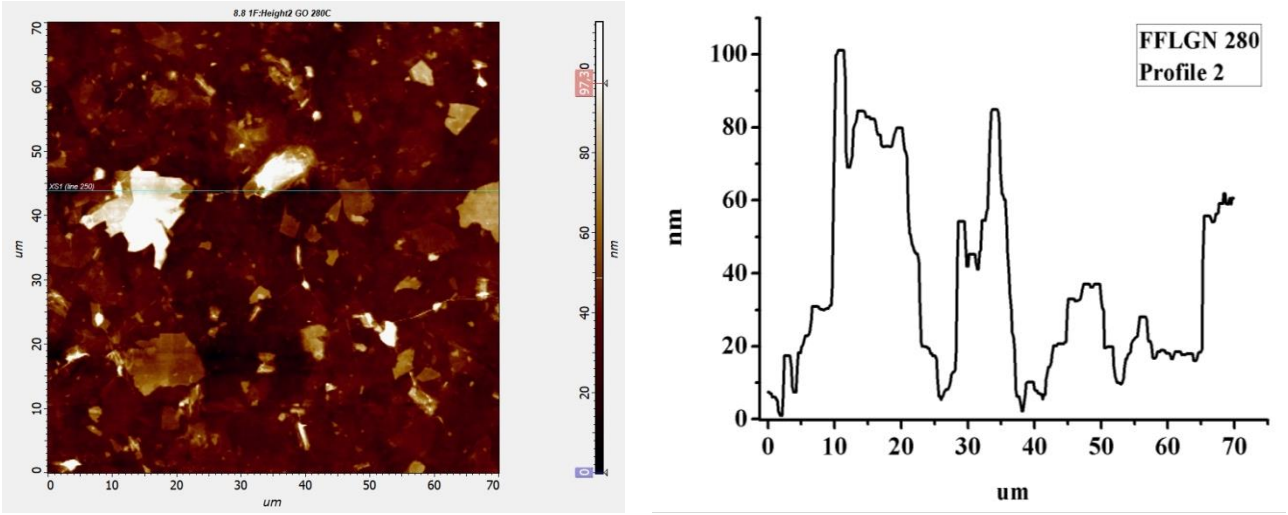

d) FFLGN 280 °C (profile 2)

Figure 34, page 2

One of the most important properties is the electrical resistance of FFLGN, which was studied after thermal reduction in air, where they were reduced within 20 minutes in a muffle furnace. After thermal reduction at the following temperatures of 25 °C, 80 °C, 120 °C, 160 °C, 200 °C, 240 °C, 280 °C, a conductive silver varnish was applied to the samples to ensure good electrical contact and left to dry overnight.

Then, using Keithley 6517A meter, the sheet resistance of samples without chlorine and sulfur was checked, which varied from 5-2.5 MΩ/square at temperatures of 200 °C and 280 °C, that is, the sample at 200 °C had 5 MΩ/square, 240 °C showed 4.2 MΩ/square and 280 °C was equal to 2.5 MΩ/square.

If compare the sheet resistance of pure FFLGN with the sheet resistance of impure graphene oxide purchased from Goographene with the presence of sulfur and chlorine, the sheet resistance of the pure FFLGN at 280 °C is more than 5 times lower than the sheet resistance of the impure FFLGN and is equal to 13 MΩ/square.

The reason for this changing can be the different distribution of flakes on the surface for pure and impure FFLGN, which in turn can affect to the contact between the FFLGN flakes.

Based on the obtained results, decreasing in electrical resistance with increasing temperature of thermal reduction of FFLGN samples is observed and this decrease in electrical resistance is detected at temperatures of 200 °C, 240 °C, 280 °C. According to well-known literature data, this phenomenon is associated with the process of chemical and thermal reduction, resulting in the removal of oxygen-containing functional groups, such as epoxy, hydroxyl, carbonyl, and carboxyl, resulting in decreased electrical resistance [199-202].

Thus, the influence of thermal reduction on FFLGN samples contributed to the change in optical and electrical characteristics. The results of the transmission spectrum of visible light of the reduced samples of FFLGN show significant changes between temperatures RT and 160 °C, as well as 200 °C and 280 °C, where the percentage of transmission decreases approximately from 20-30%, that is, according

to the data when the reduction temperature increases the percentage of transmission decreases. By analyzing the Raman AFM map, it was found that the most obvious changes in thickness from the initial sample were observed at 280 °C, where the average thickness of the reduced FFLGN decreased by 50 %. Also, the most significant changes were shown by data on electrical characteristics, in which, with an increase in the temperature of thermal reduction, the values of electrical sheet resistance decreased from 5-2.5 MΩ/square at temperatures of 200 °C and 280 °C. According to well-known literature, a decrease or increase in the values of optical, electrical and AFM characteristics are associated with the removal of unstable and stable oxygen-containing groups of FFLGN, depending on the temperature of thermal reduction, and are presumably associated with the binding energies of the groups. Also, the most important process in studying the properties of FFLGN is the synthesis of separately standing membranes of FFLGN and the study of its characteristics, which are presented in the following subsections, and its practical application for the humidity sensor and the study of electrophysical characteristics are discussed in Section 3.2.8.

3.2.3 Preparation and investigation of the FFLGN membrane and its characteristics after thermal reduction

We specified in sections 1.4, 1.5 that the most important in the study of FFLGN is the preparation and investigation of reduced FFLGN, therefore, in this section, FFLGN membrane was obtained and reduced at different temperatures in the flow tube in a hydrogen atmosphere.

During preparation process of the FFLGN membrane we used 40 ml of FFLGN solution with a concentration of 1.5 mg/ml. The FFLGN membrane was left to dry overnight at room temperature and then separated from the filter. Figure 35 shows the FFLGN membrane obtained using the vacuum filtration method, in which the FFLGN dispersion was carried out using a porous alumina membrane filter with a pore size of 800 nm and a diameter of 40 mm. The main methods and steps for the preparation of the FFLGN membrane are presented in section 1.4.

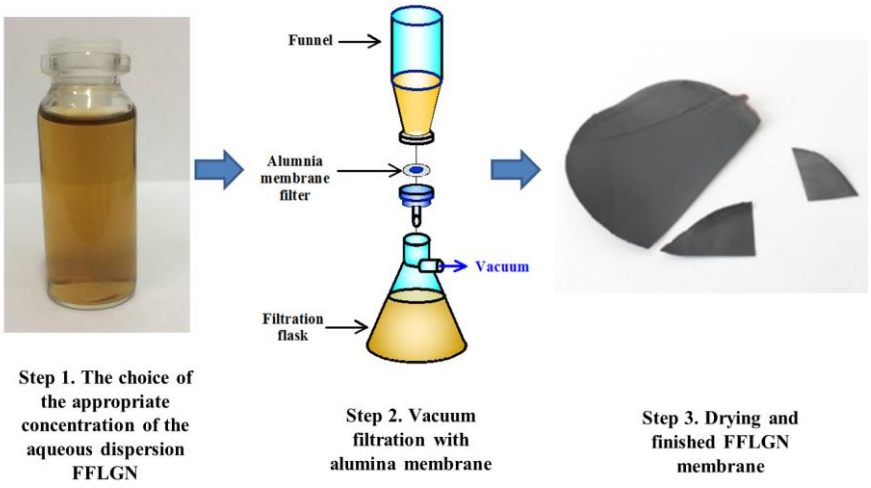

Figure 35 – Membrane FFLGN

SEM images of the surface and cross-section of the resulting FFLGN membrane are shown in section 3.2.4, which confirms that the resulting membrane has a two-dimensional highly ordered sheet-like layered structure, and the film thickness is about 20 μm (section 3.2.4, figure 37).

FFLGN cannot be used as a conductive nanomaterial without further processing when it is thermally unstable and electrically isolated. It has been demonstrated that the reduction of FFLGN can significantly improve its thermal stability and electrical conductivity, close to the level of graphite. In this work, in order to obtain a few-layer graphene list, FFLGN was reduced by heat treatment [199-202].

This section presents the results of the reduction of FFLGN. The effect of temperature was studied at: 150 °C, 300 °C, 500 °C, 900 °C in a hydrogen atmosphere on the structure and composition of FFLGN.

Using TGA we determined the change in mass under the influence of temperature. Thermogravimetry or TGA is a method of thermal analysis that records the change in the mass of a sample, measures changes in the physical and chemical properties of materials depending on temperature [199-201].

TGA of reduced FFLGN was performed in a flow tube in a stream of hydrogen at temperatures: 150 °C; 300 °C; 500 °C; 900 °C and their masses were recorded using a Sartorius instrument. The masses of these samples were measured before and after annealing, then the masses of the removed chemical functional groups of the reduced FFLGN were calculated.

Figure 36 shows a TGA of reduced FFLGN in a hydrogen atmosphere at various temperatures. This graph shows the weight loss and removal of certain functional groups of FFLGN with increasing temperature.

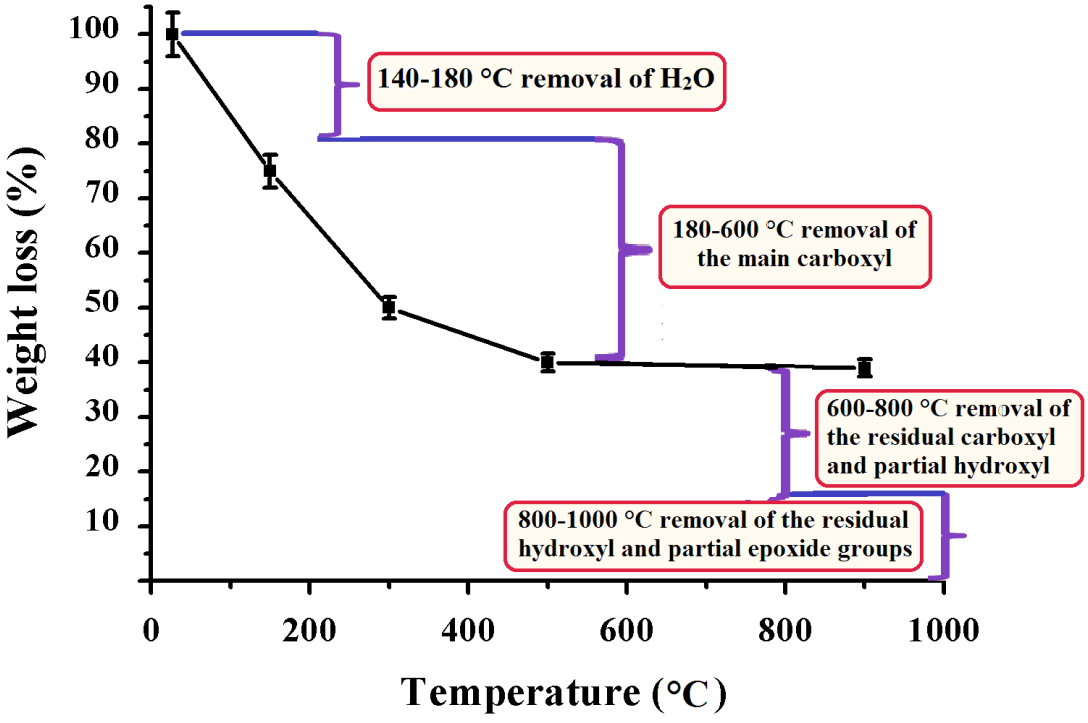

Figure 36 – TGA of reduced FFLGN

In this graphic (Figure 40) we can observe the process of thermal reduction, which includes four important temperature zones, at which chemical functional groups are removed from the reduced FFLGN. At temperatures of 140-180°C water is removed; at 180–600 °C removes the main carboxyl groups, at 600–800 °C removes residues of carboxyl and partially hydroxyl groups, at 800–1000 °C removes residues of hydroxyl and partially epoxy groups [199, 201].

Figure 37 (a, b, c, d, e) shows the elemental analysis of FFLGN and temperature-reduced FFLGN in a hydrogen atmosphere at various temperatures.

We performed an elemental analysis of 4 samples reduced FFLGN in a hydrogen atmosphere at temperatures of 150 °C, 300 °C, 500 °C, 900 °C. According to this graph, it is observed that with increasing temperature the atomic fraction of oxygen decreases. Figure 37 (a) shows the spectrum of reduced FFLGN 150 °C, where the sample contains impurities such as sulfur and chlorine (C – 74.24 at.%, O – 23.60 at.%, S – 1.39 at.%, Cl – 0.77 at.%); b) reduced FFLGN 300 °C contains (C – 85,86 at.%, O – 14.14 at.%); c) reduced FFLGN 500 °C contains (C – 91,49 at.%, O – 8.51 at.%); d) reduced FFLGN 900 °C contains (C – 97,13 at.%, O – 2.87 at.%).

Elemental analysis of each sample shows the changing of the C/O ratio, that is 4.18 at a temperature of 150 °C; 8.09 at 300 °C; 14.31 at 500 °C; 45.08 at 900 °C (Figure 36 (e)).

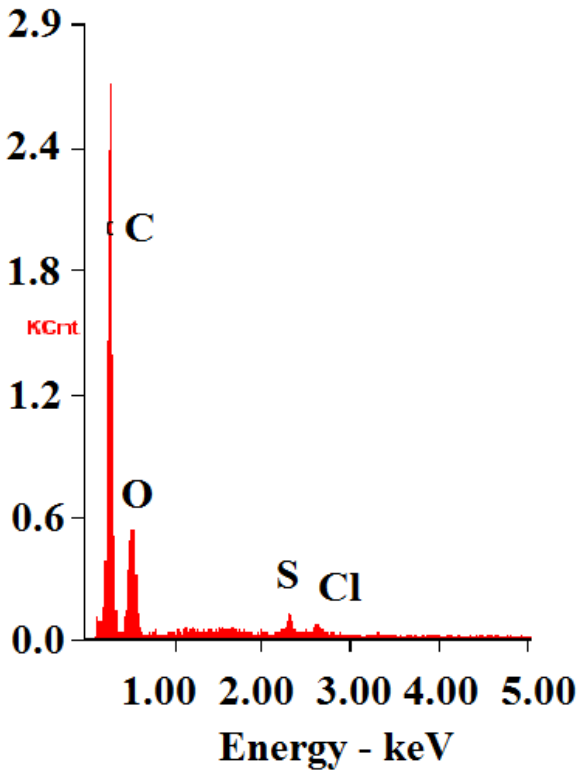

a) reduced FFLGN 150 °C

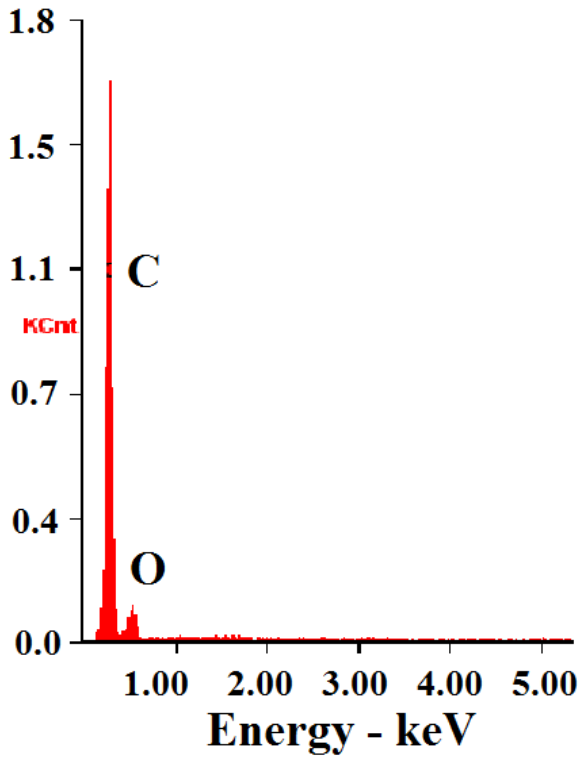

b) reduced FFLGN 300 °C

Figure 37 – Elemental analysis of the reduced FFLGN, page 1

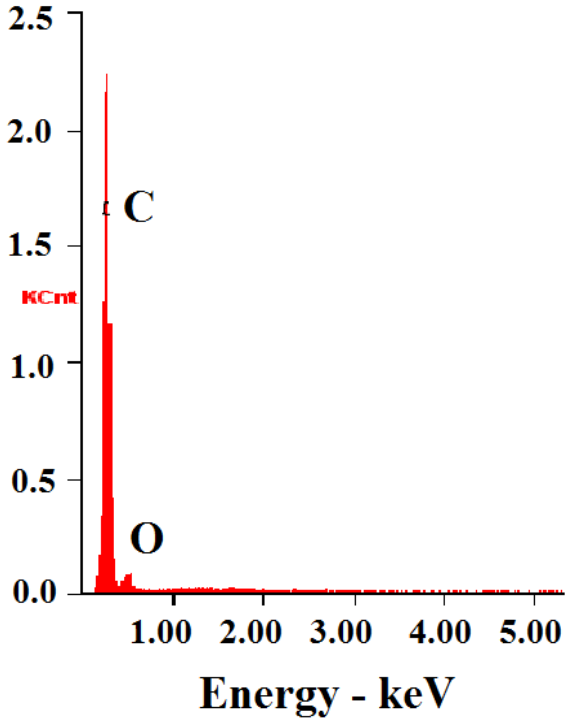

c) reduced FFLGN 500 °C

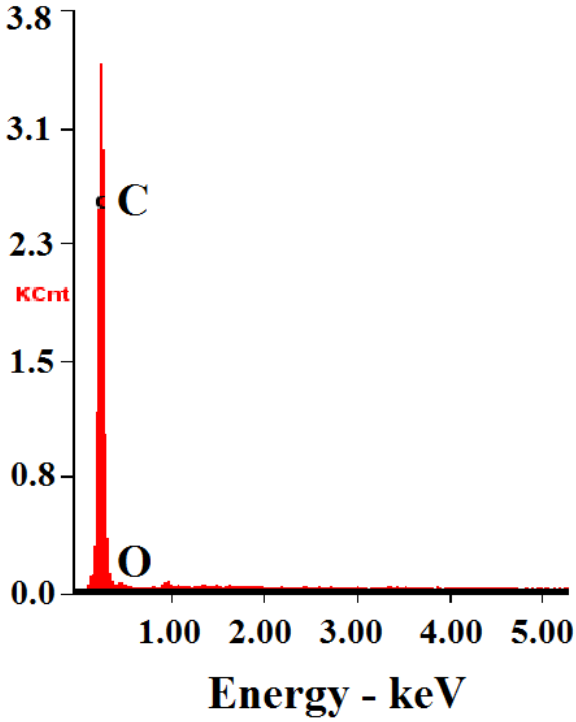

d) reduced FFLGN 900 °C

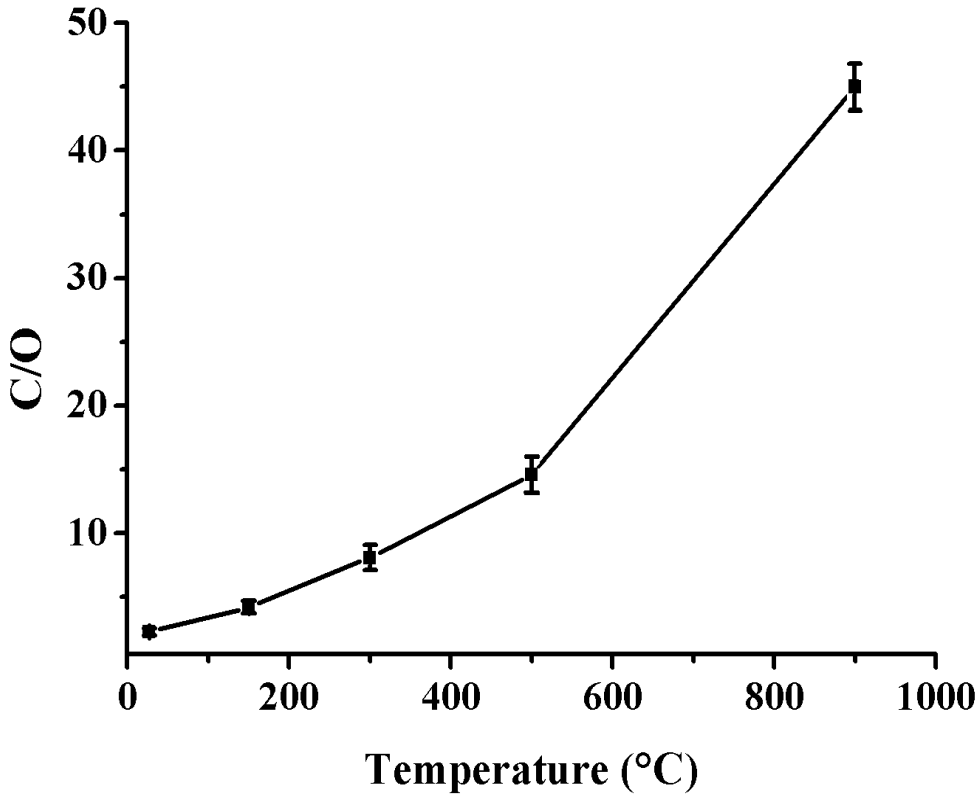

e) C/O ratio of reduced FFLGN (150 °C, 300 °C, 500 °C, 900 °C)

Figure 37, page 2

The results of the thermogravimetric and elemental analysis on the isolation of functional groups and the decrease of oxygen depending on temperature according to well-known studies [199-201] depend on the strong or weak binding energy between carboxyl, hydroxyl, epoxy groups, and reduced FFLGN.

Thus, the synthesis of free-standing FFLGN membranes using the vacuum filtration method (vacuum-assisted filtration) due to characteristics such as a layered structure and specific surface area are promising for absorption materials, due to these properties it can be widely used in various gas sensors, particular as a sensitive humidity sensor, and the experimental data of which are discussed in detail in section 3.2.8.

The results of reduced FFLGN membranes in a flow tube in a hydrogen atmosphere at a temperatures of 150 °C, 300 °C, 500 °C, 900 °C [199-201] show that with increasing annealing temperature occurs a loss of mass and the removal of chemical functional groups of the FFLGN. The result of the TGA in a hydrogen atmosphere demonstrated that at a temperature of 150 °C most of the mass leaves from 300-900 °C, the allotment of functional groups is much weaker. In addition, the elemental analysis performed by the EDS method demonstrates a decrease in the level of oxygen; also temperature changes in the rates of allotment of functional groups and oxygen coincide with known results and are presumably associated with the binding energies of the groups. The characteristics of FFLGN and thermally reduced FFLGN samples using Raman spectroscopy, SEM, EDS, TGA, and XRD studies are discussed in the following sections.

3.2.4 SEM of FFLGN and reduced FFLGN membranes

To determine the elemental composition of the reduced FFLGN, Quanta 3D 200i EDS equipment was used. The method of EDS is an analytical technique for the elemental analysis of a solid material based on the analysis of the emission energy of its X-ray spectrum is described in detail in Section 2.1.

The SEM images of FFLGN in Figure 38 (a – is the surface, b – is the cross section) clearly show that FFLGN has a two-dimensional sheet-like structure. From the images (Figure 38 (a, b)) of SEM, it can be seen that the films are stacked one above the other, and there are wrinkled areas on the FFLGN membrane surface. According to Figure 38 (b), the SEM image of the cross-section clearly shows that the FFLGN membrane obtained by us is layered and has a highly ordered lamellar structure, and the film thickness is about 20 μm.

Based on the above literature data for the production of the FFLGN membrane in section 1.4, our membrane has a relatively flat surface, a large area, and is also flexible and mechanically strong enough when processing by tweezers (Table 3) [205, 206].

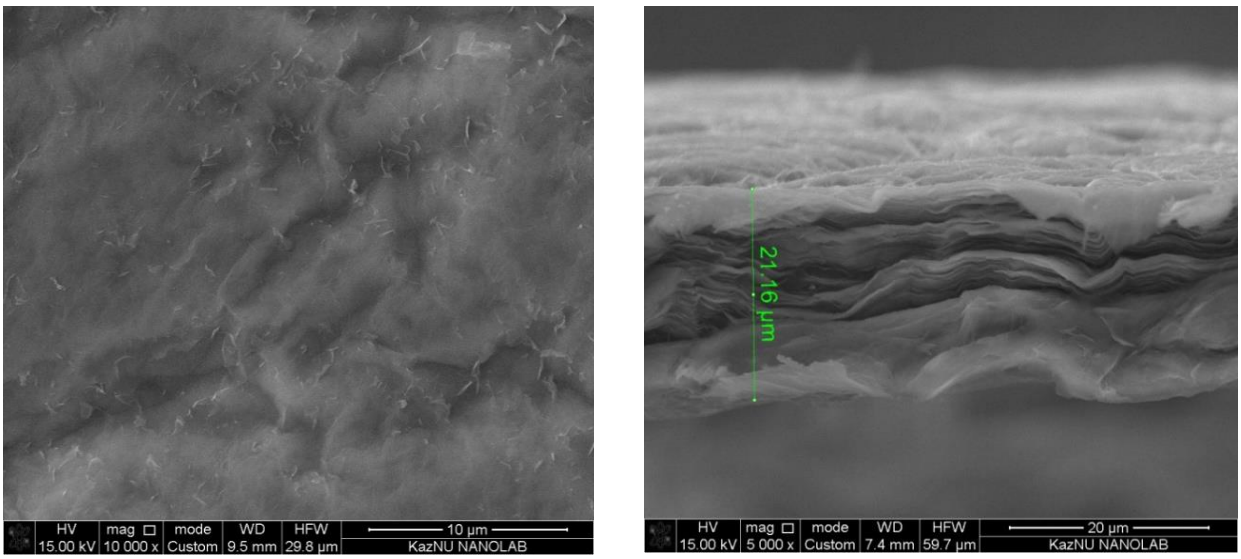

a) surface b) cross-section

Figure 38 – SEM images of initial FFLGN

In figure 39 (a, b, c, d, e, f, g, k) are shown images of FFLGN samples reduced at temperatures of 150 °C, 300 °C, 500 °C, 900 °C. These images were investigated on an SEM. The surfaces of reduced FFLGN membranes at different temperatures do not differ much between themselves; their thickness decreases by ~37 % (from 22 to 14 μm), with an increase in the temperature of reduction, which is explained by removal of oxygen-containing functional groups. As the temperature increases and as the release of water and functional groups, the specific surface of the reduced FFLGN increases.

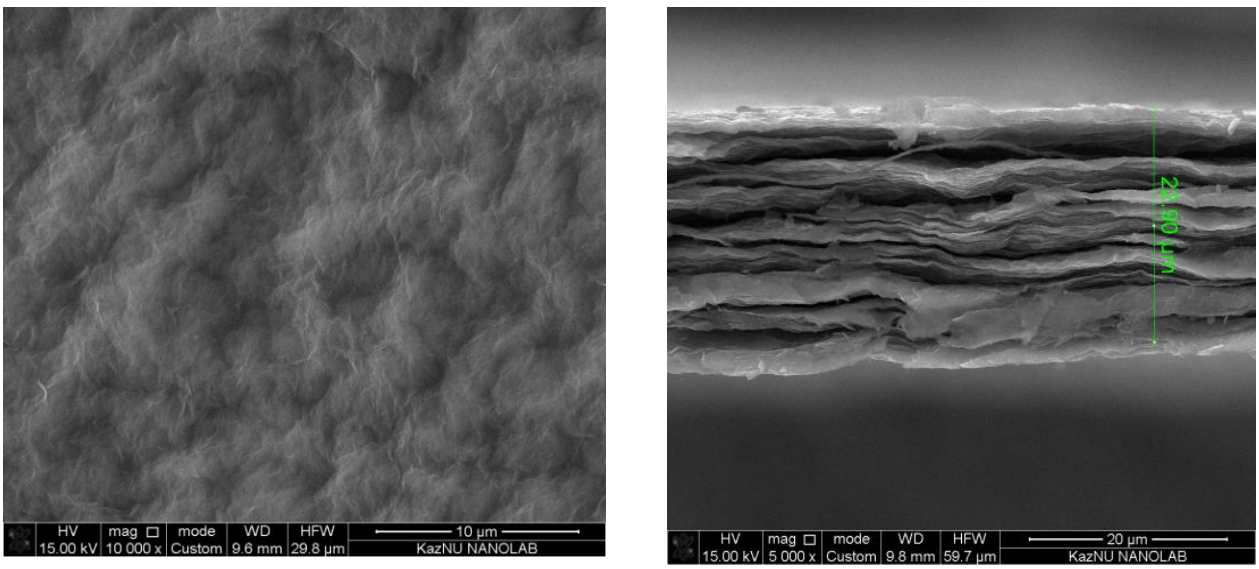

a) surface b) cross-section

reduced FFLGN 150 °C

Figure 39 – Images of temperature-reduced FFLGN, page 1

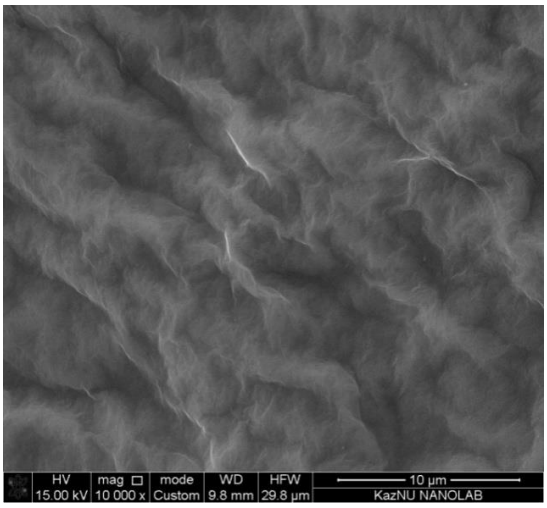

c) surface

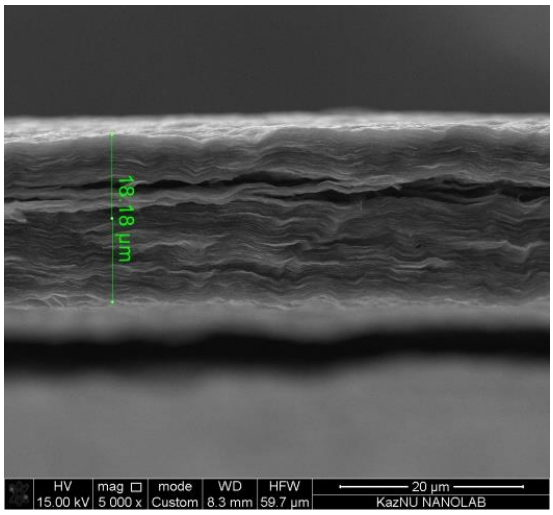

d) cross-section

reduced FFLGN 300 °C

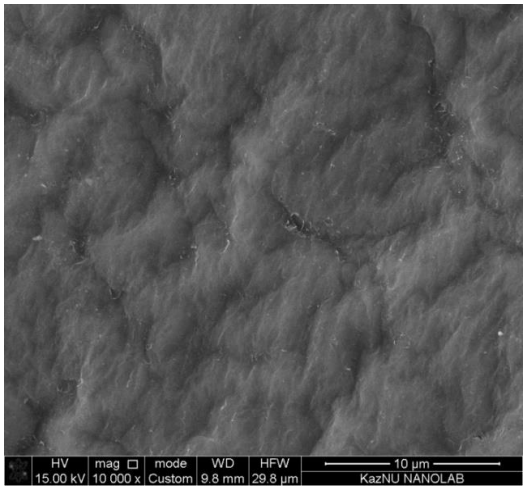

e) surface

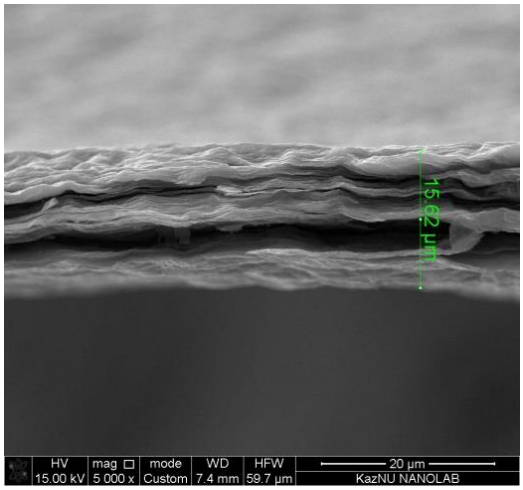

f) cross-section

reduced FFLGN 500 °C

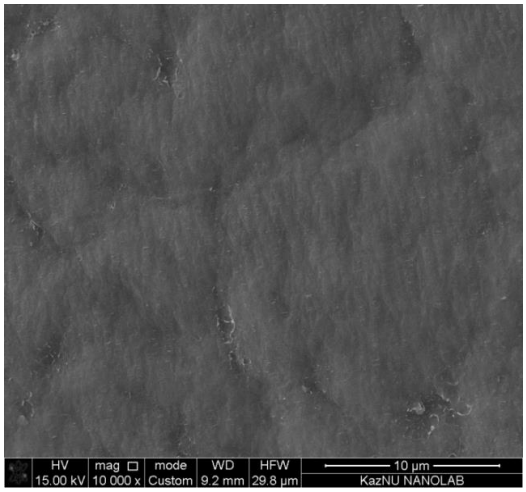

g) surface

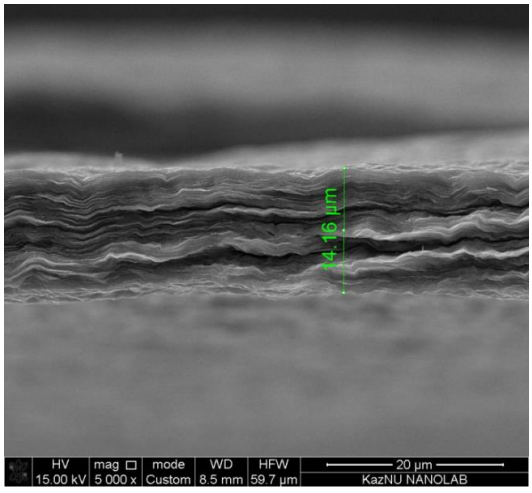

k) cross-section

reduced FFLGN 900 °C

Figure 39, page 2

Thus, based on the obtained images, it can be concluded that reduced FFLGN have a developed layered structure, in turn, can be considered as promising materials in the manufacture of electronic devices, electrical sources, in particular, lithium-ion batteries, and can also be used in gas sensors, biosensors. One of the most important research methods for characterizing the structures of the FFLGN and reduced FFLGN samples is Raman spectroscopy, which in turn will show significant changes when exposed to temperature annealing in the next subsection.

3.2.5 Raman spectroscopy of FFLGN and reduced FFLGN membranes

The FFLGN obtained by us was studied using well-known Raman spectroscopy equipment, which is intended to study the characteristics of carbon nanostructures, as well as to describe the quality of graphene in industrial processes and studies, insofar as Raman spectroscopy is not destructive, discussed in detail in sections 1.6, 2.2.

In section 1.6 is reviewed, that the ratio D/G indicates a large number of defects in the crystal lattice, and this ratio also increases during chemical reduction. Figure 40 (a, b, c) shows the Raman spectra of FFLGN and reduced FFLGN. According to Figure 40 (a), the D band is located in the region of 1350 cm^{-1}, the G-band is in the region of 1587 cm^{-1}, and the ratio of these bands corresponds to 0.85, which is consistent according to the literature data in section 1.6.

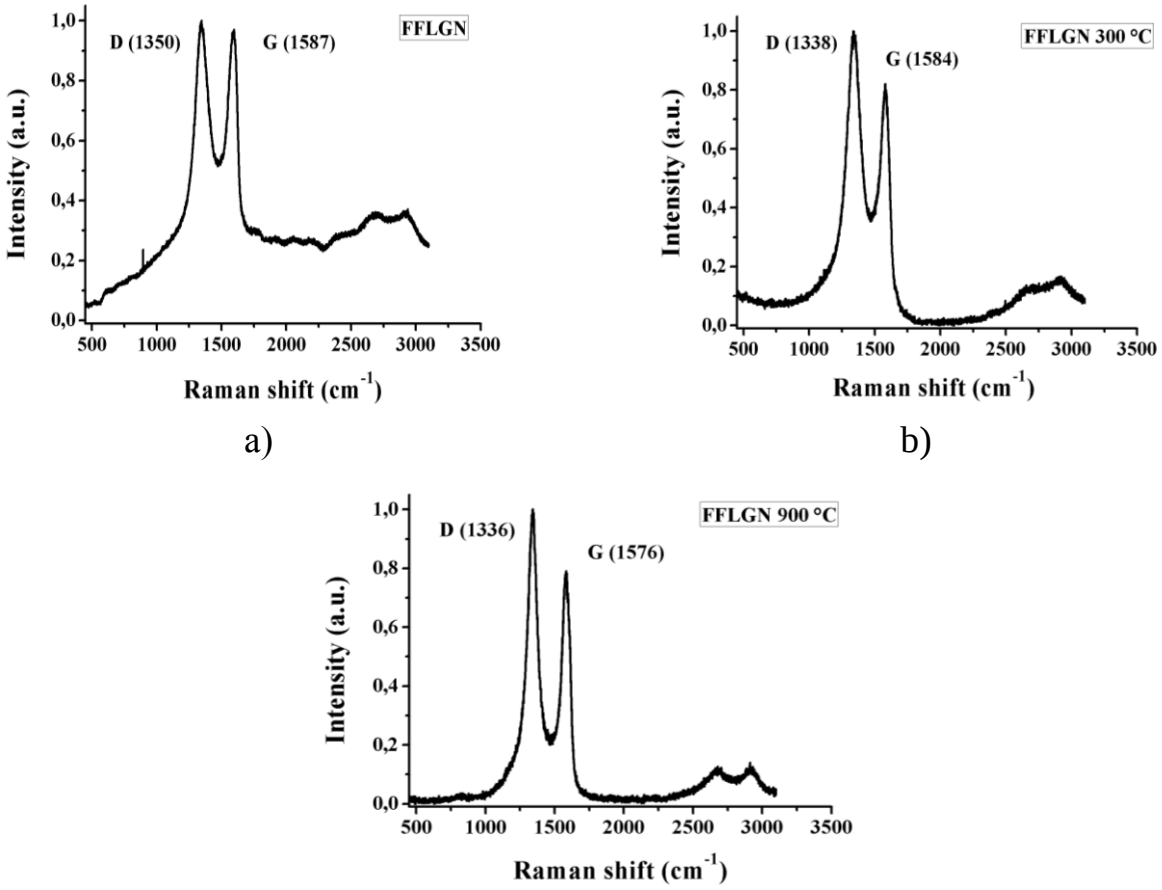

Figure 40 – TGA of FFLGN and reduced FFLGN samples

Beside of the initial FFLGN, we studied reduced FFLGN samples, which were exposed to reduction at different temperatures in a hydrogen atmosphere. The reduction of FFLGN was carried out at temperatures of 150 °C, 300 °C, 500 °C and 900 °C. Samples after reduction were investigated by using Raman spectroscopy, which is shown in Figure 40 (a, b, c). According to the table, when the annealing temperature changes the intensity and the ratio of the G and D bands change, as shown in the table, the intensity of the G band decreases from 1587 to 1576 with an increase in the reduction temperature from initial FFLGN to 900 °C, and this changes are observed at the intensity of the D band, which in turn also decreases.

Table 4 shows the values of the bands G and D. These changes in band intensities and changes in the ratio of bands mean that the removal of oxygen-containing functional groups with the thermal treatment of FFLGN [199, 201].

Table 4 – Intensity G and D bands of the FFLGN and reduced FFLGN samples at temperatures: initial, 300 °C, 900 °C.

Samples, °C	**G – band (cm^{-1})**	**D – band (cm^{-1})**
FFLGN	1587	1350
Reduced FFLGN 300°C	1584	1338
Reduced FFLGN 900°C	1576	1336

Thus, Raman spectroscopy of FFLGN and reduced FFLGN can provide important information about the state of the grating disorder, the size of the sp^2 carbon regions and electronic doping from chemical additives during the oxidation, reduction or functionalization process. According to the obtained results, it was revealed that the thermal treatment of the FFLGN membrane at different temperatures affects the intensity change and the ratio of the bands of the Raman spectroscopy, which is explained by removal of oxygen-containing functional groups.

3.2.6 XRD of the FFLGN and reduced FFLGN membranes

In this section, we used XRD, which is a non-destructive method for the characterization of crystalline materials, to study the characteristics of FFLGN. This instrument allows us to provide information about the structure, phase, preferred crystal orientation (texture), average grain size, crystallinity, deformation and crystal defects, as well as the atomic interval.

Via XRD we investigated FFLGN and reduced FFLGN samples at next reduction temperatures (150 °C, 300 °C, 500 °C, 900 °C) which were reduced in a hydrogen atmosphere. To compare the interplanar spacing before and after thermal reduction, an XRD analysis of initialFFLGN XRD and HOPG was performed, which were studied on a DRON-7 instrument [199-206]. Figure 41 shows the spectra of the initial FFLGN and HOPG.

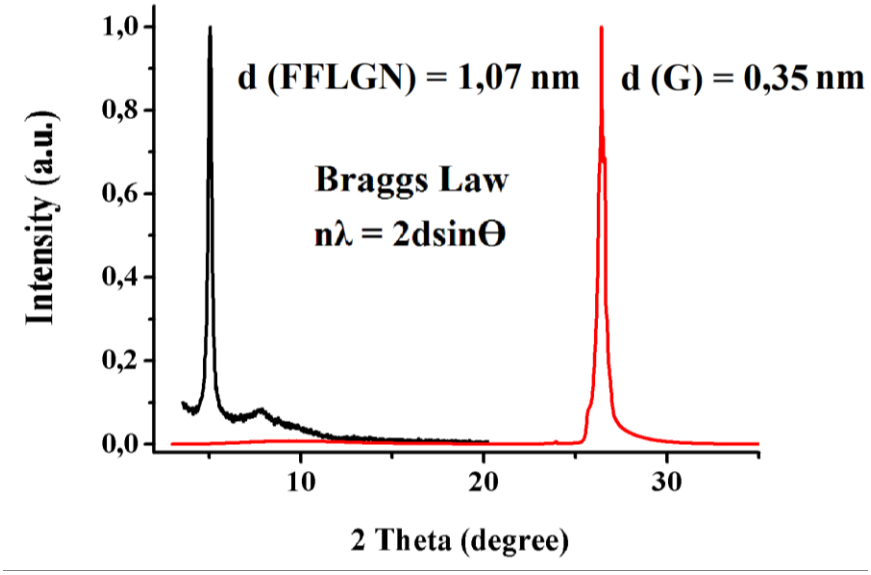

Figure 41 – XRD of graphite and FFLGN

Interpretation of the diffractogram allows to determine the interplanar distance in the initial FFLGN (d = 0.79 nm) and in graphite (d = 0.35 nm). The results obtained are closely correspond with the literature data [199-201, 203-206].

According to Figure 41, compared with HOPG, the initial FFLGN has a more interlayer distance (d_{GO}) due to its intercalated H_2O molecules and various oxide groups.

The temperature dependence of the XRD of the FFLGN and reduced FFLGN samples were measured after reduction at various temperatures of 150 °C, 300 °C, 500 °C, 900 °C has shown in figure 42 (a, b, c, d, e).

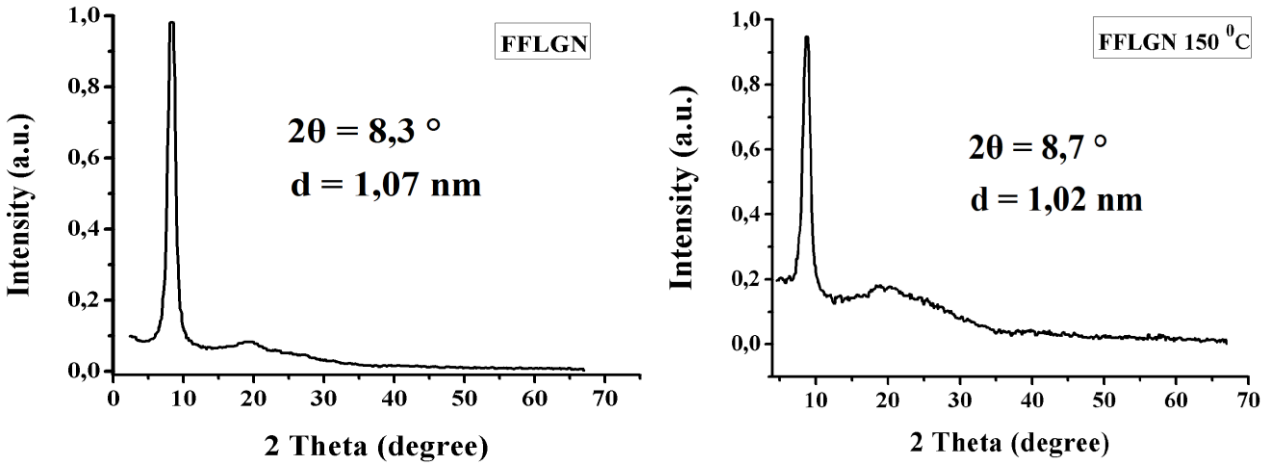

a) b)

Figure 42 – XRD spectra of the FFLGN and reduced FFLGN, page 1

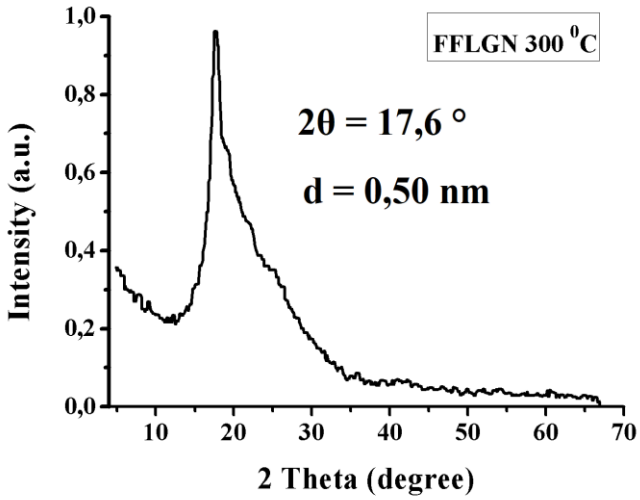

c)

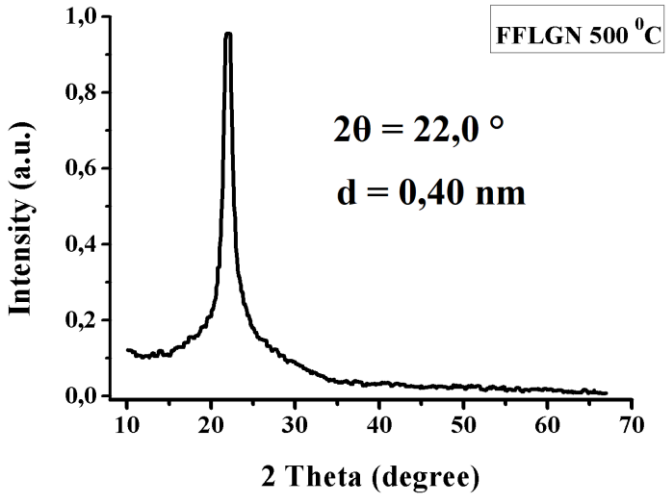

d)

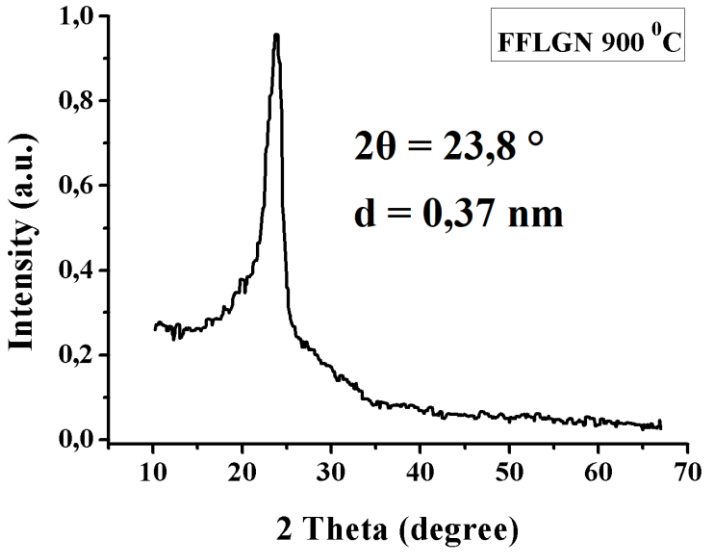

e)

Figure 42, page 2

According to Figure 42, we can observe that with increasing reduction temperature of the sample the interplanar distance FFLGN decreases. This means that as the temperature increases water molecules first evaporate, then the process of decomposition of labile (unstable) oxygen-containing functional groups such as carboxyl, aldehyde, hydroxyl, carbonyl occurs, then stable oxygen-containing groups (mainly epoxides) are removed, which changes the interplanar distance.

Table 5 shows the interplanar distances of the FFLGN samples at thermal reduction temperatures of 150 °C, 300 °C, 500 °C, 900 °C.

Table 5 XRD of FFLGN and reduced FFLGN samples at 150 °C, 300 °C, 500 °C, 900 °C.

№	Sample Name	2θ	d interplanar distance (nm)
1	FFLGN	8,3	1,07
2	reduced FFLGN 150 ˚C	8,7	1,02
3	reduced FFLGN 300 ˚C	17,6	0,50
4	reduced FFLGN 500 ˚C	22,0	0,40
5	reduced FFLGN 900 ˚C	23,8	0,37

According to table 5 we can see an increasing in 2θ=8.3-23.8˚ and a decreasing in the interplanar distance d=1.1-0.3 nm. The highest peaks of 2θ are detected at 22.0 and 23.8˚ at reduction temperatures of 500 ˚C, 900 ˚C, and the smallest interplanar spacing 0.4 and 0.3 nm in these samples is observed.

In the initial FFLGN, the interplanar distance was d=1.1 nm, and 2θ=8.3˚, after the reduction of this sample at 150 ˚C d is 1.0 nm, and 2θ = 8.7, according to these values, a slight change is observed. This change is explained by the fact that when FFLGN 150 ˚C is reduced, water molecules evaporate, therefore, the interplanar distance decreases. A significant change can be seen in the reduced sample FFLGN 300 ˚C. Compared with the reduced FFLGN sample of 150 ˚C on the reduced FFLGN sample of 300 ˚C, the interplanar spacing is d = 0.5 nm, two times smaller than the reduced FFLGN 150 ˚C, and 2θ doubled, which equals 17.6.

This is due to the decomposition of labile (unstable) oxygen-containing functional groups, such as carboxyl, aldehyde, hydroxyl, carbonyl. Due to the removal of unstable and stable oxygen-containing groups, a significant change is observed on the reduced FFLGN 500˚C sample. Compared with sample reduced FFLGN of 300 ˚C,during the thermal treatment of the reduced FFLGN 500˚C, hydroxyl and carboxyl groups are removed between 500 and 600˚C, therefore, the interplanar distance is d = 0.4 and 2θ = 22.0.

Between the temperatures of 600 and 1000 °C the remaining hydroxyl and epoxy groups belonging to the stable oxygen-containing groups are gradually removed, as a result of which there is a slight change is observed on the sample of the reduced FFLGN 900 °C in comparison with reduced FFLGN 500 °C. The interplanar spacing of the reduced FFLGN 900 °C is d = 0.4, and 2θ = 23.8. Based on the XRD spectra discussed above we can observe a significant shift on the reduced FFLGN sample at 300 °C compared to the reduced FFLGN at 150 °C, and at further sample reduction temperatures slight changes are observed.

Thus, according to the results obtained, the thermal treatment of FFLGN samples affects decreasing the interplanar spacing d from 1.1 to 0.3 nm, which is explained by the removal of oxygen-containing functional groups. In addition, the most important process of thermal reduction of FFLGN at different temperatures contributes to the large-scale production of few-layer graphene nanostructures. Also,

the most important is the creation of a humidity sensor based on the FFLGN membrane and the study of its electrophysical characteristics, which are presented in the next chapter.

3.2.7 TGA of the FFLGN and reduced FFLGN membranes

To characterize the FFLGN membrane after reduction at different temperatures in a hydrogen atmosphere, we determined chemical functionalization using TGA, which is the appropriate equipment for this analysis. TGA of FFLGN samples was investigated by using TGA Q50 equipment.

The experiment was performed under the following conditions: balanced nitrogen gas, flow rate 40 ml/min; the flow rate of gas on the sample 60 ml/min; heating rate 20 °C/min; final temperature 900 °C. FFLGN TGA consists mainly of three stages in weight loss. At the first stage, approximately 10 % of the mass is lost at a temperature of 100 °C, in which the H_2O molecules are removed in the FFLGN layers. At the second stage, at a temperature of 225 °C about 30% of the mass accompanying the thermal decomposition of unstable and stable oxygen-containing functional groups are lost. In the last stage, 45% of the mass is lost at a temperature about 620 °C, mainly due to the burning of the carbon skeleton.

We investigated the TGA of FFLGN and reduced FFLGN at the temperatures of 150 °C, 300 °C, 500 °C, 900 °C. Using this method, thermal stability and chemical functionalization were determined, that is a quantitative assessment of the surface functional groups FFLGN and reduced FFLGN, the results of which are shown in Figure 43 (a, b, c, d, e).

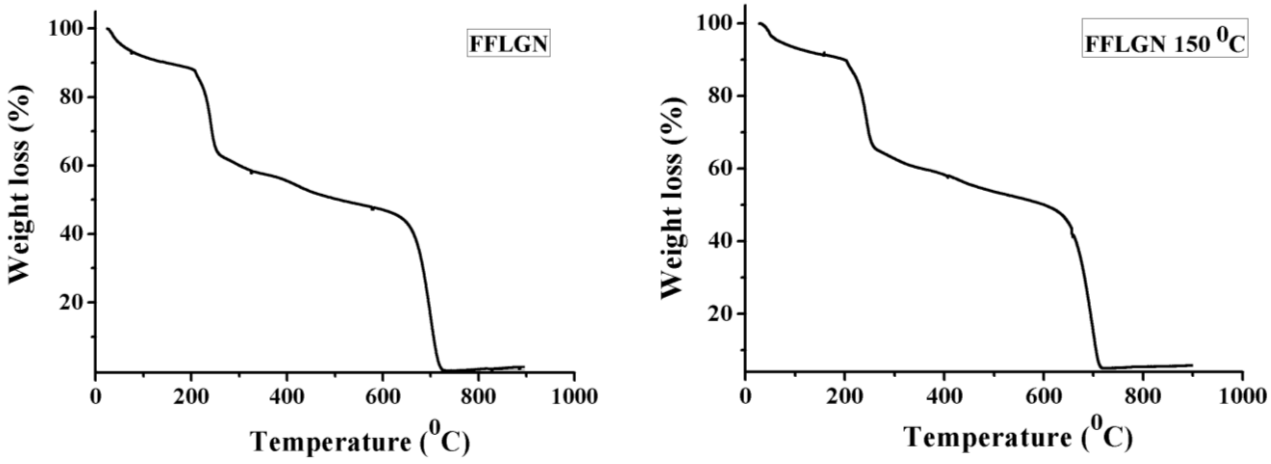

a) b)

Figure 43 – TGA of FFLGN and reduced FFLGN samples, page 1

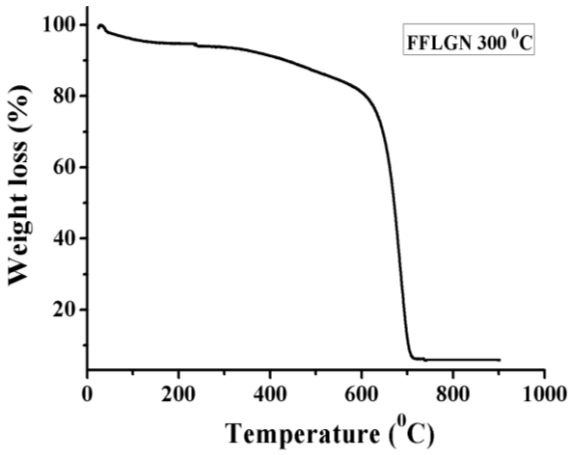

c)

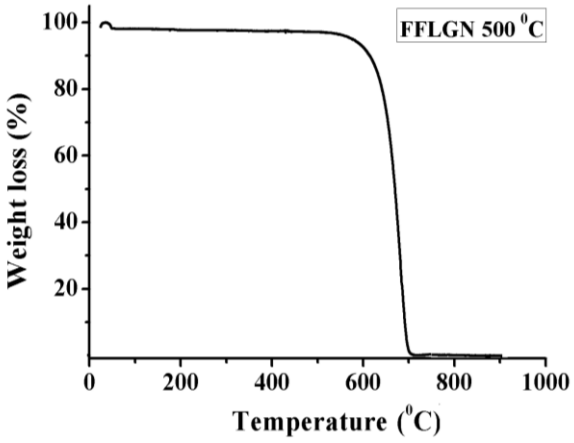

d)

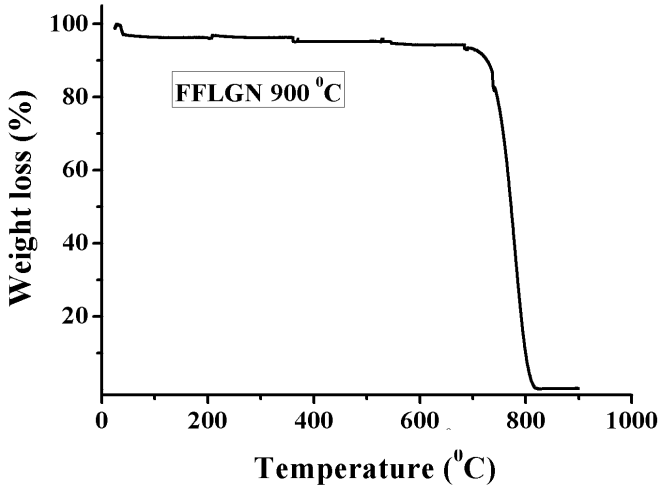

e)

Figure 43, page 2

Figure 43 (a) shows the analysis of the TGA conducted to verify the stability of the initial FFLGN. The first stage can be seen up to 100°C, which corresponds to the evaporation of the H_2O molecule. The second peak is reflected in the region of 250 °C, in connection with the pyrolysis of labile oxygen-containing groups, which corresponds to the evolution of CO and CO_2 from FFLGN. The third exothermic peak is observed at 700 °C due to the burning of the carbon skeleton of FFLGN. According to TGA, the mass loss of FFLGN occurred in three stages. At the first stage, at temperatures from 25 °C to 100 °C, about 10% of the sample mass is lost due to evaporation of adsorbed H_2O molecules in FFLGN [199, 200]. In the second stage, between 100 °C and 250 °C, there is a mass loss of about 30% due to the decomposition of labile (unstable) oxygen-containing functional groups such as carboxyl, aldehyde, hydroxyl, carbonyl and carboxylic acid with the formation of CO, CO_2 and H_2O [199-201]. Also, it is stated that at a temperature of ~ 200 °C, FFLGN will be effectively reduced to a highly conducting reduced FFLGN. In the third stage, between 250-650 °C, about 50 % of the sample mass is lost and mass loss is observed more slowly due to the decomposition of stable oxygen-containing

groups (mainly epoxides), and this is also due to the burning of the FFLGN skeleton [199-201]. At the end, at temperatures of 650-750˚C, the carbon skeleton is completely burned. According to Figure 43 (b), the main mass loss of reduced FFLGN 150˚C occurs in the following three main stages: about 100 °C; 250 °C; 650 °C. At a temperature of about 100 °C, about 10 % of the mass is lost; at 250 °C, about 32% is lost; at a temperature of 650 °C, about 50 % mass loss occurs. The results of the sample reduced FFLGN 150 °C show that the adsorbed water molecules first evaporate, then unstable oxygen-containing functional groups are removed, such as carboxyl, aldehyde, hydroxyl, carbonyl, and eventually the carbon skeleton burns (figure 43 (b)). According to the spectrum of TGA in figure 43 (c) compared with reduced FFLGN 150 °C, mass loss of reduced FFLGN 300 °C occurs at temperatures from 250-650 °C about 40% of mass is lost, which is accompanied by the removal of stable oxygen-containing groups, then from 650 °C begins the combustion of carbon.

The TGA reduced FFLGN 500°C, which is introduced in Fig. 43 (g), the main mass loss, occurs at 650 °C and, compared with the previous samples, the removal of unstable groups is not observed and the remaining stable oxygen-containing functional groups are gradually removed. Basically, unstable functional groups and part of the stable oxygen-containing functional groups were removed during the thermal reduction of FFLGN 500°C. According to figure 43 (e) reduced FFLGN 900 °C, the mass loss is observed in the region from 650-780 °C, in which the carbon skeleton is burned. Also, the results of this sample of FFLGN 900 °C are similar to the reduced FFLGN at 500 °C, which does not remove oxygen-containing functional groups, since they were removed during thermal reduction to 500 °C.

Thus, TGA is the appropriate equipment for determining thermal stability and chemical functionalization, that is, quantifying the surface functional groups FFLGN and reduced FFLGN.

This analysis method allows obtaining information at what temperatures of thermal reduction, unstable and stable functional oxygen-containing groups are removed, which is carried out according to comparison with known literature data on three stages of mass loss, as well as on four important temperature zones [199-201]. According to the obtained results of TGA it is shown that at temperatures from 150-300 °C, the main mass leaves, from 300-900 °C, the release of functional oxygen-containing groups is much weaker, which agrees well with experimental data in section 3.2.3.

3.2.8 Creation a humidity sensor based on an FFLGN membrane and studying its electrophysical characteristics

In this section, we present the results of the humidity sensor research on the stability of the capacitance reading and electrical resistance under different levels of constant humidity as a function of time, also, the dependence of capacitance and the dependence of the electrical resistance on humidity. The FFLGN membrane sensor was tested under fixed humidity conditions in a wide range at room temperature for 10 hours [203-206].

The most important process in the creation of a sensor is a synthesis of initial material. In our condition, FFLGN membrane was used as initial material. To obtain this membrane, FFLGN was originally synthesized using the modified Hummers method, the synthesis of this material and its characteristics are discussed in Section 3.2.1 in Figure 28. After the synthesis of FFLGN, the FFLGN membrane was obtained from its liquid solution using vacuum filtration, the details of the preparation are indicated in section 3.2.3 in Figure 34. The characteristics of the obtained initial material FFLGN and the membrane FFLGN were investigated using SEM, Raman spectroscopy, XRD, optical microscopy, TGA results are discussed in subsections 3.2.4-3.2.7 in Figures 37, 38, 40 (a), 41 (a), 42, 43 (a). The obtaining results confirm with the properties of FFLGN and these results correspond with known literature data.

The design of the humidity sensor is shown in Figure 44, where the FFLGN membrane was mounted on a dielectric substrate and connected at opposite ends with copper wire (0.15 mm in diameter) as electrodes with an FFLGN sample. These electrodes were covered with conductive silver paint contacts and left to dry overnight to ensure good electrical contact [205, 206].

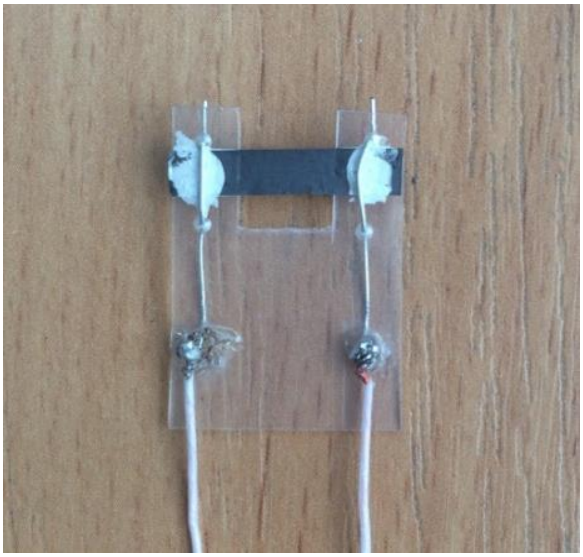

Figure 44 – Structure of the humidity sensor.

The substrate of the sensor has following dimensions: 2.5*1.8 cm, the FFLGN membrane thickness is about 20 μm, as shown in Figure 41 (b), the length is 2.5 cm, and width is 0.5 cm. The surface of the FFLGN membrane is open on both sides, which allows to react sensitively to the relative humidity of the environment.

As can be seen from the schematic in Figure 44, a humidity sensor based on FFLGN and an exemplary DHT 22 sensor by the Arduino platform are placed together in the testing chamber, which was used to control the humidity and DHT 22 sensor has the following technical characteristics: calculated to measure the level of humidity in the range from 0 to 100 % and the measurement accuracy is in the range of 2-5 %. Schematic representation of installation for investigating the sensitivity of the sensor to humidity shows in Figure 45.

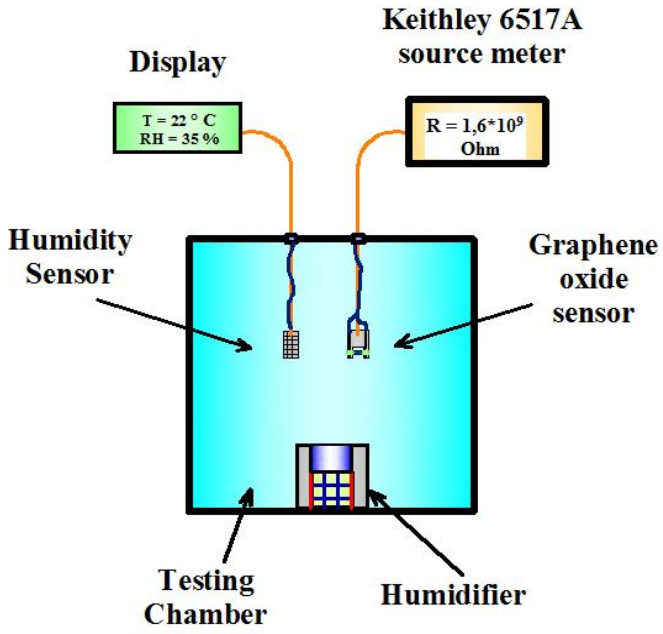

Figure 45 – Schematic view of the installation

The electro-physical parameters were studied as a function of humidity to determine the operating characteristics of the device. The stability of the electrical capacitance was monitored using the Keithley 6517A meter attached to the copper electrodes with alligator clips. The results of testing the sensor for the stability of the electrical capacitance under various levels of constant humidity, depending on the time are shown in Fig. 46. It can be seen from the results that the deviation of the electrical capacitance values of the structure for a long time does not exceed 2 %

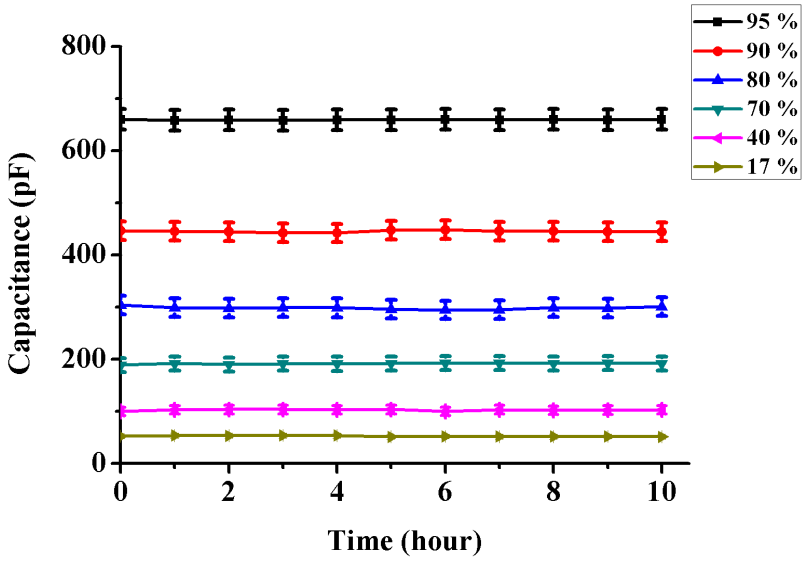

Figure 46 – Testing the humidity sensor for the stability of the capacitance reading under various levels of constant humidity as a function of time

The humidity sensor was kept in the sealed chamber with humidity levels controlled at 5 %, 25 %, 50 %, 75 %, 100 % for 10 hours. The results of testing the sensor for the stability of the electrical resistance under various levels of constant humidity, depending on the time are shown in Figure 47. It can be seen from the results that the deviation of the electrical resistance values of the structure for a long time does not exceed 2 %.

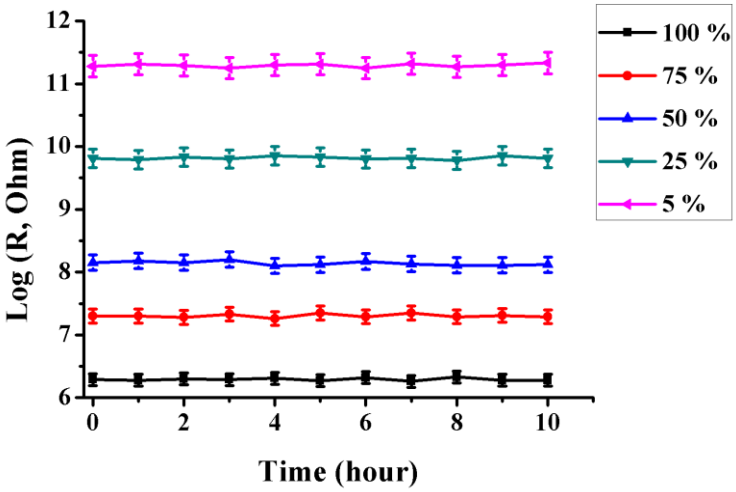

Figure 47 – Testing the humidity sensor on the stability of the electrical resistance readings under different humidity levels

Figure 48 shows the dependence of capacity on humidity. This figure shows that as the humidity level increases, the capacity of the sensor increases. Significant changes in capacity are observed at 70%, 80%, 90%, 95% humidity, this is due to the fact that a large amount of water vapor penetrates into the interplanar distance of FFLGN membrane and due to the high dielectric permeability (constant) increases the electrical capacitance.

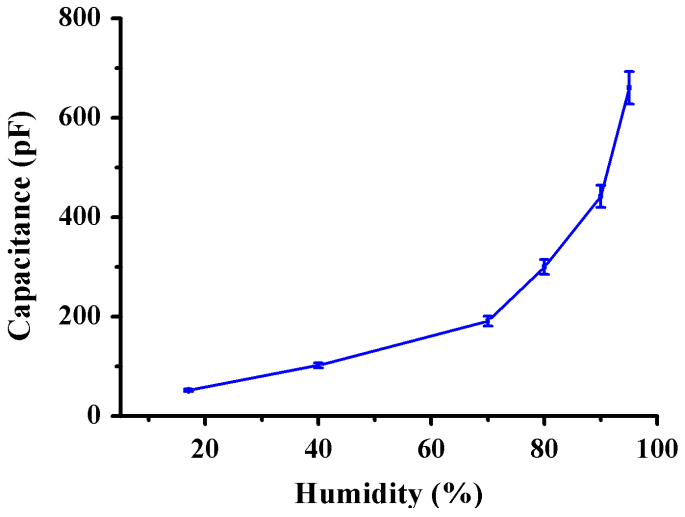

Figure 48 – Dependence of capacity on humidity

The electrical resistance versus humidity is presented in Figure 49. This image shows that the electrical resistance of the sensor decreases from 11,5 to 6,3 Log (R, Ohm) with increasing humidity at the range of 5-100 %.

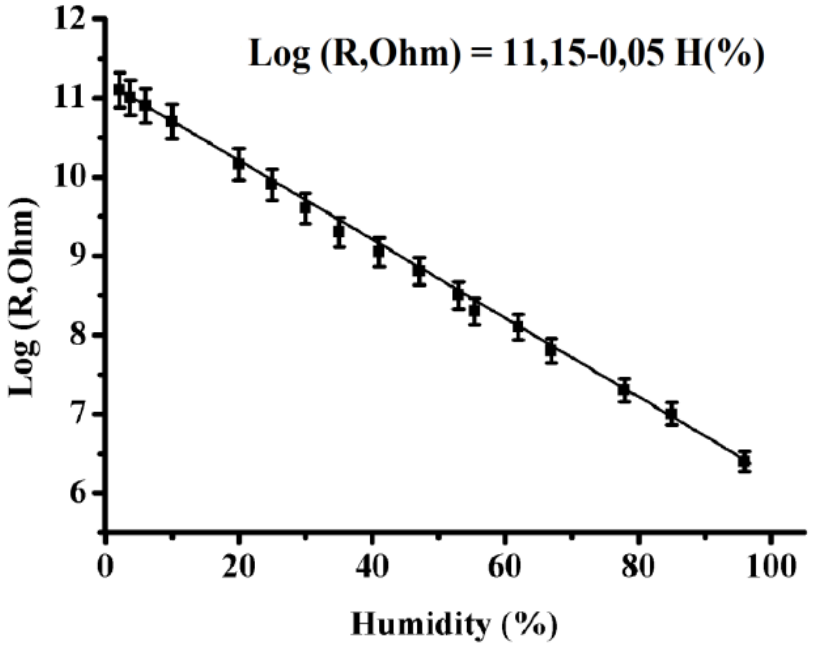

Figure 49 – Dependence of the electrical resistance on humidity.

In the process of raising the humidity in the chamber, a drastic decrease in electrical resistance is observed, this would indicate a large amount of water vapor penetrated into the interplanar distance and is also adsorbed on the surface of the sample altering the resistance.

We also studied the recovery and response of the humidity sensor. The recovery and response time of the sensor was tested at the range from 5 to 100 % humidity. Response dynamics and recovery were measured in the same way as we measured the stability of the electrical resistance.

The dynamics of the response of the humidity sensor as a function of time was studied using the sealed chamber with handmade humidifier. According to Figure 50, a decrease in electrical resistance is observed in entire range of relative humidity. This is because a large number of water molecules are adsorbed on the FFLGN surface, which significantly increases its conductivity due to proton-electron exchange between FFLGN and the adsorbed molecules. There is also the similar mechanism of changes in electrical conductivity, due to the influence of a water molecule as a result of which proton-electronic changes occur [203-206]. Figure 50 shows the dynamics of the humidity sensor response.

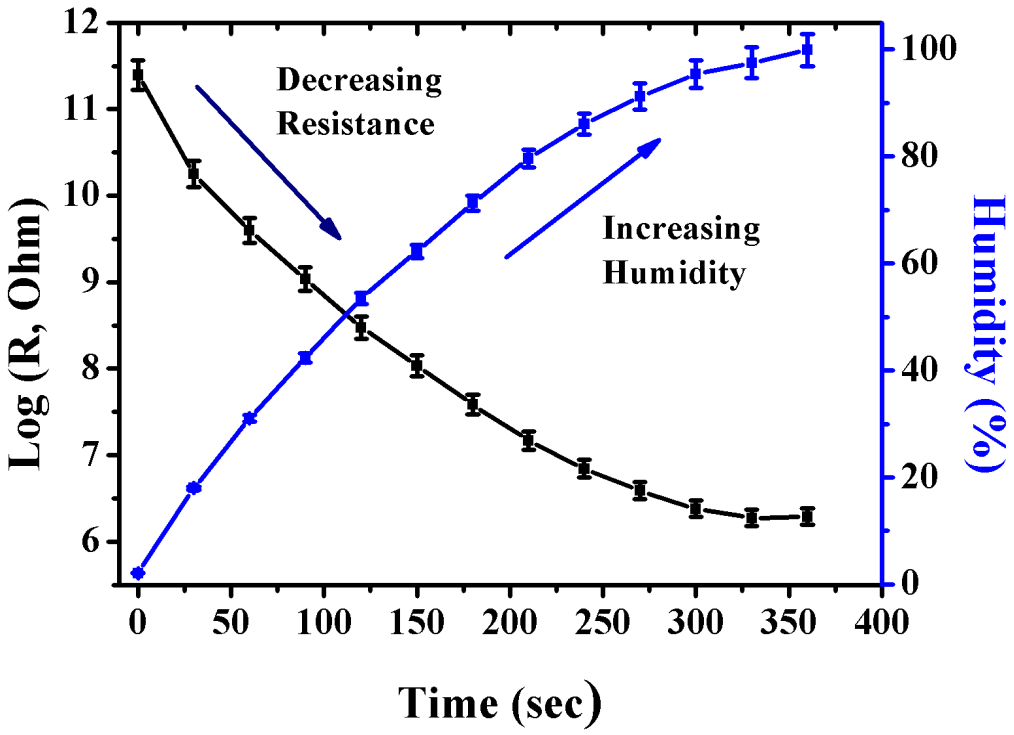

Figure 50 – Dynamics of the response.

Recovery time of the sensor can be seen in Fig. 51. Increasing electrical resistance of the structure was recorded as a function of time using the Keithley 6517A source meter

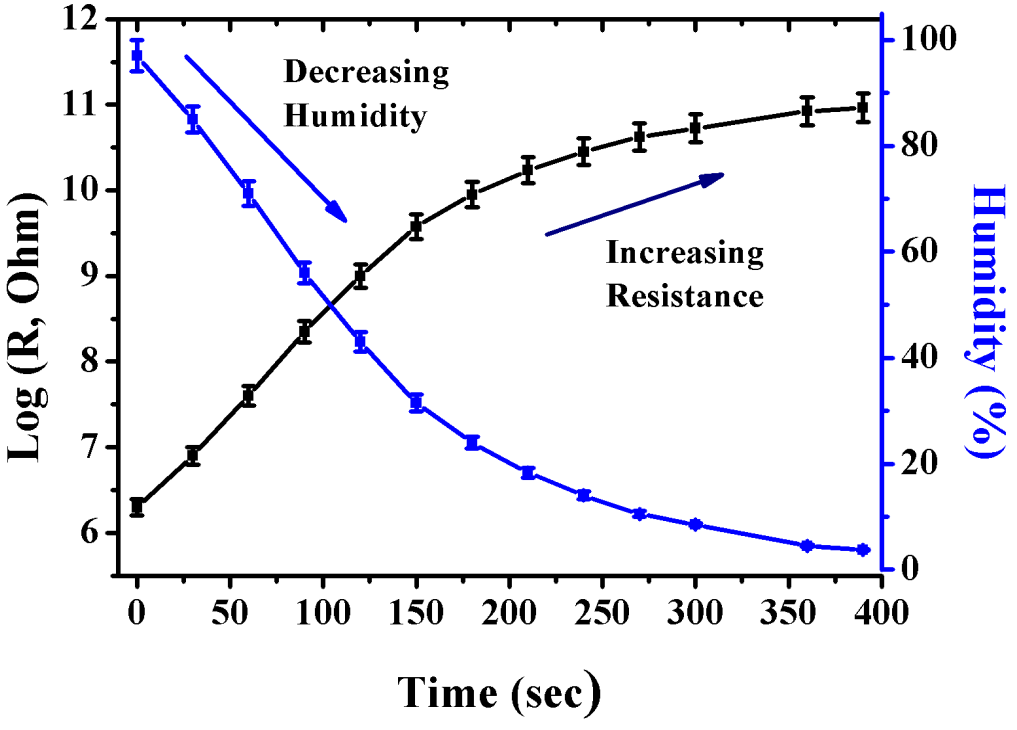

Figure 51 – Recovery dynamics.

Figure 52 shows the response and recovery dynamics of the humidity sensor.

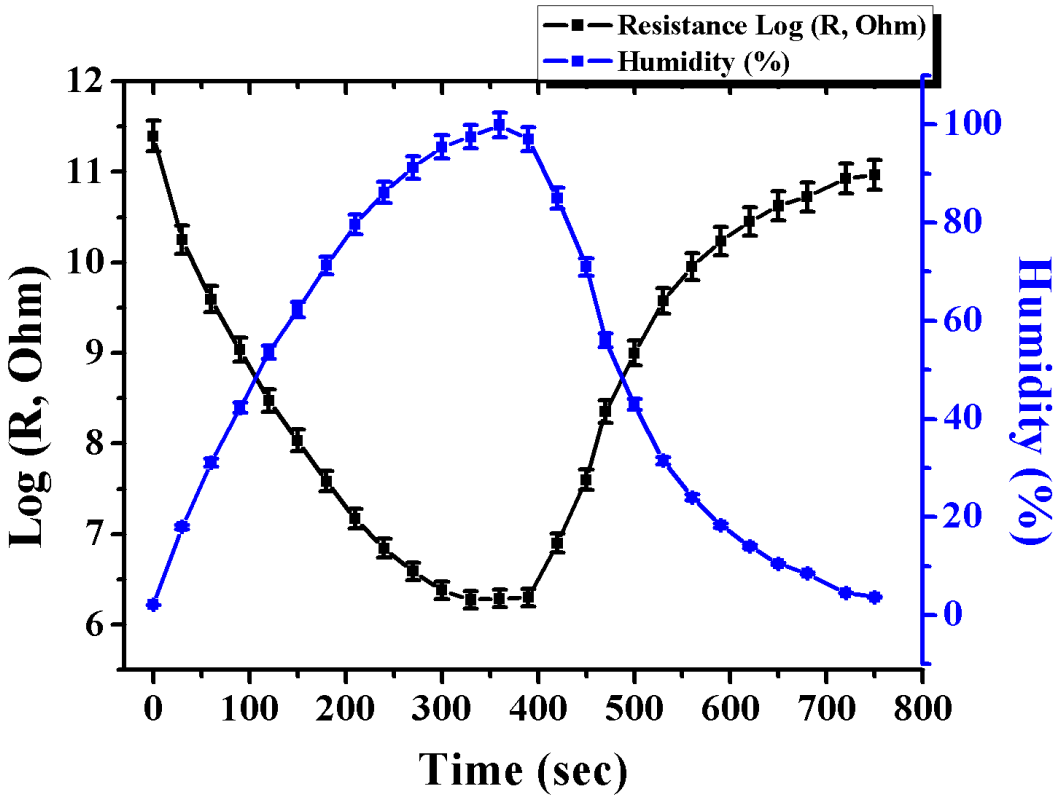

Figure 52 – Dynamics of response and recovery.

The changing in the electrical resistance of the sample mainly depends on the adsorption of the water molecule on the surface of FFLGN membrane, therefore the electrical conductivity depends on water molecule on the surface. When the humidity level decreases from 100 to 5 % (RH), adsorbed water molecules are removed, this leads to increased resistance. Significantly increases in the electrical resistance of the sample observed at the humidity level from 100 to 20 % and resistance changes from 6,4 up to 10 Log (R, Ohm).

In section 1.11 (Table 2) we made a comparison of the performance of humidity sensors based on FFLGN with similar types of humidity sensors according to the following characteristics: dynamics of response and recovery, humidity detection range. According to the table 2, in comparison with sensors our device [206] has an advantage in response and recovery time, which has the same time of 360 s, as well as a wide range of relative humidity from 5-100%.

Thereby in this thesis we created humidity sensor based on FFLGN membrane, which FFLGN membrane was obtained from FFLGN aqueous dispersion. The FFLGN aqueous dispersion was synthesized via a modified Hummers method by using a pure natural graphite with various acids, then from this FFLGN aqueous via vacuum filtration, FFLGN membrane was produced. The created humidity sensor was tested in a wide range of humidity level from 5 to 100 % (RH) for studying electro-physical characteristics. The humidity sensor was tested for the stability of the

electrical resistance at next multiple humidity levels: 5 %, 25 %, 50 %, 75 %, 100 % for 10 hours at room temperature and obtained measurement results show the stability of the sensor (±2 %) in the entire humidity range. Based on obtained results significant changes in the values of electrical resistance were observed, which are associated with the absorption of a water molecule on the surface and penetration into the interplanar distance of FFLGN membrane. According to the obtained electro-physical characteristics, we can say that the sensor is able to work stably at a wide range of humidity and respond rapidly to changes in humidity, which allows it to be useful as a precise and sensitive device.

Conclusions for section 3

Computer simulations of some possible stable structures of graphene and few-layer graphene, functionalized by Ga, FFLGN, reduced FFLGN and calculating their energy and structural characteristics were performed.

The technology of obtaining FFLGN and the FFLGN membrane using the modified Hammers method was optimized, which leads to the large-scale production of graphene and also several time filtration and washing with a 5% HCl solution with a centrifuge helps to obtain a clean FFLGN solution.

Reduced FFLGN samples at different temperatures contribute to the changes in the optical, electrical, and structural characteristics.

The thermal reduction of FFLGN films led to a decrease sheet resistance both for clean and with chlorine and sulfur impurities, also average thickness of layers decreased.

Also, the reduced membranes were investigated by Raman spectroscopy and XRD, which demonstrates the removal of functional groups.

Thus, a humidity sensor based on FFLGN was created, which compared to a similar sensitive element had the advantage of a wide range of sensitivity and a symmetrical response due to the use of purified initial FFLGN.

CONCLUSION

1. Computer simulation shows typical configurations of Ga-doped graphene and various arrangements of their atoms, types of oxygen bonds with graphene, a model of the possible reduce process of FFLGN, and also the binding energies of the functionalizing graphene-O and graphene-O-H groups were theoretically investigated.

2. The technology of obtaining FFLGN in strong oxidants such as H_2SO_4, $NaNO_3$, $KMnO_4$ was developed. Then FFLGN films were obtained and their optical and electrical characteristics were investigated depending on the reduction in the temperature range from 80-280 °C. It was experimentally established that with increasing of temperature of reduction the significant changes of visible light transmission are observed between temperatures RT and 160 °C, as well as 200 °C and 280 °C, where the percentage of transmission decreases approximately by 30 % from initial position, also sheet resistance decreased from 5 to 2.5 MΩ/square at temperatures of 200 °C - 280 °C and sheet resistance of the pure FFLGN at 280 °C is more than 5 times lower than the sheet resistance of the impure FFLGN and is equal to 13 MΩ/square, and according the AFM results average thickness was decreased by 50 % from the initial sample thickness at 280 °C.

3. The technology of preparation FFLGN membrane was developed. The influence of temperature on the structure and composition of the FFLGN membrane was studied by SEM and EDS, Raman spectroscopy, TGA, XRD, optical microscopy. FFLGN membranes were reduced in a hydrogen atmosphere at temperatures of 150 °C, 300 °C, 500 °C, 900 °C, as a result of which TGA showed that the main mass loses at temperatures from 150-300 °C, from 300-900 °C much weaker. The elemental analysis by the EDS method showed changing in the C/O ratio from 4.18 to 45.08, as well as a decreasing in the interplanar distance from 1,07 to 0,37 nm and the thickness decreased by ~37%, that is explained by removal of oxygen-containing functional groups.

4. The electrophysical characteristics of the humidity sensor based on the FFLGN membrane were experimentally investigated, and the following characteristics of the sensor were achieved when exposed to different humidity levels: a wide range of relative humidity measurements from 5 to 100%; identical response and recovery time of 360 seconds, stability (+/- 2%) over the entire humidity range.

REFERENCES

1 Novoselov K.S., Jiang D., Schedin F., Booth T.J., Khotkevich V.V., Morozov S.V. and Geim A.K. Two-Dimensional Atomic Crystals // Proceedings of the National Academy of Sciences of the USA. – 2005. – Vol. 102, № 30. – P. 10451-10453.

2 Web-Resource, Scientifc Background on the Nobel Prize in Physics 2010. Graphene. http://www.nobelprize.

3 Hongwei Zhu., Zhiping Xu., Dan Xie.,Ying Fang. Graphene Fabrication, Characterizations, Properties and Applications. – United Kingdom: Academic Press. Elsevier Inc, 2018. – P. 272.

4 Boehm H.P., Clauss A., Hofmann U., and Fischer G.O. Thin Carbon Leaves // Zeitschrift Für Naturforschung. – 1962. – Vol. 17. – P. 150 - 153.

5 Oshima C., Itoh A., Rokuta E., and Tanaka T.. A hetero-epitaxial-double-atomic-layer system of monolayer graphene/monolayer h-BN on Ni (111) // Solid State Communications. – 2000. – Vol. 116, № 1. – P. 37 - 40.

6 Dreyer D.R., Ruoff R.S., Bielawski C.W. From conception to realization: an historical account of graphene and some perspectives for its future // Angew Chem. Int. Ed. – 2010. – Vol. 49. – P. 9336–9344.

7 Boehm H.-P. Setton R., Stumpp E. Nomenclature and terminology of graphite intercalation compounds // Carbon. – 1986. – Vol. 24. – P. 241- 245.

8 Boehm H.-P. Graphene-how a laboratory curiosity suddenly became extremely interesting // Angew. Chem. Int. Ed. – 2010. – Vol. 49. – P. 9332 - 9335.

9 Park S., Ruoff R.S. Chemical methods for the production of graphenes // Nature Nanotechnology. – 2009. – Vol. 4. – P. 217 - 224.

10 Stankovich S., Piner R.D., Chen X., Wu N., Nguyen S.T., Ruoff R.S. Stable aqueous dispersions of graphitic nanoplatelets via the reduction of exfoliated graphite oxide in the presence of poly(sodium 4-styrenesulfonate) // Journal of Material Chemistre. – 2006. – Vol. 16. – P. 155–158.

11 Shin H.-J., Kim K.K., Benayad A., et al. Efficient Reduction of Graphite Oxide by Sodium Borohydride and Its Effect on Electrical Conductance // Advanced functional materials. – 2009. – Vol. 19. – P. 1987 - 1992.

12 Geim A.K. Graphene prehistory // Physica Scripta. – 2012. – Vol. 2012, T 146. – P. 4.

13 Web-Resource, Dale A. C. Brownson, Craig E. Banks. The Handbook of Graphene Electrochemistry // Springer-Verlag London Ltd. P. 330. – 2014.

14 Kroto H.W., Heath J.R., Obrien S.C., Curl R.F., and Smalley R.E. C60: Buckminster fullerene // Nature. – 1985. – Vol. 318. – P. 162-163.

15 Oberlin A., Endo M., and Koyama T.. Filamentous growth of carbon through benzene decomposition // Journal of Crystal Growth. – 1976. – Vol. 32. – P. 335-349.

16 Iijima S., and Ichihashi T. Single-shell carbon nanotubes of 1-nm diameter // Nature. – 1993. – Vol. 363. – P. 603–605.

17 Bethune D.S., Kiang C.H., Devries M.S., Gorman G., Savoy R., Vazquez J., and Beyers R. Cobalt-catalysed growth of carbon nanotubes with single-atomic-layer walls // Nature. – 1993. – Vol. 363. – P. 605–607.

18 Hiremath N., Mays J., Bhat G., Recent developments in carbon fibers and carbon nanotube-based fibers: a review // Polymer Reviews. – 2017. – Vol. 57, № 2. – P. 339-368.

19 Arbuzov A.A., Muradyan V.E., and Tarasov B.P. Synthesis of few-layer graphene sheets via chemical and thermal reduction of graphite oxide // Proceedings of the International Conference Nanomaterials: Applications and Properties. – 2012. – Vol. 1, №. 1. – P. 4.

20 Singh V., Joung D., Zhai L., Das S., Khondaker S.I., and Seal S. Graphene based materials: past, present and future // Progress in Materials Science. – 2011. – Vol. 56, №.8. – P. 1178–1271.

21 Web-Resource, Sharon M., et al. Graphene: An Introduction to the Fundamentals and Industrial Applications. – USA: John Wiley & Sons, 2015. – P. 294.

22 Novoselov K.S., Geim A.K., Morozov S.V., et al. Two-dimensional gas of massless dirac fermions in graphene // Nature. – 2005. – Vol. 438. (7065) – P. 197-200.

23 Zhang Y.B., Tan Y.W., Stormer H.L., et al. Experimental observation of the quantum hall effect and berry's phase in graphene // Nature. – 2005. – Vol. 438. (7065) – P. 201-204

24 Berger C., Song Z.M., Li T.B., et al. Ultrathin epitaxial graphite: 2D electron gas properties and a route toward graphene-based nanoelectronics // J. Phys. Chem. B. – 2004. – Vol. 108, № 52. – P. 19912-19916.

25 Son Y.W., Cohen M.L., Louie S.G. Half-metallic graphene nanoribbons // Nature. – 2006. – Vol.444, № 7117. – P. 347-349.

26 Avouris P., Chen Z., Perebeinos V.. Carbon-based electronics // Nat. Nanotechnol. – 2007. – Vol. 2, № 10. – P. 605-613.

27 Nair R.R., Blake P., Grigorenko A.N., et al. Fine structure constant defines visual transparency of graphene // Science. – 2008. – Vol.320, № 5881. – P. 1308.

28 Ni Z.H., Wang H.M., Kasim J., et al. Graphene thickness determination using reflection and contrast spectroscopy // Nano Lett. – 2007. – Vol. 7, № 9. – P. 2758-2763.

29 Lee C., Wei X., Kysar J.W., et al., Measurement of the elastic properties and intrinsic strength of monolayer graphene // Science. – 2008. – Vol. 321, № 5887. – P. 385-388.

30 Stankovich S., Dikin D.A., Dommett G.H.B., et al. Graphene-based composite materials // Nature. – 2006. – Vol. 442, № 7100. – P. 282-286.

31 Stoller M.D., Park S., Zhu Y., et al. Graphene-based ultracapacitors // Nano Lett. – 2008. – Vol. 8, № 10. – P. 3498-3502.

32 Novoselov, K.S., Geim, A.K., Morozov, S.V., Jiang, D., Zhang, Y., Dubonos, S.V., Grigorieva, I.V., and Firsov, A.A. Electric field effect in atomically thin carbon films // Science. – 2004. – Vol. 306. – P. 666-669.

33 Shivaraman, Sh., Barton R.A., Yu X., Alden J., Herman, L. Chandrashekhar M., Park J., McEuen P.L., Parpia J.M., Craighead H.G. and Spencer M.G. Free-Standing Epitaxial Graphene // Journal of nano Letter. – 2009. – Vol. 9. – P. 3100-3105.

34 Reina, A., Jia, X.T., Ho, J., Nezich, D., Son, H., Bulovic, V., Mildred Dresselhaus, S., Kong, J. Large area, few-layer graphene films on arbitrary substrates by chemical vapor deposition // Nano Lett. – 2009. – Vol. 9, № 1. – P. 30–35.

35 Wonbong Choi, Jo-won Lee. Graphene Synthesis and Applications. – USA New York: Taylor & Francis Group, 2016. – P. 394.

36 Keun Soo Kim, Yue Zhao, Houk Jang, Sang Yoon Lee, Jong Min Kim, Kwang S. Kim, Jong-Hyun Ahn, Philip Kim, Jae-Young Choi, and Byung Hee Hong. Large-scale pattern growth of graphene films for stretchable transparent electrodes. // Nature. – 2009. – Vol. 457, № 7230. – P. 706–710.

37 Parvez K., Li R., Puniredd S.R., Hernandez Y., Hinkel F., Wang S., Feng X., Mu¨ llen K. Electrochemically exfoliated graphene as solution-processable, highly conductive electrodes for organic electronics // ACS Nano. – 2013. – Vol. 7, № 7. – P. 3598-3606.

38 Su C.Y., Lu A.Y., Xu Y., Chen F.R., Khlobystov A.N., Li L.J. High-quality thin graphene films from fast electrochemical exfoliation // ACS Nano. – 2011. – Vol. 5, № 7. – P. 2332-2339.

39 Liu N., Luo F., Wu H., Liu Y., Zhang C., Chen J. One-Step Ionic-Liquid-Assisted Electrochemical Synthesis of Ionic-Liquid-Functionalized Graphene Sheets Directly from Graphite // Advanced Functional Materials. – 2008. – Vol. 18. – P. 1518-1525.

40 Singh V.V et al. Greener Electrochemical Synthesis of High Quality Graphene Nanosheets Directly from Pencil and its SPR Sensing Application // Advanced Functional Materials. – 2012. – Vol. 22, № 11. – P. 2352–2362.

41 Ching-Yuan Su et al. High-quality thin graphene films from fast electrochemical exfoliation // ACS Nano. – 2011. – Vol. 5, № 3. – P. 2332-2339.

42 Sergey D, Scott G et al. A One-step, solvothermal reduction method for producing reduced graphene oxide dispersions in organic solvents // ACS Nano. – 2010. – Vol. 4, № 7. – P. 3845–3852.

43 Lerf A, He H, Forster M, Klinowski J. Structure of Graphite Oxide Revisited // J Phys Chem B. – 1998. – Vol. 102. – P. 4477–4482.

44 Cai W, Piner RD, Stadermann FJ, Park S, Shaibat MA, Ishii Y, Yang D, Velamakanni A, An SJ, Stoller M. Synthesis and solid-state NMR structural characterization of C-labeled graphite oxide // Science. – 2008. – Vol. 321. – P. 1815–1817.

45 He H, Riedl T, Lerf A, Klinowski J. Solid-State NMR Studies of the Structure of Graphite Oxide // J Phys Chem. – 1996. – Vol. 100. – P. 19954.

46 Ilyin A.M., Beall G.W., Tsyganov I.A. Simulation and study of bridge-like radiation defects in the carbon nanostructures // Journal of Computational and Theoretical Nanoscience. – 2010. – Vol. 7, № 10. – P. 2004-2007.

47 Ilyin A.M., Guseinov N.R., Tsyganov I.A. et al. Computer simulation and experimental study of graphane-like structures formed by electrolytic hydrogenation // Physica E. – 2011. – Vol. 43, № 6. – P. 1262-1265.

48 Yuhai Hu and Xueliang Sun. Chapter 7 Chemically Functionalized Graphene and Their Applications in Electrochemical Energy Conversion and Storage. Advances in Graphene Science, 2013. – P. 162-189.

49 Sharma R, Baik J, Perera C. Anomalously large reactivity of single graphene layers and edges toward electron transfer chemistries // Nano Letters. – 2010. – Vol. 10, № 2. – P. 398-405.

50 Lim H, Lee J, Shin H. Spatially resolved spontaneous reactivity of diazonium salt on edge and basal plane of graphene without surfactant and its doping effect // Langmuir. – 2010. – Vol. 26, № 14. – P. 12278-12284.

51 Da Chen, Hongbin Feng, and Jinghong Li. Graphene Oxide: Preparation, Functionalization, and Electrochemical Applications // Chem. Rev. – 2012. – Vol. 112, № 11. – P. 6027−6053. dx.doi.org/10.1021/cr300115g

52 Chernozatonskii, L.A. et al., Novel graphene-based nanostructures: physicochemical properties and applications., // Russian Chemical Reviews. – 2014, – Vol. 83, № 3. – P. 251-279.

53 Berger, C., Song, Z., Li, X., Wu, X., Brown, N., Naud, C., Mayou, D., Li, T., Hass, J., Marchenkov, A.N., Conrad, E.H., First, P.N. and De Heer, W.A. Electronic Confinement and Coherence in Patterned Epitaxial Graphene // Science. – 2006. – Vol. 312. – P. 1191-1196.

54 He H., Klinowski J., Forsterb M., Lerf A.A new structural model for graphite oxide // Chemical Physics Letters. – 1988. – Vol. 287, № 1-2. – P. 53-56.

55 Web-Resource, Sun L, Fugetsu B. Massive production of graphene oxide from expanded graphite https://arxiv.org/ftp/arxiv/papers/1301/1301.3253.pdf

56 Liao K.H, Mittal A, Bose S, Leighton C, Mkhoyan K.A, Macosko C.W. Aqueous only route toward graphene from graphite oxide // ACS Nano. – 2011. – Vol. 5, №.2. – P. 1253-1258.

57 Mei XG, Ouyang JY. Ultrasonication-assisted ultrafast reduction of graphene oxide by zinc powder at room temperature // Carbon. – 2011. – Vol. 49, №.15. – P. 5389-97.

58 Dey R.S, Hajra S, Sahu R.K, Raj C.R, Panigrahi M.K: A rapid room temperature chemical route for the synthesis of graphene: metal-mediated reduction of graphene oxide // Chem Commun. – 2012. – Vol. 48, № 12. – P. 1787-1789.

59 Najafi F., Rajabi M. Thermal gravity analysis for the study of stability of graphene oxide–glycine nanocomposites // Int Nano Lett. – 2015. – Vol. 5. – P. 187–190. DOI 10.1007/s40089-015-0154-7.

60 Algothmi, W.M., Murthy Bandaru, N., Yu, Y., Shapter, J.G., Ellis, A.V. Alginate–graphene oxide hybrid gel beads: an efficient copper adsorbent material // J. Colloid Interface Sci. – 2013. – Vol. 397. – P. 32–38.

61 Dimiev A.M. and Tour J.M. Mechanism of Graphene Oxide Formation // ACS Nano. – 2014. – Vol. 8, № 3. – P. 3060–3068.

62 Huitao Yu, Bangwen Zh, Chaoke B, Ruihong Li & Ruiguang X. High-efficient Synthesis of Graphene Oxide Based on Improved Hummers Method // Scientific Reports. – 2016. – Vol. 6, № 1. – P. 36143. DOI: 10.1038/srep36143.

63 Eda, G.; Chhowalla, M. Chemically Derived Graphene Oxide: Towards Large-Area Thin-Film Electronics and Optoelectronics // Adv. Mater. – 2010. – Vol. 22, № 12. – P. 2392.

64 Spitalsky, Z., Danko, M. & Mosnacek, J. Preparation of functionalized graphene sheets // Curr Org Chem. – 2011. – Vol. 15. – P. 1133–1150.

65 Da Chen, Hongbin Feng and Jinghong Li. Graphene Oxide: Preparation, Functionalization, and Electrochemical Applications // Chem. Rev. – 2012. – Vol. 112. – P. 6027−6053.

66 Li, X. L.; Zhang, G. Y.; Bai, X. D.; Sun, X. M.; Wang, X. R.; Wang, E. G.; Dai, H. J. Highly conducting graphene sheets and Langmuir-Blodgett films // Nat. Nanotechnol. – 2008. – Vol. 3, № 9. – P. 538-542.

67 Kim, F.; Cote, L. J.; Huang, J. X. Graphene oxide: surface activity and two-dimensional assembly // Adv. Mater. – 2010. – Vol. 22, № 17. – P. 1954-1958.

68 Kuila T, Bose S, Mishra AK, Khanra P, Kim NH, Lee JH. Chemical functionalization of graphene and its applications // Prog Mater Sci. – 2012. – Vol. 57, № 7. – P. 1061-105.

69 Vimlesh C, Kwang S. Highly Selective Adsorption of Hg2+ by polypyrrole-reduced graphene oxide composite // Chemical Communications. – 2011. – Vol. 47, № 13. – P. 3942-3944.

70 Paulchamy B, Arthi G, Lignesh BD. A simple approach to stepwise synthesis of graphene oxide nanomaterial // Journal of Nanomedicine & Nanotechnology. – 2015. – Vol. 6, № 1. – P. 253.

71 Eda G, Chhowalla M. Chemically derived graphene oxide: towards large-area thin-film electronics and optoelectronics // Adv Mater. – 2010. – Vol. 22, № 22. – P. 2392–2415.

72 Brodie B.C. On the atomic weight of graphite // Philosophical Transactions of the Royal Society of London. – 1859. – Vol. 149. – P. 249–259.

73 Hummers W.S, Offeman R.E. Preparation of graphitic oxide // Journal of the American society. – 1958. – Vol. 80, № 3. – P. 1339.

74 Marcano D.C, Kosynkin D.V, Berlin J.M, Sinitskii A, Sun Z, Slesarev A, Alemany L.B, Lu W, Tour J.M. Improved synthesis of graphene oxide // ACS Nano. – 2010. – Vol. 4. – P. 4806–4814.

75 Alam S.N, Sharma N., Kumar L. Synthesis of Graphene Oxide (GO) by Modified Hummers Method and Its Thermal Reduction to Obtain Reduced Graphene Oxide (rGO) // Graphene. – 2017. – Vol. 6, №.1. – P. 1-18.

76 Staudenmaier L . Verfahren zur Darstellung der Graphit säure // Berichte der deutschen chemischen Gesellschaft. – 1898. – Vol. 31, № 2. – P. 1481–1487.

77 Hofmann U and Holst R. Über die säurenatur und die methylierung von graphit oxyd // Berichte der deutschen chemischen Gesellschaft. A and B. – 1939. – Vol. 72, № 4. – P. 754–771.

78 Marcano D.C. et al. Improved synthesis of graphene oxide // ACS Nano. – 2010. – Vol. 4, № 8. – P. 4806–4814.

79 JIA T.T., SUN B.Zh. et al. Bonding of Hydroxyl and Epoxy Groups on Graphene: Insights from Density Functional Calculations // JIEGOU HUAXUE Chinese J. Struct. Chem. – 2013. – Vol 32, № 10. – P. 1475─1484.

80 Rourke J.P. et al.. The real graphene oxide revealed: stripping the oxidative debris from the graphene-like sheets // Angew. Chem. Int. Ed. – 2011. – Vol. 50, № 14. – P. 3173–3174.

81 Jinxia Ma, Dan P. and Xinfa D. Recent Developments of Graphene Oxide-Based. Membranes: A Review // Membranes. – 2017. – Vol. 7, № 52. – P. 29. doi:10.3390/membranes7030052.

82 Kim J, Cote LJ, Huang J. Two dimensional soft material: new faces of graphene oxide // Acc Chem Res. – 2012. – Vol. 45, № 8. – P. 1356-64.

83 Du J. and Cheng H.M. The Fabrication, Properties, and Uses of Graphene/Polymer Composites // Macromolecular chemistry and physics. – 2012. – Vol. 213, № 10-11. – P. 1060-1077.

84 Piner, R.D.; Ruoff, R.S.; Stankovich, S.; Zimney, E.J.; Evmenenko, G.; Dikin, D.A.; Dommett, G.H.B.; Nguyen, S.T. Preparation and characterization of graphene oxide paper // Nature 2007. – 2014. – Vol. 448, № 7152. – P. 457–460.

85 Dreyer D.R, Park S, Bielawski C.W., Ruoff R.S. The chemistry of graphene oxide // Chem Soc Rev. – 2010. – Vol. 39, № 1. – P. 228-40. doi: 10.1039/b917103g.

86 Stankovich S., Dikin D.A., Piner R.D., Kohlhaas K.A., Kleinhammes A., Jia Y., Wu Y., Nguyen S.T. and Ruoff R.S. Synthesis of graphene-based nanosheets via chemical reduction of exfoliated graphite oxide // Carbon. – 2007. – Vol. 45, № 7. – P. 1558–1565.

87 Stankovich S, Dikin D.A, Dommett G.H.B, Kohlhaas K.M, Zimney E.J, Stach E.A, et al. Graphene-based composite materials // Nature. – 2006. – Vol. 442, № 7100. – P. 282–286.

88 Schniepp H.C, Li J-L, McAllister M.J, Sai H, Herrera-Alonso M, Adamson D.H, et al. Functionalized single graphene sheets derived from splitting graphite oxide // J Phys Chem B. – 2006. – Vol. 110, № 17. – P. 8535–8539.

89 Zhu Y, Murali S, Stoller M.D, Velamakanni A, Piner R.D, Ruoff R.S. Microwave assisted exfoliation and reduction of graphite oxide for ultracapacitors // Carbon. – 2010. – Vol. 48, № 7. – P. 2118–2122.

90 Zhang Y, Guo L, Wei S, He Y, Xia H, Chen Q, et al. Direct imprinting of microcircuits on graphene oxides film by femtosecond laser reduction // Nanotoday. – 2010. – Vol. 5, № 1. – P. 15–20.

91 Kaniyoor A, Baby T.T, Arockiadoss T, Rajalakshmi N, Ramaprabhu S. Wrinkled graphenes: A study on the effects of synthesis parameters on exfoliation-reduction of graphite oxide // J Phys Chem C. – 2011. – Vol. 115. – P. 17660–17669.

92 Zhou M, Wang Y, Zhai Y, Zhai J, Ren W, Wang F, et al. Controlled synthesis of large-area and patterned electrochemically reduced graphene oxide films // Chem Euro J. – 2009. – Vol. 15, № 25. – P. 6116–6120.

93 Ramesha G.K, Sampath S. Electrochemical reduction of oriented graphene oxide films: an in situ raman spectro electrochemical study // J Phys Chem C. – 2009. – Vol. 113, № 19. – P. 7985–7989.

94 Seung H.H. Chapter 5 Thermal Reduction of Graphene Oxide. Physics and Applications of Graphene - Experiments, 2011. – P.73-90.

95 Sundaram R.S, Gomez-Navarro C, Balasubramanian K, Burghard M, Kern K. Electrochemical modification of graphene // Adv Mater. – 2008. – Vol. 20. – P. 3050–3053.

96 Tuinstra F. and Koenig J.. Raman spectrum of graphite // Journal of Chemistry Physics. – 1970. – Vol. 53. – P. 1126-1130.

97 Sansone L., Malachovska V., La M.P. et al. Nanochemical fabrication of a GO-based nanohybrid for label-free optical sensing with fiber optics // Sens. Actuators B: Chem. – 2014. – Vol. 202. – P. 523–526.

98 Liu X.L, Ren N.Q, Zhang Y. Experimental study on treatment of traditional Chinese medicine wastewater by electronically controlled recoil // Journal of Harbin Institute of Technology. – 2006. – Vol 6. – P. 881-883.

99 Kudin K.N., Ozbas B., Schniepp H.C., et al.. Raman spectra of graphite oxide and functionalized graphene sheets // Nano Lett. – 2008. – Vol. 8, № 1. – P. 36–41.

100 Chen J.-L., Yan X.-P.. A dehydration and stabilizer-free approach to production of stable water dispersions of graphene nanosheets // J. Mater. Chem. – 2010. – Vol. 20, № 21. – P. 4328–4332.

101 Das A., Pisana S., Chakraborty B.. et al., Monitoring dopants by Raman scattering in an electrochemically top-gated graphene transistor // Nature Nanotechnology. – 2008. – Vol. 3, № 4. – P. 210–215.

102 Ang P.K., Wang S., Bao Q.. et al., High-throughput synthesis of graphene by intercalation−exfoliation of graphite oxide and study of ionic screening in graphene transistor // ACS Nano. – 2009. – Vol. 3, № 11. – P. 3587–3594.

103 Voggu, R.; Das, B.; Rout, C.S.; Rao, C.N.R., Effects of the charge-transfer interactions of graphene with electron-donor and -acceptor molecules examined by Raman spectroscopy and cognate techniques // J. Phys. Condens. Matter. – 2008. – Vol 20. – P. 472204.

104 Arsat R., Breedon M., Shafiei M. et al. Graphene-like nano-sheets for surface acoustic wave gas sensor applications // Chem. Phys. Lett. – 2009. – Vol. 467, № 4-6. – P. 344–347.

105 Zhang L.S., Wang W.D., Liang X.Q. et al. Characterization of partially RGO as room temperature sensor for H_2 // Nanoscale. – 2011. – Vol. 3, № 6. – P. 2458–2460.

106 Tan C., Huang X., Zhang H. Synthesis and applications of graphene-based noble metal nanostructures // Mater. Today. – 2013. – Vol. 16, № 1-2. – P. 29–36.

107 Du Y., Xue Q., Zhang, Z., Xia F. Great enhancement in H_2 response using graphene-based Schottky junction // Mater. Lett. – 2014. – Vol. 135. – P. 151–153.

108 Hu N., Yang Z., Wang Y. et al. Ultrafast and sensitive room temperature NH_3 gas sensors based on chemically RGO // Nanotechnology. – 2014. – Vol. 25, № 2. – P. 025502.

109 Russo P.A., Donato N., Leonardi S.G. et al. Room-temperature hydrogen sensing with hetero nanostructures based on RGO and tin oxide // Angew. Chem. Int. Ed. – 2012. – Vol. 51, № 44. – P. 11053–11057.

110 Dutta D., Hazr S.K., Das J. et al. Studies on p-TiO2 /n-graphene heterojunction for hydrogen detection // Sens. Actuators B: Chem. – 2015. – Vol. 212. – P. 84–92.

111 Esfandiar A., Irajizad A., Akhavan O. et al. Pd–WO3 /RGO hierarchical nanostructures as efficient hydrogen gas sensors // Int. J. Hydrogen Energy. – 2014. – Vol. 39, № 15. – P. 8169–8179.

112 Guo L., Jiang H.B., Shao R.Q. et al. Two-beam-laser interference mediated reduction, patterning and nanostructuring of GO for the production of a flexible humidity sensing device // Carbon. – 2012. – Vol. 50, № 4. – P. 1667–1673.

113 Han D.D., Zhang Y.L., Jiang H.B. et al. Moisture-responsive graphene paper prepared by self-controlled photoreduction // Adv. Mater. – 2014. – Vol. 27, № 2. – P. 332–338.

114 Yu H.W., Kim H.K., Kim T. et al. Self-powered humidity sensor based on GO composite film intercalated by poly (sodium 4-styrenesulfonate) // ACS Appl. Mater. Interfaces. – 2014. – Vol. 6, № 11. – P. 8320–8326.

115 Hwang S.H., Kang D., Ruoff R.S. et al. Poly (vinyl alcohol) reinforced and toughened with poly (dopamine)-treated GO, and its use for humidity sensing // ACS Nano. – 2014. – Vol. 8, № 7. – P. 6739–6747.

116 Mao S., Cui S., Lu G. et al., Tuning gas-sensing properties of RGO using tin oxide nanocrystals // J. Mater. Chem. – 2012. – Vol. 22. – P. 11009–11013.

117 Zhang D., Tong, J., Xia B. Humidity-sensing properties of chemically reduced graphene oxide/polymer nanocomposite film sensor based on layer-by-layer nano self-assembly // Sens. Actuators B: Chem. – 2014. – Vol. 197. – P. 6–72.

118 Gao W. Graphene Oxide, Reduction Recipes, Spectroscopy, and Applications. – Los Alamos, NM, USA: Springer International Publishing Switzerland, 2015. – P. 147.

119 Ni Zh., Wang Y., Yu T. and Shen Z. Raman Spectroscopy and Imaging of Graphene // Journal of Nano Review. – 2008. – Vol. 1. – P. 273-291.

120 Challa S.S.R. Kumar. Raman Spectroscopy for Nanomaterials Characterization. – USA: Springer-Verlag Berlin Heidelberg, – 2012. – P. 645.

121 Ferrari A.C., Basko D.M., Raman spectroscopy as a versatile tool for studying the properties of graphene // Nature Nanotechnol. – 2013. – Vol. 8, № 4. – P. 235–246.

122 Eigler S., Hof, F.; Enzelberger-Heim M.; et al. Statistical-Raman-microscopy and atomic-force-microscopy on heterogeneous graphene obtained after reduction of graphene oxide // J. Phys. Chem. C. – 2014. – Vol. 118, № 14. – P. 7698–7704.

123 Web-Resource, Leo P. Kadanoff. Excellence in computer simulation https://www3.nd.edu/~powers/ame.60614/kadanoff.pdf

124 Web-Resource, Roger McHaney. Understanding Computer Simulation. https://library.ku.ac.ke/wp-content/downloads/2011/08/Bookboon/IT,Programming%20and%20Web/understanding.pdf

125 Web-Resource, Molecular dynamics simulations https://afire.asnet.am/asnetvm/index.php/molecular-dynamics-simulations

126 Web-Resource, Markus J. Buehler. Introduction to classical molecular dynamics Lecture 2. https://ocw.mit.edu/courses/civil-and-environmental-engineering/1-978-from-nano-to-macro-introduction-to-atomistic-modeling-techniques-january-iap-2007/lecture-notes/lec02.pdf

127 Web-Resource, Chapter 8 Monte Carlo Simulation. http://web.mst.edu/~dux/repository/me360/ch8.pdf

128 Web-Resource, Dirk P. Kroese. Why the Monte Carlo Method is so important today. https://people.smp.uq.edu.au/DirkKroese/ps/whyMCM_fin.pdf

129 Ilyin A.M., Daineko E.A. & Beall G.W. Computer Simulation and Study of Radiation Defects in Graphene // Physica E. – 2009. – Vol. 42, №. 21. – P. 67-69.

130 Ilyin A., Guseinov N., Nikitin A. and Tsyganov I. Characterization of thin graphite layers and graphene with energy dispersive X-ray analysis // Physica E. – 2010. – Vol. 42, №. 8. – P. 2078-2080.

131 Ilyin A.M., Nemkaeva R.R., Kudryashov V.V. Computational study of graphene and few –layer graphene –metal composites, induced by radiation // J.Mater. Sci& Engineering, B3. – 2013. – Vol. 3. – P. 161-166.

132 Ilyin A.M., Guseinov N.R., Nemkaeva R.R., Asanova S.B., Kudryashov V.V. Bridge-like radiation defects in few-layer graphene // Nucl.Instrum & Methods in Phys.Res., B. – 2013. – Vol. 315. – P. 192-196.

133 Ilyin A.M., Kudryashov V.V., Guseinov N.R. Computer Simulation of Few-Layer Graphene Intercalated by Lithium for Power Sources // Journal of Electrochemical Society. – 2015. – Vol.162, №. 8. – P. A1544-A1546.

134 Guseinov N., Baigarinova G., Ilyin A. Structural damaging in few-layer graphene due to the low energy electron irradiation // Advances in Nano Research. – 2016. – Vol. 4, №. 1. – P. 45-50.

135 Farahani H., Wagiran R. and Hamidon M.N.. Review Humidity Sensors Principle, Mechanism, and Fabrication Technologies // A Comprehensive Review Sensors. – 2014. – Vol. 14. – P.7881-7939;

136 Chia Y.L. and Gwo B.L. Humidity Sensors: A Review // SENSOR LETTERS. – 2005. – Vol. 3. – P. 1-14.

137 Naik G., Krishnaswamy S. Room-Temperature Humidity Sensing Using Graphene Oxide Thin Films // Graphene. – 2016. – Vol. 5. – P. 1-13.

138 Lee, C. & Lee, G. Humidity sensors: A Review // Sens. Lett. – 2005. – Vol. 3. – P. 1-15.

139 Hengchang B, Kuibo Y, Xiao X, Jing J, Shu W, Litao S, Mauricio T & Mildred S.. Ultrahigh humidity sensitivity of graphene oxide // Scientific Reports. – 2013. – Vol. 3. – P. 1-7.

140 Schedin F., Geim, A.K., Morozov S.V., Hill E.W., Blake P., Katsnelson M.I. and Novoselov K.S. Detection of Individual Gas Molecules Adsorbed on Graphene // Nature Materials. – 2007. – Vol. 6. – P. 652-655.

141 Lu G., Ocola L.E. and Chen J. Reduced Graphene Oxide for Room-Temperature Gas Sensors // Nanotechnology. – 2009. – Vol. 20, № 44. – P. 445-502.

142 Lu G., Ocola L.E. and Chen J. Gas Detection Using Low-Temperature Reduced Graphene Oxide Sheets // Applied Physics Letters. – 2009. – Vol. 94, № 8. – P. 083-111.

143 Lange U., Hirsch T., Mirsky V.M. and Wolfbeis O.S. Hydrogen Sensor Based on a Graphene-Palladium Nanocomposite // Electrochimica Acta. – 2011. – Vol. 56. – P. 3707-3712.

144 Nomani M., Shishir R., Qazi M., Diwan D., Shields V., Spencer M., Tompa G.S., Sbrockey N.M. and Koley G. Highly Sensitive and Selective Detection of NO_2 Using Epitaxial Graphene on 6H-SiC // Sensors and Actuators B: Chemical. – 2010. – Vol. 150. – P. 301-307.

145 Jeong H.Y., et al. Flexible Room-Temperature NO_2 Gas Sensors Based on Carbon Nanotubes/Reduced Graphene Hybrid Films // Physics Letters. – 2010. – Vol. 96. – P. 213105.

146 Gautam Naik, Sridhar Krishnaswamy. Room-Temperature Humidity Sensing Using Graphene Oxide Thin Films // Graphene. – 2016. – Vol. 5, № 1. – P. 1-13.

147 Meng-Chu Chen, et al. Fabrication of Humidity Sensor Based on Bilayer Graphene // Ieee electron device letters. – 2014. – Vol. 35, № 5. – P. 590-592.

148 Weng H.L. et al. All-Optical Graphene Oxide Humidity Sensors // Sensors. – 2014. – Vol. 14, № 1. – P. 24329-24337.

149 Sourav Gh, Ruma Gh, Prasanta K.G and Tarun K.B. Humidity Sensor Based on High Proton Conductivity of Graphene Oxide // IEEE Transactions on Nanotechnology. – 2015. – Vol. 14, № 5. – P. 931-937.

150 Daniel H.R, Grissel R.R, Rodrigo M.M. and Ernesto S.G. A Capacitive Humidity Sensor Based on an Electrospun PVDF/Graphene Membrane // Sensors. – 2017. – Vol. 17, № 1009. – P. 1-11.

151 Anderson D. Smith etc., Resistive graphene humidity sensors with rapid and direct electrical readout // Nanoscale. – 2015. – Vol. 7, № 45. – P. 19099-19109.

152 Anderson D. Smith etc., Graphene-based CO_2 sensing and its cross sensitivity with humidity // The Royal Society of Chemistry Advances. – 2017. – Vol. 7. – P. 22329–22339.

153 Massera E., Ferrara, V.L.A., Miglietta M., Polichetti, T., Nasti I. and Francia G.D.I. Gas Sensors Based on Graphene // Chemistry Today. – 2011. – Vol. 29. – P. 39-41.

154 Boudaden J, etc., Polyimide-Based Capacitive Humidity Sensor // Sensors. – 2018. – Vol. 18, № 5. – P. 1-15.

155 Ghosh A., Late D.J., Panchakarla L.S., Govindaraj A. & Rao C.N.R. NO_2 and humidity sensing characteristics of few-layer graphene // Journal of Experimental Nanoscience. – 2009. – Vol. 4, № 4. – P. 313–322.

156 Popov V.I. etc., Graphene based humidity sensors: The origin of alternating resistance change // Nanotechnology. – 2017. – Vol. 28, № 35. – P. 14.

157 Wang Y., Park S., Yeow J.T., Langner A., Müller F. A Capacitive humidity sensor based on ordered macroporous silicon with thin film surface coating. Sens. Actuators B Chem. – 2010. – Vol. 149, № 1. – P. 136–142.

158 Web-Resource, O. Olea-Mejia, R. Contreras-Bulnes et al. Scanning electron microscopy and energy dispersive spectroscopy microanalysis applied to human dental specimens under laser irradiation for caries prevention. http://www.formatex.info/microscopy6/book/70-77.pdf

159 Web-Resource, Ana María Valenzuela-Muñiz. ABC's of Electrochemistry series Materials Characterization techniques: SEM and EDS. https://www.ohio.edu/engineering/ceer/research/upload/sem-edx.pdf

160 Goldstein J, Newbury D, Joy D, Lyman Ch, Echlin P, Lifshin E, Sawyer L, Michael J. Scanning Electron Microscopy and XRay Microanalysis. Unated States: Springer, 2003. – P. 673.

161 Web-Resource, Калмыков К.Б., Дмитриева Н.Е. Сканирующая электронная микроскопия и рентгено-спектральный анализ неорганических материалов. http://www.chem.msu.su/rus/teaching/kalmykov-dmitrijeva-sem2017.pdf

162 Web-Resource, Susan Swapp. Scanning Electron Microscopy (SEM) https://serc.carleton.edu/research_education/geochemsheets/techniques/SEM.html

163 Web-Resource, Roger Robbins. Scanning Electron Microscope Operation Zeiss Supra-40.

https://www.utdallas.edu/~rar011300/SEM/Scanning%20Electron%20Microscope%20Operation.pdf

164 Web-Resource, Introduction to Energy Dispersive X-ray Spectrometry (EDS) https://cfamm.ucr.edu/documents/eds-intro.pdf

165 Web-Resource, D.S. Su. Scanning electron microscopy (SEM) (SEM: Sächsisches Eisenbahnmuseum). http://www.fhi-berlin.mpg.de/acnew/department/pages/teaching/pages/teaching__wintersemester__2009_2010/dangsheng_su__scanning_electron_microscopy__100129.pdf

166 Ewen Smith, Geoffrey Dent. Modern Raman Spectroscopy – A Practical Approach. – England: John Wiley & Sons Ltd, Chichester, 2005. – P. 210.

167 Web-Resource, XI. Raman spectroscopy

http://users.abo.fi/mhotokka/mhotokka/lecturenotes/ms04.d/ms04-raman-eng.pdf

168 Web-Resource, Raman Spectroscopy

http://fizika.unios.hr/~ilukacevic/dokumenti/materijali_za_studente/afs/10_Raman.pdf

169 Web-Resource, Raman Spectroscopy Basics

http://web.pdx.edu/~larosaa/Applied_Optics_464-564/Projects_Optics/Raman_Spectrocopy/Raman_Spectroscopy_Basics_PRINCETON-INSTRUMENTS.pdf

170 Web-Resource, Dr. Davide Ferri. Raman Spectroscopy https://www.ethz.ch/content/dam/ethz/special-interest/chab/icb/van-bokhoven-group-dam/coursework/Characterization-Techniques/2015/raman-spectroscopy-2015.pdf

171 Web-Resource, Введение в Рамановскую Спектроскопию http://www.bvr.by/kscms/uploads/editor/file/vvedenie_v_raman_spektroskopiyu.pdf

172 Web-Resource, Raman Spectroscopy http://instructor.physics.lsa.umich.edu/adv-labs/Raman_Spectroscopy/Raman_spect.pdf

173 Web-Resource, Siegfried Wartewig. IR and Raman Spectroscopy. http://citeseerx.ist.psu.edu/viewdoc/download?doi=10.1.1.382.8078&rep=rep1&type=pdf

174 Web-Resource, Laura Mazzei. Lab Manual: Raman Spectroscopy http://physics.gu.se/~starn/tif060/Raman/Raman_manual2014.pdf

175 Web-Resource, NTEGRA Spectra https://www.ntmdt-si.ru/data/media/files/products/ntegra/112_ntegra_spectra_2008.pdf

176 Web-Resource, http://nnlot.kz/RU/Instruments.html.

177 Web-Resource, Thermogravimetric Analysis – TGA. https://www.farmacja.umed.wroc.pl/sites/default/files/struktura/farmacja/pracownia-aebs/4_TG.pdf

178 Web-Resource, A Beginner's Guide. Thermogravimetric Analysis (TGA). https://www.perkinelmer.com/lab-solutions/resources/docs/faq_beginners-guide-to-thermogravimetric-analysis_009380c_01.pdf

179 Web-Resource, Linda Fröberg. Thermal Analysis TGA/DTA http://web.abo.fi/instut/biofuelsGS-2/kursen/%C5A/lectures/Lectrure_Thermal%20Analysis.pdf

180 Started Guide. https://engineering.tamu.edu/media/4133232/tga-q500.pdf

181 Web-Resource, TA Instruments Q Series Thermogravimetric Analyzers. http://www.tainstruments.com/pdf/literature/OLD_tgabrochure.pdf

182 Web-Resource, Термогравиметрия https://ru.wikipedia.org/wiki/%D0%A2%D0%B5%D1%80%D0%BC%D0%BE%D0%B3%D1%80%D0%B0%D0%B2%D0%B8%D0%BC%D0%B5%D1%82%D1%80%D0%B8%D1%8F

183 Web-Resource, Laboratory 10: Thermogravimetric Analysis. Experimental Method and Testing Procedures. https://sites.google.com/a/iastate.edu/laboratory-10-thermogravimetric-analysis/experimental-methods

184 Bunaciu A.A. etc. X-Ray Diffraction: Instrumentation and Applications // Critical Reviews in Analytical Chemistry. – 2015. Vol. 45, № 4. – P. 289-299

185 Web-Resource, B.D. Cullity. Elements of X-Ray diffraction https://www.researchgate.net/profile/Ahmed_Hassanien/post/What_is_the_main_purpose_of_XRD_analysis_of_materials_How_it_is_different_from_EDS_analysis/attac

hment/59d64b9279197b80779a5988/AS%3A480622478139392%401491600736594/download/B.+D.+CULLITY-Elements+of+X-RAY+DIFFRACTION-SECOND+EDITION.pdf

186 Web-Resource, Yunus Kocabozdoğan etc. X-Ray Diffraction (XRD) http://yunus.hacettepe.edu.tr/~selis/teaching/WEBkmu396/ppt/Presentations2010/XRD.pdf

187 Web-Resource, Bragg′s law. http://www.idc-online.com/technical_references/pdfs/chemical_engineering/Braggs_law.pdf

188 Bunaciu A.A., Udristioiu E.G. and Hassan Y.A. X-Ray Diffraction: Instrumentation and Applications // Critical Reviews in Analytical Chemistry. – 2015. – Vol. 45. – P. 289–299.

189 Web-Resource, Diffraction Methods http://ww2.chemistry.gatech.edu/class/6182/wilkinson/diffraction_methods.pdf

190 Web-Resource, Yoshio Waseda. X-Ray Diffraction Crystallography. https://fac.ksu.edu.sa/sites/default/files/ebooksclub.org__X_Ray_Diffraction_Crystallography__Introduction__Examples_and_Solved_Problems.pdf

191 Web-Resource, Principles of X-ray Diffraction. https://application.wiley-vch.de/books/sample/3527310525_c01.pdf

192 Web-Resource, Topic 5a XRD lectures. X-ray Diffraction (XRD) http://web.pdx.edu/~pmoeck/phy381/Topic5a-XRD.pdf

193 Web-Resource, Barbara L Dutrow etc., Geochemical Instrumentation and Analysis. X-ray Powder Diffraction (XRD). https://serc.carleton.edu/research_education/geochemsheets/techniques/XRD.html

194 Web-Resource, X-ray diffraction. https://www.unf.edu/~michael.lufaso/chem4627/ch2_solid_state.pdf

195 Web-Resource, Michael W. Davidson. Optical microscopy. http://zeiss-campus.magnet.fsu.edu/referencelibrary/pdfs/Davidson_Abramowitz_Optical_Microscopy.pdf.

196 Web-Resource, Optical Microscopy https://www.researchgate.net/publication/277704161_Optical_Microscopy

197 Web-Resource, Спектрофотометры Lambda /модели 25,35,45 www.kip-guide.ru/docs/20961-01.pdf

198 Ilyin A.M., Guseinov N.R., Kuanyshbekov T.K., Beall G.W., and Tulegenova M.A. Computer Simulation and First Principles Study of Ga-Doped Graphene Nanostructures // Journal of Computational and Theoretical Nanoscience. – 2019. – Vol. 16, №. 1. – P. 39-41.

199 Kuanyshbekov T.K., Tulegenova M.A., Baigarinova G.A., Guseinov N.R., Ilyin A.M.. Investigation of temperature influence on the process of reduction of graphene oxide // VESTNIK KazNU. – 2017. – Vol. 2, № 61. – P. 18-23.

200 Қуанышбеков Т.Қ., Гусейнов Н.Р., Ильин А.М.. Термическое восстановление оксида графена в водородной атмосфере // Сборник тезисов Международной конференции студентов и молодых ученых «Фараби Әлемі». Алматы., 2017. – P. 312.

201 Қуанышбеков Т.Қ., Тулегенова М.А., Гусейнов Н.Р. Термическое восстановление оксида графена в водородной атмосфере // ВЕСТНИК КазНИТУ имени К.И. Сатпаева, Серия техническая. – 2017. – Vol. 123, № 3. – P. 331-336.

202 Куанышбеков Т.К., Тулегенова М.А., Гусейнов Н.Р., Beall G.W., Ильин А.М. Получение графена диффузией графита // ВЕСТНИК КазНИТУ им. К.Сатпаева. – 2018, – Vol. 127, № 3. – P. 152-158.

203 Қуанышбеков Т.Қ., М.А. Тулегенова, Н.Р. Гусейнов, А.М. Ильин. Изучение стабильности датчика влажности на основе оксида графена // Сборник тезисов Международной конференции студентов и молодых ученых «Фараби Әлемі», Алматы. 2018. – P. 205.

204 Куанышбеков Т.К., Тулегенова М.А., Гусейнов Н.Р., Озюлмаз Б., Ильин А.М.. Изучение стабильности датчика влажности на основе оксида графена // ВЕСТНИК КазНИТУ им. К.Сатпаева. – 2017. – Vol. 124, № 6. – P. 210-213.

205 Kuanyshbekov T.K., Ilyin A.M., Beall G.W., Guseinov N.R., and Tulegenova M.A. Sensitive humidity sensor based on functionalized graphene // Abstract. 4th International Conference on Sensors Engineering and Electronics Instrumentation Advances (SEIA' 2018). – Amsterdam, The Netherlands, 2018. – P. 45-46.

206 Kuanyshbekov T.K., Ilyin A.M., Beall G.W., Guseinov N.R. Creation of a Humidity Sensor Based on Functionalized Graphene Nanostructures // Sensors & Transducers. – 2019. – Vol. 229, – № 1. – P. 39-46.